THE $^2H(\vec{d},\gamma)^4HE$ REACTION AT 20 TO 50 MEV AND THE D-STATE IN ^4HE

by
R. M. Whitton

Tensor and vector analyzing powers for the $^2H(\vec{d},\gamma)^4He$ reaction have been obtained as a function of angle at E_{beam}= 30 and 50 MeV. These data augment an extensive set of data obtained at TUNL and Wisconsin at E_{beam}< 15 MeV, and a measurement from IUCF at E_{beam}= 95 MeV. A direct capture calculation was performed and compared to the data, using Woods-Saxon potentials for the ground state of ^4He, and scattering wave-functions obtained from an optical model potential that was constructed by fitting the elastic scattering data. The model assumes that this reaction proceeds primarily via E2 radiation in this energy region. While the validity of this assumption has been questioned at lower energies, it is supported at these energies by the shape of the angular distributions of the tensor analyzing powers and by the small magnitude of the vector analyzing power. A value of the probability for the D-state in ^4He can be extracted by fitting the predictions of this model to the data. This calculation differs from previous direct capture calculations in that the optical model takes absorption into account in the region of the continuum state. The results of this calculation are compared to the results of a microscopic 7-channel resonating group model calculation.

The polarized beam data were obtained at the 88-inch Cyclotron of the Lawrence Berkeley Laboratory (LBL), and the unpolarized differential cross section at E_{beam}= 30 MeV

was obtained at the Kernfysisch Versneller Instituut (KVI) in Groningen, The Netherlands. All measurements were made using large anticoincidence-shielded NaI gamma-ray spectrometers. The measurements at 50 MeV required the detection of the recoiling ^{4}He nuclei in coincidence with the gamma-rays, along with time of flight criteria for clean event identification. The targets used in this work were gas cells cooled to liquid nitrogen temperature. The gas was contained within the cell by 0.0254 mm Kapton windows. The total D_2 thickness was 45 mg/cm^2.

Within the pure E2 approximation, a tensor analyzing power can only arise from a tensor force effect. The observed values are large, on the order of 30% of the allowed values, suggesting that a significant fraction of the capture cross section arises as capture to the D-state at these energies.

Below 15 MeV significant p-wave capture strength complicates the analysis of this reaction while at 95 MeV the long wavelength approximation may be invalid. The best determination of the D-state in ^{4}He may therefore be possible in the previously unprobed energy region of 30 to 50 MeV.

ACKNOWLEDGEMENTS

I would like to thank my thesis advisor, Dr. Henry Weller for his professional interest, advice and support, and for his warm personal friendship. His level of involvement has always far surpassed the line of duty, and his generosity seems boundless. I must also express my gratitude to all of the principal collaborators on this experiment. These include Drs. Evans Hayward, Bill Dodge, and Sebastian Kuhn. Not only did they make the project possible, they were a delight to work with and remain a pleasure to know.

The support of the directors of the three laboratories at which this work was done must be gratefully acknowledged. They were Drs. E.G. Bilpuch at TUNL, Robert Stokstad at the 88 Inch Cyclotron, and Rolf Siemssen at KVI. I must also thank the staff of the 88 and particularly, Ruth Mary Larimer.

I must thank Dr. Don Lehman for the discussions of the electric dipole operator. Part of this discourse is included as an appendix to this thesis. These discussions eliminated much of the confusion surrounding a fundamental piece of nuclear physics.

No project of this nature would have been possible without the help and friendship of the past and present members of the TUNL radiative capture group. This includes James Langenbrunner, Zandy Williams, Laird Kramer, Mark Balbes, Sinan Utku, Gabrielle Caloustian, Claude LaFontaine, Drs. Ron Tilley, Jerry Feldman, Bob August, and George Mitev and my classmate John Riley.

Table of Contents

1. Introduction. 1
1.1. Radiative Capture. 1
1.2. D-States in Nuclei. 5
1.3. D-States and Radiative Capture. 14
1.4. A Brief Description of This Study. 17
1.5. Motivation for These Energies. 23
2. Experimental Equipment and Techniques. 32
2.1. History of the Project. 32
2.2. The Experimental setup at KVI. 36
2.3. The Setup at LBL. 41
2.3.a. Overview. 41
2.3.b. The Polarized Source at the LBL. 45
2.3.c. The Solenoid. 48
2.3.d. Polarimeters. 49
2.3.e. NaI Spectrometers. 51
2.4. The Coincidence Technique. 54
2.4.a. Overview. 54
2.4.b. The Use of Time-Of-Flight. 55
2.4.c. Target Design Considerations. 58
2.4.d. The Particle Detectors. 63
2.4.e. Simulation of The Recoils. 67
2.5. Fast Electronics. 72
2.5.a. NaI Spectrometer Electronics. 72
2.5.b. Scintillator Electronics. 77
2.5.c. Accidental Coincidence Concerns. 81
2.6. Computers Used. 85

3. Offline Analysis. 86
3.1. Introduction. 86
3.2. Polarization Observables. 86
3.3. The Event Sorting. 92
3.3.a. Software. 92
3.3.b. Setting Gates. 92
3.3.c. Sorting and Summing the Events. 93
3.4. Finite Geometry in the Apparatus. 95
3.5. Spectra. 98
3.6. Summary of Errors and Corrections. 103
3.6.a. Analyzing Power Error 103
3.6.b. Differential Cross Section.Error 104
4. Discussion of Recent Data and Calculations. 110
4.1. Recent Attempts to Measure the D-State. 110
4.1.a. Polarization Work at Tandem Energies. 110
4.1.b. Low Energy Effects. 114
4.2. ^{4}He D-state from Modern n-n Potentials. 120
4.3. The RGM Calculation. 124
4.4. The RGM Calculation Compared to This Data. 127
4.5. A Direct Capture Calculation. 131
5. Transition Matrix Element Element Analysis. 144
5.1. Results of Transition Matrix Analysis. 150
6. Conclusions. 152
References. 154
Appendices. 162
A. Charge Polarization and the E1 Operator. 162
B. Legendre Coefficients and Transition Matrix. 178
C. Electronics Diagrams. 180
D. The Program CORRECT. 184
Biography. 197

List of Figures

1.1 The Experimental Setup in Cave 4C at the 88-inch Cyclotron at LBL. 22

1.2. Ay ($\vartheta\gamma$= 130 degrees) at "Tandem" Energies. 29

1.3. The sensitivity of Ayy at Higher Energies. 31

2.1. The layout of KVI. 40

2.2. Details of the Berkeley Setup. 44

2.3. The Hyperfine Splitting in Deuterium. 47

2.4. Particle Time of Flight Spectrum. 56

2.5. Simulated ^{4}He Time of Flight Spectrum. 60

2.6. Details of the Target Assembly. 62

2.7. The Charged Particle Detectors. 66

2.8. Simulation of the Position of the ^{4}He Nuclei. 71

2.9. Simplified View of the NaI Electronics. 76

2.10. Simplified View of Scintillator Electronics. 80

2.11. Accidental Vetoes as a Function of Timing 84

3.1. The Madison Convention. 91

3.2. Gamma-Ray Spectra from KVI at E_d = 30 MeV. 98

3.3. Gamma-ray Spectra from LBL at E_d = 50 MeV. 100

3.4. Particle Time and Energy Spectra. 102

4.1. The Ratio $R = \sigma(\pi/2)/\sigma(3\pi/4)$ at Low Energy. 119

4.2. Integrated Low Energy Cross-Section. 119

4.3. The RGM Matrix Elements from Hofmann et.al. 129

4.4. RGM A_y (ϑ_γ=130°)as a Function of Energy. 130

4.5. RGM A_{yy}(ϑ_γ=130°) as a Function of Energy. 130

4.6. Optical Model Fits to Elastic Scattering Data. 135

4.7. A_y (ϑ_γ), and A_{yy} (ϑ_γ),(E_d = 20 MeV). 137

4.8. $\sigma(\vartheta_\gamma)$, Ay(ϑ_γ), and A_{yy} (ϑ_γ),(E_d = 50 MeV). 139

4.9. $\sigma(\vartheta_\gamma)$,,and A_y (ϑ_γ),(E_d = 50 MeV). 141

4.10. A_{yy} (ϑ_γ), and T_{20} (ϑ_γ),(E_d = 50 MeV). 143

Appendix C. Complete Electronics Diagrams. 180

List of Tables

1.1. Introductory and Review Articles. 12

1.2. Experimental Values of ^{3}H and ^{3}He D-State. 13

1.3. Calculated Differences Between 10 and 50 MeV. 27

3.1. Correction Factors to the Cross Section. 107

3.2. Fractional Sources of Error. 107

3.3. Reduced and Corrected Data. 108

4.1. Table of Allowed Amplitudes. 118

4.2. Table of Potential Parameters. 133

5.1. Coefficients from Fits. 149

5.2. Matrix Element Analysis and RGM Results. 151

1. Introduction

1.1. Radiative Capture

A few words should be devoted to a general discussion of electromagnetic nuclear physics and the importance of studying radiative capture processes. It isn't possible to attempt any sort of review of this subject here. In this section mention will be made of the most qualitatively understandable and interesting aspects of electromagnetic nuclear physics, and specifically radiative capture. Also, for the purpose of review, a short bibliography of some introductory and review articles is included at the end of this section.

The detection of photons, rather than massive or charged particles, is technically difficult. Some aspects of the nucleus are most easily accessed in this way however, because of the nature of radiative capture processes.

Two aspects of the electromagnetic interaction make it unusually useful in studying the atomic nucleus. First of all it is an interaction for which a specific Hamiltonian is known. From first principles, operators are available to calculate the electromagnetic part of the interaction thereby isolating it from the the rest of it, such as the purely strong nuclear force. The other aspect unique to electromagnetic nuclear physics is that the strength of the force is such that it can be reliably described by a perturbation theory expansion, while still strong enough to be useable in making measurements. These are in essence the reasons why such an interest has developed in this seemingly difficult branch of nuclear physics, motivating the electron facilities now being built, along with de-

velopments of a theoretical nature, such as the ability to make the radiative corrections necessary in extracting information from electron studies. Radiative capture studies involve the transition from an initial scattering state to a final state through the emission of a photon, and of course are motivated by these same reasons.

As will be discussed in Sections 1.3 and 4.1, analyzing powers are sensitive to the interference of transition amplitudes. Polarization observables are therefore extraordinarily useful in examining small components of the nuclear wave-function, as small amplitudes can produce large effects through interference. The technical difficulties of producing either polarized targets or polarimeters for reaction products often motivates one to study polarization observables in photonuclear studies using the inverse channel of radiative capture. No double scattering experiments or optically pumped or frozen targets are required when a polarized beam is used in the capture channel.

The lowest term in a perturbative expansion of the radiation field is the electric dipole (E1). Nuclear systems are partly bound by the exchange of charged mesons and the simple current given by the proton charge is modified by an exchange current associated with the charged pions. The Siegert form of the E1 operator implicitly includes the effects of exchange currents in a simple fashion (Siegert, 1937). This form of the electromagnetic operator can be extended to include meson exchange currents in all electric multipoles (Friar, 1984), but not in the magnetic multipoles. Magnetic transitions are therefore viewed as a good testing ground for various theoretical treatments of meson exchange currents, as their effects must be added in a model dependent fashion. A good example is the theoreti-

cal interest in accessing the exchange currents in the deuteron via the M1 radiation present in the $^{1}H(n,g)^{2}H$ reaction at thermal and low energies (Riska, 1972). The electric transitions on the other hand allow exchange current effects to be absorbed in the operator, simplifying the interpretation of some data, as in this study of the $^{2}H(\vec{d},\gamma)^{4}He$ reaction.

Table 1.1. Introductory and Review Articles

(Refer to reference list for publication and page.)

Hayward (1970), "Photonuclear Reactions"
(an introduction, with emphasis on data and the giant resonance region).

Giannini and Ricco (1985), "Photoreactions Above the Giant Resonance"
(an introduction to the study of photonuclear reactions with real photons).

Gari and Hebach (1981), "Photonuclear Reactions at Intermediate Energies"
(a review with emphasis on meson exchange currents).

Gibson (1981), "The Photodisintegration of Light Nuclei"
(A = 3,4).

Walecka (1983), "Electron Scattering"
(virtual photons).

1.2. D-States in Nuclei

It has long been known that in addition to the $L = 0$ (S-state) component of the ground state of the deuteron, there is present at the 4 to 7 percent level, an $L = 2$ (D-state) component. In fact, as early as 1939 Schwinger pointed out that the quadrupole moment of the deuteron provided conclusive evidence for a tensor component of the nuclear force. The tensor force doesn't conserve either the spin (S) or the orbital angular momentum (L), but only the total angular momentum (J), therefore allowing mixing between the predominant spherically symmetric S-state and configurations with $L = 2$ (the D-state component).

Three observables that are associated with the deuteron D-state are Q_d; the quadrupole moment, $\eta(^2H)$; the ratio of the deuteron's D-wave to S-wave asymptotic normalization constants, and $F^d_Q(q)$; the electromagnetic quadrupole form factor. Q_d and $\eta(^2H)$ can be understood in term of the two-nucleon tensor interaction, and specifically, to an accuracy of about one percent, the one-pion-exchange (OPE) piece of the tensor interaction. While Q_d and $\eta(^2H)$ depend primarily on the part of the deuteron wave-function that is external to the range of the nuclear interaction, the D-state probability $P_D(^2H)$ is an integral over the entire nuclear wave-function, and therefore it really isn't an observable. The non-zero values of the observables assure that $P_D(^2H)$ is also non-zero, but do not determine its value, as that would require a dynamical model of the entire nuclear wave-function. Electron polarization measurements are required to extract D-state information via $F^d_Q(q)$. Because of the scarcity of polarized electron beam, this work hasn't progressed far. It does however

hold promise with the development of new electron facilities.

Ericson and Rosa-Clot(1984, 1985) argue that it is reasonable to think of the entire deuteron wave-function as one pion exchange (OPE) dominated. This is based on the success of the OPE model in describing Q_d and $\eta(^2H)$ to within about a percent, making them the best understood dynamical quantities in nuclear physics. They emphasize that this is an accident of nature due to the near cancellation of the attractive and repulsive parts of the short range force leaving the deuteron nearly unbound. The OPE is a longer range interaction and it is generally agreed that the OPE tensor component is responsible for about 70% of the deuteron's binding. Within that model they suggest that the deuteron's D-state probability is ~6%. They also note that because of the success of the OPE in describing the deuteron's external quantities Q_d and $\eta(^2H)$ without free parameters, strong constraints are placed on exotic N-N models by the rather simple asymptotic part of the deuteron wave-function. In other words, calculations that include the short range forces through exotic means such as the quark bag description must do so properly to preserve the delicate cancellation in the deuteron's binding energy and to properly reproduce the asymptotic D-state observables.

The asymptotic normalization constant is a dimensionless quantity that reflects the dynamics of the entire wave-function through an overall normalization. There are separate constants for each of the L -waves, but it is the ratio of the D-wave to S-wave asymptotic normalization constants that is the quantity η most often referred to in the context of D-state studies. The normalized deuteron

wave-function can be written, using S- and D-state radial wave-functions u(r) and w(r), as

$$\Psi_{J,M} = \frac{1}{\sqrt{4\pi}}\left\{\frac{u(r)}{r} + \frac{w(r)}{\sqrt{8}\,r} S_{12}(\hat{r})\right\}\chi_{1M} ,$$

where χ_{1M} is the normalized spin wave function. Outside the range of the nuclear interaction, the radial wave-functions are completely determined by the deuteron binding energy ε and the asymptotic normalization constants A_s and $A_d = \eta A_s$:

$$u(r) \equiv A_S \tilde{u}(r) \xrightarrow[r\to\infty]{} A_S e^{-\alpha r},$$

$$w(r) \equiv A_D \tilde{w}(r) \xrightarrow[r\to\infty]{} \eta A_S \left[1 + 3/\alpha r + 3/(\alpha r)^2\right] e^{-\alpha r},$$

where $w(r)$ and $u(r)$ are respectively the D and S-state components of the deuteron, $\alpha^2 = \varepsilon M$, ε is the binding energy, and M is the reduced mass of the nucleon. The use of exponentials for the asymptotic forms is intended to be descriptive, a more accurate treatment should of course use asymptotic Coulomb wave-functions (Santos, 1982, 1984). See (Weller, 1988) for a detailed summary of the more complete treatment.

Consider the deuteron in a potential description. The S- and D-state wave functions then satisfy the coupled equations:

$$u''(r) = [\alpha^2 + U_{00}(r)]u(r) + U_{02}(r)w(r),$$

$$w''(r) = [\alpha^2 + 6/r^2 + U_{22}(r)]w(r) + U_{02}(r)w(r).$$

The terms $U_{ij} = MV_{ij}$ are linear combinations of central, tensor, spin-orbit, and quadratic spin-orbit potentials V_C, V_T, V_{LS}, and V_{LL} : $V_{00} = V_C$; $V_{02} = V_{20} = \sqrt{8}\, V_T$; $V_{02} = V_C - 2V_T - 3V_{LS} - 3V_{LL}$. Note that the S-D coupling is produced only in the non-diagonal tensor interaction. The D-state admixture in the deuteron is therefore generated by the tensor term $U_{20}(r)u(r)$. The asymptotic D/S ratio η is given by the following simple and exact expression:

$$\eta = \int_0^\infty dr\, \eta(r) = \sqrt{8}\, M \int_0^\infty dr\, r\, J_2(r) V_T(r)\, \tilde{u}.$$

Here $J_2(r)$ is the regular solution of the homogeneous D-wave equation normalized to the corresponding spherical Bessel function at large r :

$$J_2(r) \xrightarrow[r\to\infty]{} j_2(i\alpha r).$$

The parameter D_2 in the formalism of the distorted-wave Born approximation (DWBA), is closely akin to η :

$$D_2 = \frac{1}{15}\frac{\int_0^\infty dr \quad r^4 w(r)}{\int_0^\infty dr \quad r^2 u(r)} , \qquad D_2 \cong \frac{\eta}{\alpha^2} , \qquad \alpha^2 = \varepsilon M .$$

Sub-Coulomb stripping reaction studies have been used to extract values for the parameter D_2., and these are in excellent agreement with theory. It should be emphasized that this is an external property of the deuteron, and since all modern theories correctly treat the one pion exchange potential which dominates this region, they too are in agreement.

The helium isotopes and tritium (spin 0 and 1/2), unlike the deuteron, do not possess static quadrupole moments, therefore they only display a D-state component in their ground states through the non-zero ratios of their D-wave to S-wave asymptotic normalization constants. This aspect has only recently been accessed. The configurations in the trinucleon with total orbital angular momentum $L = 2$ can be a deuteron orbited by a nucleon in a relative D-wave; the deuteron could be in an internal D-wave configuration orbited by a nucleon in a relative S-wave, or there could be a correlated pair in an internal P-wave configuration, orbited by a P-wave nucleon. As discussed above for the deuteron, each of these cluster configurations can be separated into S- and D-wave amplitudes A_S and A_D given by the asymptotic behavior of the normalized wave-function:

$$u(r) \rightarrow A_S \exp(-\alpha r), \qquad w(r) \rightarrow \eta A_S [1 + 3/\alpha r + 3/(\alpha r)^2]\exp(-\alpha r).$$

$$\eta = \sqrt{8}\, M\, S(A) \int_0^\infty dr\, r j_2(i\alpha r)\, V_T(r)\, \tilde{u}(r).$$

The first studies of D-states in these nuclei were accomplished via sub-Coulomb stripping reactions (Knutson, 1975). The method of exchange pole extrapolation has also been used to extract values for η in the tri-nucleon from $(\vec{d},t)$ transfer reactions. (Sen, 1982; Knutson, 1981;

Here r is the relative distance between the center of mass of the two components and $\alpha^2 = 2\, M_R\, \varepsilon$, where M_R is the reduced mass and ε is the binding energy of the configuration. The average tensor potential acting between the asymptotic constituents is $\bar{V}_T(r) = \sqrt{8}\, S(A) V_T(r)$, where $V_T(r)$ is the n-n tensor potential in the I=0 channel, and S(A) is a kinematical factor that accounts for spin summation and takes the values 1, -1, and -2 for 2, 3, and 4 nucleon systems respectively. Then, within the Born approximation,

1979). The agreement here is not so good. Table 1.2 contains experimental values of ^{3}H and ^{3}He D-state observables. It is a condensation of Table 1 from the review article of (Weller, 1988); see that reference for the sources of the numbers.

The ^{4}He D-state can be asymptotically realized between two bound-state fragments only for two deuterons with relative orbital angular momentum of 2 and total spin angular momentum of 2 coupled to a total angular momentum of 0. The first qualitative experimental evidence for the D-

state in ^{4}He was obtained by Plattner et.al. (1975) by application of a forward-angle dispersion relation to p+ ^{4}He scattering. It can be shown that a 3N-exchange amplitude is proportional to the $^5D_0$ probability (Ericson, 1970). This analysis showed non-vanishing exchange contributions, and provided a model independent demonstration of a D-state component in the ^{4}He ground state.

Table 1.2. Three body D-state measurements, taken from Weller (1988).

The methods for extracting D-state observables are abbreviated as follows.

a. Analytical continuation of tensor analyzing powers.

b. Exact finite range / Distorted-wave Born approximation (DWBA).

c. Same as b. with tensor component of the deuteron distorting potential.

d. Local energy approximation / DWBA with tensor component of deuteron distorting potential.

e. Local energy approximation / DWBA without tensor component of deuteron distorting potential.

f. Local energy approximation / DWBA (sub-Coulomb).

Experimental Values of ^3H and ^3He D-State Observables.

Quantity	^3H	^3He	Method/Date
η	0.050+/-0.006	0.035+/-0.006	a. 1987
	0.051/-0.005		a. 1982
	O.O48+/-0.007		a. 1981
$D_2(fm^2)$	-0.25+/-0.05	-0.24+/-0.04	b. 1988
	-0.20+/-0.04	-0.25+/-0.05	c. 1987
	-0.16+/-0.03	-0.17+/-0.04	d. 1983
	-0.22+/-0.03	-0.21+/-0.04	e. 1983
	-0.259+/-0.014		f. 1982
	-0.288+/-0.011		f. 1982
	-0.279+/-0.012		f. 1981
	-.022+/-0.02	-0.22+/-0.02	d. 1981
		-.034	b. 1980
		-.036	b. 1980
	-0.275(P_d=.18)	-0.339	f. 1979
		-0.22	b. 1977
	-0.30	-0.37	b. 1977
	-0.24		b. 1975

1.3. D-State and Radiative Capture

The specific selection rules that apply to capture reactions can accentuate the effects of D-states in light nuclei. The formal expression for all of the spherical tensor analyzing powers involve the Racah coefficient $W(x\ S\ x\ S';\ a\ 2\ )$, where x and a are the spins of the projectile and target, and S and S' correspond to channel spins associated with any pair of T-matrix elements T and T' (Seyler, 1979). S, S' and 2 must triangulate (in terms of quantum mechanical vector addition, $|\vec{S} + \vec{S}'| = 2$) in order that the coefficient be non-zero.

Consider first the capture reaction $^1H(\vec{d},\gamma)^3He$. Because this reaction proceeds primarily via E1 radiation (Belt, 1970; Skopik, 1983), it should have $\Delta S = 0$ (neglecting the small spin dependent part of the E1 operator). In a simple p+d model of the ^3He ground state (with no D-state), $L = 0$, $S = {}^1/_2$, $J^\pi = {}^1/_2{}^+$, so for $\Delta S = 0$ the continuum state must also have $S = {}^1/_2$. No tensor analyzing power is therefore expected, because S, S' and 2 cannot triangulate. It is clear that if a D-state component is included in the ground state of ^3He, one has L=2, $S = {}^3/_2$, $J^\pi = {}^1/_2{}^+$. E1 capture from the L=1, $S = {}^3/_2$ continuum is therefore allowed, as well as capture from the the L=3, $S = {}^3/_2$ continuum since they both obey the $\Delta S = 0$ rule. Then with $S = {}^3/_2$, S' can equal $^1/_2$ or $^3/_2$, so that S, S' and 2 can triangulate and a non-zero tensor analyzing power can be expected.

$T_{20}(\vartheta)$ for the capture reaction $^1H(\vec{d},\gamma)^3He$ was first measured at the McMaster University Enge split pole spectrograph, detecting the recoiling ^3He nuclei (Vetterli,

1985). This measurement was made at 19.8 MeV, and the analysis that accompanied this study suggested a 5 to 9% D-state admixture in the ground state of ^{3}He. These data were also used to extract a value for the asymptotic D-to-S state ratio η . Their analysis indicated that for a reasonable inner cutoff radius of 2.5 fm in calculating the integrals and almost any reasonable assumption about the inner form of the ^{3}He bound state wave-function, a stable value of η (^{3}He) = 0.035 +/- 0.010 was required to fit their data. This is not inconsistent with the lower range of the values of this quantity that have been deduced from transfer reactions, and is in agreement with modern calculations (Friar, 1988; Klepacki, 1988; Ishikawa, 1986). Measurements of the tensor analyzing power A_{yy} in this reaction have since been made at E_d = 29.2 and 45.3 MeV for ϑ_{lab} = 90 degrees (Jourdan, 1986), and $A_{yy}(\vartheta)$ has been measured at E_d =95 MeV (Pitts, 1988). All of these measurements yield reasonably consistent results regarding the D-state. The D-State admixture in the ground state of ^{3}He has thus been accessed via radiative capture. Indeed the mere non-zero value of a tensor analyzing power in this reaction provides good evidence for a D-State, without complicated analysis and assumptions.

As with ^{3}He and ^{3}H, the existence of a non-zero tensor analyzing power in the ^{2}H($\vec{d}$,γ)^{4}He reaction is also strong evidence of a D-state component in the ground state of ^{4}He. In this case the fact that the particles in the incoming channel are identical bosons requires that L+S be even. This forbids $\Delta S = 0$ E1 transitions since L = 1 is required in the incident channel to form a 1^- state, so that S must equal 1. The ground state, on the other hand has L = 0, S = 0, ($J^\pi = 0^+$), only the small spin flip ΔS = 1 part of the E1 operator can therefore contribute (this

be discussed in more detail in appendix 1). In addition the isospin selection rule forbids E1 since $\Delta T = \pm 1$ in a self conjugate nucleus. Since $T = 0$ for a deuteron, the continuum state will have $T = 0$, as does the ground state of ^{4}He so that $\Delta T = 0$ here. $\Delta S = 0$, E2 radiation is allowed from a 2^+ state formed via $l = 2$, $s = 0$ going to the $^1S_0$ ground state (here the notation $^{2S+1}L_J$ is being used), and by a state formed with $l = 0,2,4$ and $s = 2$ going to the $^5D_0$ component (D-state) of the ^{4}He ground state. As $S = 0$ and $S = 2$ can triangulate with 2, an interference of the predominant d wave capture to the large S-state part of the ^{4}He ground state, with s, d or g wave capture leading to the small D-state part is expected to produce a tensor analyzing power.

The first measurement of such a tensor analyzing power was done at TUNL (Weller, 1984). This experiment measured T_{20} and showed indeed that it was large in value (~-0.2), and isotropic within the accuracy of the measurement. Isoptropy of T_{20} is a result that was expected from a pure E2 model if second order terms of the $s = 2$, $s' = 2$ type are neglected (see Section 4.1.a). Simple calculations accompanied this work, and from them values of $P_D(^4He)$, and η were extracted. This first work, though simplistic by the standards of today, was a fairly model independent verification of the ^{4}He D-state that aroused the fairly intense theoretical interest that has accompanied the study of this reaction.

1.4. A Brief Description of This Study; The $^2H(d,\gamma)^4He$ Reaction in the Region of 20 to 50 MeV

An effort to extend the measurements in $^2H(\vec{d},\gamma)^4He$ reaction to energies above the range accessible with an FN tandem Van de Graaff accelerator has been completed or very nearly so. This work has been carried out at the eighty-eight-inch cyclotron at the Lawrence Berkeley Laboratory (LBL), and to a lesser extent at the Kernfysisch Versneller Instituut (KVI) in Groningen, The Netherlands.

The vector (A_y) and tensor (A_{yy}) analyzing powers have been measured as a function of angle (θ), at beam energies of 20, 30 and 50 MeV. The differential cross section (σ) has been measured as a function of angle, at beam energies of 30 and 50 MeV. A_{yy} is related to the D-state admixture in the ground state of ^4He. Our measurements show that $A_{yy}(\theta)$ remains fairly isotropic but increases in magnitude with increasing energy. This is an interesting result in light of the fact that we are probing a region of smaller radius in the ^4He nucleus where the D-state wave-function is more uncertain. The vector analyzing power $A_y(\theta)$ arises primarily as a result of interference of the predominant E2 radiation with other multipoles, probably E1 and/or M2. While A_y is rather large at low energies, our measurements show that it becomes small at around 15 MeV and remains fairly consistent with zero on up to 50 MeV (See Fig. 1.2). The origin of this radiation of odd parity has been the object of some confusion in discussions among practitioners of electromagnetic nuclear physics. It has been supposed that charge polarization of the deuterons breaks conservation of isospin and thus may be the mechanism that produces E1 transitions. It is shown in Appendix A that this cannot be the case. E1 can however come about

through the isoscalar spin dependent part of the E1 operator. This small part of the operator is often ignored, but is more important in this reaction because the larger non-spin-flip part of the operator is forbidden both by symmetry and isospin considerations.

The tensor analyzing power $A_{zz}(\theta)$ at 50 MeV was also measured. The model calculations that have fit the A_{yy} data at tandem energies fairly well (ref. Section 4.1.a.) have failed to fit A_{zz}. S-wave capture to the D-state of ^{4}He contributes in first order to A_{zz} but not to A_{yy}. An explanation (Santos 1986) of the failure of the model to fit A_{zz} is that the S-wave scattering state is highly distorted. The D-state of the deuteron can also play a stronger role in S-wave capture. This is because an $l = 0$ scattering state can couple via E2 to the large $L = 0$ part of the ^{4}He ground state if there is an internal $\Delta L = 2$ transition which occurs in a deuteron. This could be a transition from the deuteron D to S-state, S to D-state, or a D to D-state. An $l = 2$ scattering state can couple to the D-state component of 4He in this same way, but the D-state is small, so this isn't expected to be important. There is not enough internal angular momentum to couple an $l = 4$ scattering state to the $L = 0$ ground state in this way. It seemed useful to look at a different energy region to help unravel the effects of distortion versus the internal deuteron transitions. This measurement required that the spin axis normally defined by the magnetic field of the cyclotron, not be perpendicular to the scattering plane, as it is when measuring A_{yy}. A large solenoid was installed in the capture beam-line at Berkeley for the purpose of precessing the spin axis about the beam axis in order to measure A_{zz}. It is interesting to note that the most recent calculations which are described in Section

4.2.a. are also least successful at predicting A_{zz}. The reason for this failure may be due to the omissions in this calculation, mentioned in Section 4.2.a.

There were a number of major difficulties that had to be overcome in order to successfully accomplish these measurements. The cross section for this reaction is very small (~ 10 nb/sr), while the $^{2}H(d,n)^{3}He$ reaction produces an intense background of energetic and thermal neutrons. Since there is no way to produce a pure deuterium target, there is also a neutron and gamma ray background associated with the target windows. As the energy is increased the advantage of the high Q-value of this reaction is lost, (see section 2.4.a, or 2.3 b iv), and the Coulomb barrier in heavy materials is overcome. It was therefore necessary to build an alpha recoil detection system that would make it possible to use the coincidence of the recoiling ^{4}He nuclei with the gamma rays in order to identify capture events at the limit of the beam energy at LBL. (This is currently 50 MeV in the beam-line where our setup is installed.)

The system takes advantage of the fact that the recoiling ^{4}He nuclei are kinematically coupled in angle to the angle of the outgoing gamma ray, and are restricted to a narrow forward cone in the region of < 7 degrees from the direction of the beam. Unfortunately there is an intense background of elastically scattered deuterons from the beam in this region. A count rate of the order of ten megahertz was expected in the recoil detectors due to the scattered beam. A system was constructed where the alpha particles of interest were separated from the beam bursts by time of flight, see Figure 1.1. A flight path of two meters was chosen to allow ~ 20 nsec between the arrival

times of the scattered deuterons and the alphas. This was enough to allow the recoiling alphas to be resolved from the beam bursts.

Four identical detectors were employed, two on each side of the beam. The detectors were thin planes of fast plastic scintillator (BC 418, 4.5" x 2.75" x .030") viewed by 2" diameter photomultiplier tubes, through Lucite light pipes, see Figure 2.5. The thickness was chosen so that the alpha particles of interest stopped in the first plane. The second plane was used to provide a fast veto to reduce the rate in some of the slower components of the electronics; when a deuteron was detected in the rear plane the pulse was vetoed in the very early part of the circuit while the time to pulse height converters and slow amplifiers remained ready to process the signal from an alpha particle that might arrive ~ 20 nsec later.

Figure 1.1 The experimental setup in cave 4C at the 88- inch cyclotron at LBL.

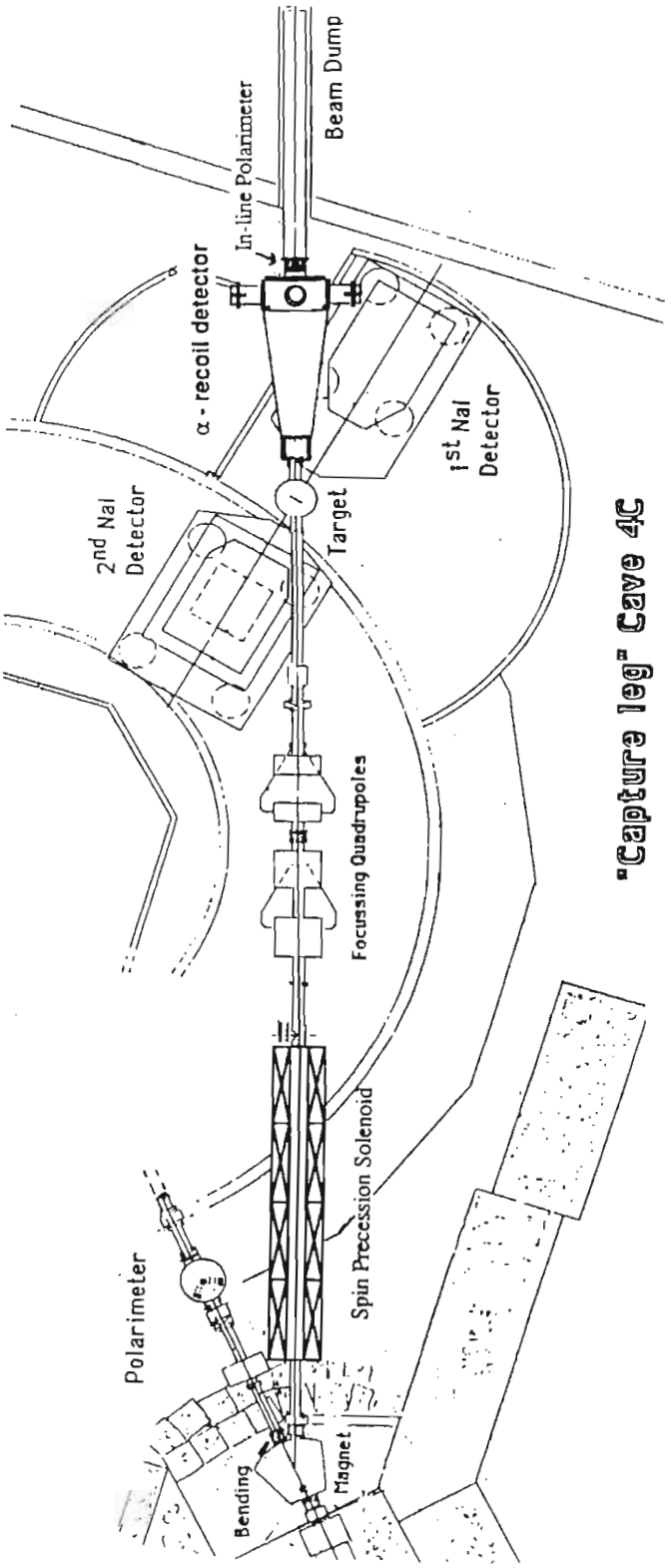
"Capture leg" Cave 4C
Beam Dump
In-line Polarimeter
α - recoil detector
1st NaI Detector
2nd NaI Detector
Target
Focussing Quadrupoles
Spin Precession Solenoid
Polarimeter
Bending Magnet

1.5. Motivation for Measurements at Deuteron Energies Greater Than 20 MeV.

The motivation for this experiment has been both to study the D-state in ^{4}He, and to study the dynamics of the ^{2}H$(\vec{d},\gamma)^4$He reaction. These are related motives, because a clearer understanding of the reaction dynamics allows a clearer interpretation of the observables that are related to the D-state. The presence of non-E2 transitions is an example of reaction dynamics making the interpretation of the tensor analyzing more difficult. This complication may be much less important in certain energy regions.

As previously pointed out, the tensor analyzing powers are sensitive to the interference of the predominant d-wave capture to the S state in ^{4}He with s, d, and g-wave capture to the D-state in ^{4}He. A_{yy} would be zero in a pure E2 direct capture model if there were no tensor force. This observable therefore gives us a fairly simple way to look at the small D-state component of the ground state of ^{4}He. The vector analyzing power $A_y(\theta)$ arises primarily as a result of interference of the predominant E2 radiation with other multipoles, probably E1 or M2 (or both). While A_y is rather large at low energies, calculations and the general trend of the tandem data suggest that it is small in an energy region above 15 MeV, see Figure 1.2. This suggests that the simplifying assumption of a pure E2 transition may be better in this higher energy region. Although the statistical uncertainty in the measurements at 20 to 50 MeV is large, the data proved to be in general agreement with this idea.

As the energy is increased, a region deeper into the nuclear wave-function is probed. The group of Santos, Eiró

and Arriaga have made calculations which show that the fractions of the capture amplitudes arising from the region within three Fermis are five to seven times larger at 50 MeV than at 10 MeV (see Table 1.3). This increased sensitivity to the region of small radius gives us a probe of the non-asymptotic part of the D-state wave-function. Probing the non-asymptotic part of the nucleus contains new information, but models are required to extract D-state information, as the asymptotic normalization is no longer an appropriate quantity to consider. Calculations from this same group show an increased sensitivity to the form of the wave-function at higher energies. Figure 1.3 shows this calculation of Ayy at 130 degrees, as a function of energy. The curves are for wave-functions generated from a Woods-Saxon potential, a variational calculation of the wave function from the Urbana group, and a microscopic Gaussian potential of their own construction. Note that the curves diverge at higher energy, motivating an interest in obtaining data in this region.

The cross section for the $^{2}H(\vec{d},\gamma)\ ^{4}He$ reaction is very small, and the data set for it is still rather sparse. The wealth of information that is available from studying this reaction was only first publicized in 1984 by Weller et. al., and it was pointed out how within the approximation that the reaction proceeds by an E2 transition, a non-zero tensor analyzing power implies a ^{4}He D-state component. Since that time an effort has been underway within Weller's research group at TUNL to make measurements from 400 keV to 15 MeV (Langenbrunner, 1988; Weller, 1986). The most complete data sets have however been measured at Wisconsin at 4 and 10 MeV (Mellema, 1986). These data sets were complete enough for a multipole decomposition to be made, and it was clear from them that E1 and M2 radiations contribute sig-

nificantly to the cross section at these lower energies. Subsequent measurements at TUNL revealed evidence for significant P-wave capture strength in the energy region E_d < 3 MeV, characterized by a peak in the magnitude of the vector analyzing power A_y = -.22 at E_d =1.2 MeV (Langenbrunner,1988) (Fig 1.2).

It has been suggested that the low energy region (E_d< 1 MeV) may be the best for the study of the D-state because the D-wave E2 capture to the S-state will be suppressed by the angular momentum barrier, thus enhancing the effects of the S-wave E2 capture going to the D-state. Besides the effects of non-E2 strength, the study of S-wave capture is complicated by the fact that the $\langle {}^1S_0 | E2 | {}^5S_2 \rangle$ capture amplitude involves the deuteron D-state, while the other S-wave amplitude, the $\langle {}^5D_0 | E2 | {}^5S_2 \rangle$ is known to be affected by strong distortions in the S-wave scattering state (labeled as $\langle {}^4He$ ground state component|Multipolarity|Initial State$\rangle$ and with notation $^{2S+1}L_J$). The very low energy region is therefore apparently not such a simple region for D-state studies as it may appear when the enhancement of S-wave capture to the D-state is first considered.

The only other polarization data that exists were taken at Indiana at E_d = 95 MeV(Pitts, 1988). These data show A_{yy} to be consistent with the large positive and fairly isotropic results observed at tandem energies, and A_y to be consistent with zero, as the trend of the tandem data suggested may occur at higher energy. This A_{yy} result is inconsistent with direct capture model calculations that have worked well at 10 MeV (Tostevin, 1986), but when extended to E_d = 95 MeV predict that A_{yy} should change signs. Cross section measurements at $E_d \cong$ 200 MeV from Bonn and

Saclay (Arends, 1976; Silverman, 1984) indicate an angular distribution more consistent with E1 than with E2 radiation. One could conclude that either the isospin selection rules, valid only in the long wavelength limit, are violated at high energy, or isoscalar spin-flip E1 transitions contribute significantly. The Indiana work may also be affected by the breakdown of the long wavelength approximation.

The tandem Van de Graaff work suffers from the rather strong P-wave strength at low energies making the data difficult to interpret, while cyclotron data have been at energies where long wavelength and asymptotic approximations are questionable. Before the work of this dissertation, the energy region 15 MeV < E_d < 95 MeV was unprobed, and some of the most interesting information may be contained here.

Table 1.3. Contributions From Different Regions; for Different Amplitudes and Energies.

(Calulations from Santos, Eiró and Arriaga)

	Inside 3 Fermis.	Outside 3 Fermis	% of total X-section	% of Capt to D-state
S-wave capture to the D-state:				
10 MeV	9%	91%	1.8%	50%
50 MeV	67%	33%	2.7%	23%
D-wave capture to the D-state:				
10 MeV	14%	86%	1.8%	50%
50 MeV	69%	49%	3.8%	33%
G-wave capture to the D-state:				
10 MeV	1.3%	99%	0.01%	.03%
50 MeV	7.7%	92%	5%	43%

Figure 1.2. A_y ($\vartheta\gamma$= 130 degrees) as a function of energy. It can be seen that the general trend is for the magnitude of this observable to diminish as energy is increased. This may indicate that the approximation that the $^2H(\vec{d},\gamma)^4He$ reaction goes by an E2 transition is better at energies greater than ~30 MeV.

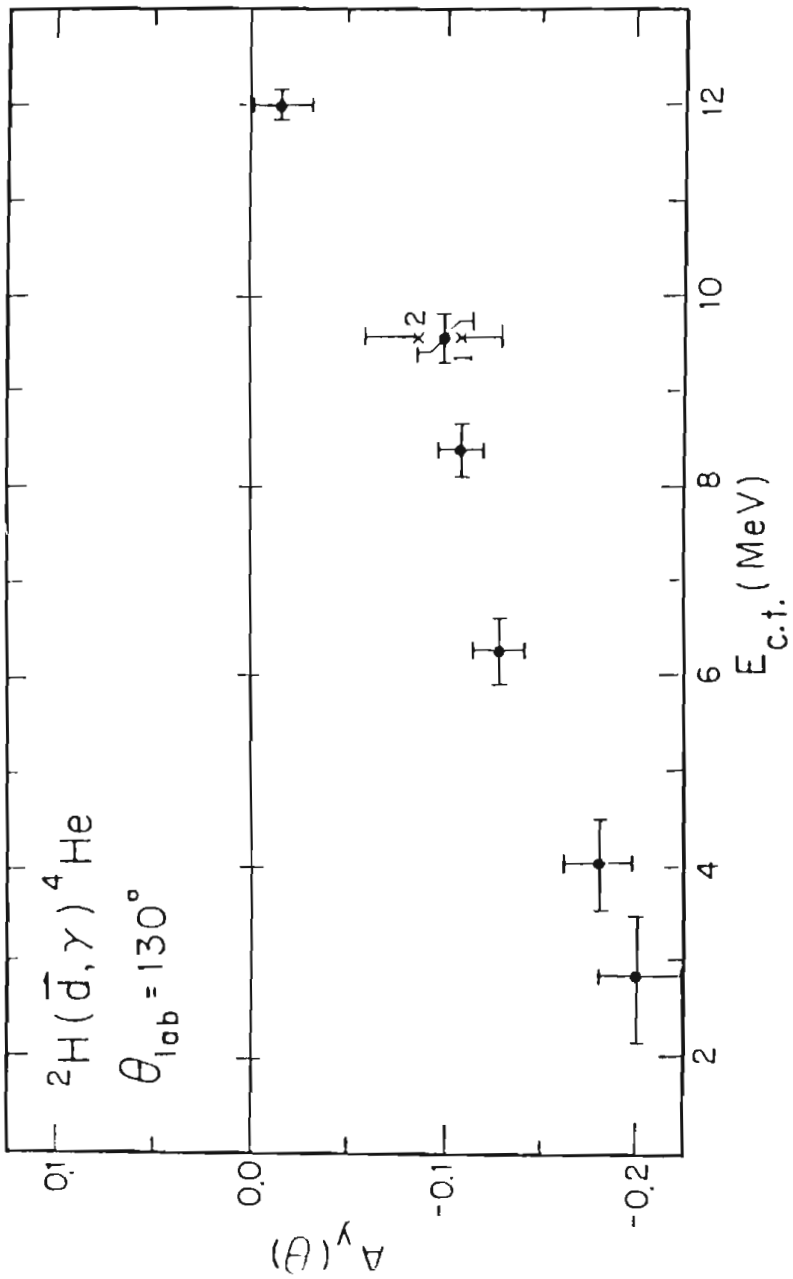
$^2H(\vec{d},\gamma)^4He$
$\theta_{lab} = 130°$
$A_y(\theta)$
$E_{c.t.}$ (MeV)
0.1
0.0
-0.1
-0.2
2
4
6
8
10
12
x2
x1

Figure 1.3. A_{yy} ($\vartheta\gamma$= 130 degrees) as a function of energy. The curves are from the Lisbon group of Santos Eiró and Arriaga, using several different forms of the ground state wave-function. They are derived from a Wood-Saxon potential, the Urbana potential of Pandharipande et. al., and a microscopic Gaussian potential of their own construction. This figure demonstrates both the large magnitude of this observable and the sensitivity of the potential model calculations to the form of the wave-function used in this energy region.

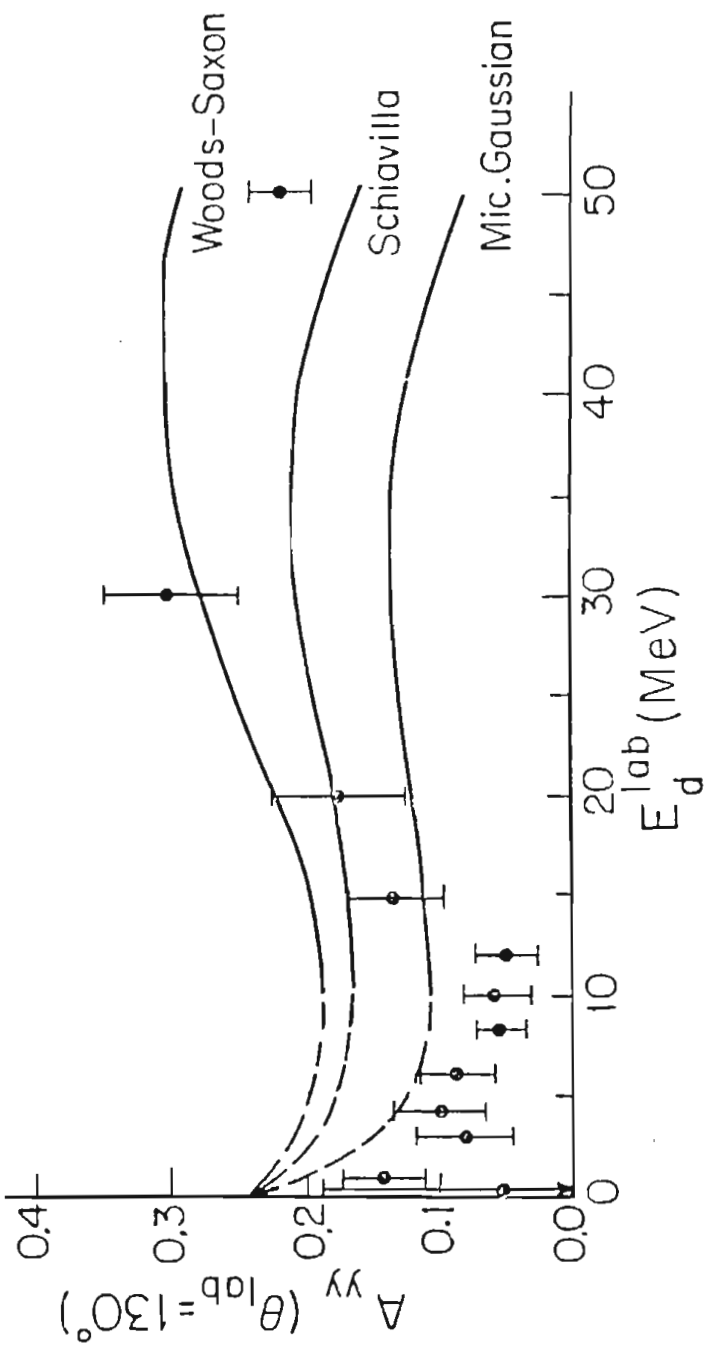
Woods-Saxon
Schiavilla
Mic.Gaussian
A_{yy} (θ_{lab}=130°)
E_d^{lab} (MeV)
0.0
0.1
0.2
0.3
0.4
0
10
20
30
40
50

2. Experimental Equipment and Techniques

2.1. History of the Project.

The development of the radiative capture program at the Lawrence Berkeley Laboratory began when in August 1985 the first of two large sodium-iodide spectrometers was moved to the eighty eight inch cyclotron laboratory. During that month, the spectrometer was carefully tested and the beam-line was designed along with the goneometer to position the gamma-ray spectrometer.

At that stage, the beam-line included only a small chamber with a good beam dump in the hillside. A liquid nitrogen cooled gas cell target similar to the ones used in refs.(Weller, et. al., 1984)) was built at TUNL. This target was used in a test run in November '85, at which time it was verified that the $^{2}H(d,\gamma)^{4}He$ reaction could be studied at higher energies than are available at the TUNL tandem. It was also discovered that the beam geometry at the cyclotron would require a larger target cell, and the time structure of the beam wasn't adequate for clean neutron gamma separation with reasonable flight paths between the target and the spectrometer. This was a hint at the extensive development of timing techniques that would be required to complete this study.

The following spring was spent at Kernfysisch Versneller Instituut (KVI), in Groningen, the Netherlands. While at that laboratory, development continued in our ability to do this experiment. An attempt was made in April '86 to measure the angular distribution of the cross section at 30 MeV beam energy. During this run a deuterated polyethylene target was used. The total thickness was about 11 mg/cm^2, so the thickness of deuterium was about 3 mg/cm^2.

This target produced much nicer spectra than the gas cell that we had tested at Berkeley the previous fall. The quality of these data was still marginal, mainly because of poor statistics caused by the thin target. An additional problem in the use of the polyethylene target was the monitoring of its thickness, as it tended to be burned away by the beam. The relatively thick surface barrier detectors tended to be unreliable and the angle from which they effectively saw the target would change with beam position. Since the scattering cross section is angle dependent, motion of the beam made the monitors unreliable during this first run at KVI.

Upon returning to the United States in the summer of '86, the group was joined by the very able NATO fellow, Dr. Sebastian Kuhn, formerly from The Bonn University, and by Drs. Evans Hayward and W.R. Dodge of the National Bureau of Standards. The group at Bonn has had a long history of collaboration with the polarization program at Berkeley, and though the ion source there was not actively being used, Dr. Kuhn was able to rehabilitate it in short order. The NBS collaborators contributed a second ten inch shielded NaI spectrometer.

In August, we undertook to measure the tensor analyzing power A_{yy}, and the vector analyzing power A_y at the beam energy of 20 MeV. We used a deuterated polyethylene target, similar to the one used at KVI. The monitoring of the beam and target thickness was not a problem for this measurement because it wasn't necessary to measure any absolute yields, only relative yields between polarization states. Polarization states were changed on a time scale of one second, averaging out any effect of a slow degrada-

tion of the target. The problem of poor counting statistics persisted, however.

Having successfully made some measurements, and having assembled a sophisticated beam-line, a large collaboration and a bit of experience, we began to think about working up to 50 MeV (the limit of the switching magnet in our beam-line). In November of 1986 the group met at TUNL and plans were laid to further develop the setup into one in which the recoiling ^{4}He nuclei could be detected in coincidence with the gamma rays. This technique promised to unambiguously identify radiative capture events even though the gamma rays could not be separated from other radiation coming from the target. This was a large project which required resources at TUNL, NBS, and LBL. Instrument makers at all three laboratories completed the project in time to test it during a run which was scheduled for March of 1987.

At TUNL, two test runs of around four days each were devoted to the study of the charged particle detectors, and the extremely high count rates that would be encountered in this experiment. Parallel plate avalanche counters were tested, but it was determined that thin fast plastic scintillators were more reliable and easier to use.

The changes that were made that winter also included a major rethinking of the target. It was decided that there were significant advantages to a liquid nitrogen cooled gas cell, but this time a much larger one with large openings and Kapton windows would be tried (see section 2.4.d). This assembly was built at the NBS instrument shop. A large extension to the scattering chamber had to be built in order to provide a flight path for the recoiling 4He nuclei. This was built at one of the LBL

shops. At TUNL we concentrated on the particle detectors, along with the apparatus to position them. The whole system was assembled in March just prior to the difficult but successful test run during which A_y and A_{yy} were measured in singles and in coincidence at 30 MeV.

Based on what was learned during the March '87 run, the alpha recoil detectors were changed in shape and size, but nothing else had to be modified to take data at 50 MeV. Ay and Ayy were measured in June.

In August of that same summer we (HW, EH, and RMW) returned to KVI for another run there. It had been agreed at the time of our previous stay at that laboratory that we would be given more beam time at some point when they weren't plagued by the accelerator problems of the spring of '86. The 88 inch cyclotron at Berkeley is highly subscribed, and the time at KVI was very much appreciated. A liquid nitrogen cooled gas target similar to the one that we were by then using at Berkeley was built at TUNL and sent to KVI. In early September of 1987 a careful measurement of the angular distribution of the cross section was made at 30 MeV. Because of the symmetry of the projectile and the target, the differential cross section must be symmetric about ninety degrees with respect to the center of mass reference frame. This removed the need to measure at forward angles where the background radiation is worse and hence removed the need of recoil detection.

Around that same time, a solenoid to precess the spin axis was being installed in our beam-line at Berkeley. This made it possible for the tensor analyzing power A_{zz} to be measured in January 1988. A portion of a run mostly devoted to a different experiment was used to clarify an ambiguity in the data in May of 1988.

Slightly less than three years were spent from the time that the first NaI spectrometer was moved to the 88 inch cyclotron, to the time that this experiment is considered more or less complete, at least for now. Much was learned in this endeavor, from experimental technique to the nature of the ^{4}He nucleus. Notably, the gas target proved to be a key ingredient both in obtaining quality spectra and reasonable statistics. The modern 300 MHz electronics from the Phillips Instrument Co. were crucial to the fast timing in the recoil detection system. It was found that working in the user mode at highly subscribed laboratories produced an environment where a short test run was needed to assure that the setup was completely debugged. Most runs were around five days long, preceded by a setup run of about 24 hours in length. It was usually scheduled with the two runs situated around a weekend or other shutdown, so that interfacing electronics, etc., would not need to be disturbed by other experimenters.

The analyzing powers that were observed at these higher energies were large, at some angles they were on the order of 40 percent of the maximum allowed values for these observables. Since these polarization observables are related to small components in the 4He wave-function, and to small admixtures of multipolarities, they are a useful window providing access to the more subtle aspects of this nucleus and the dynamics of the $^2H(\vec{d},\gamma)^4He$ reaction.

2.2. The Experimental setup at KVI

The unpolarized angular distribution of the cross section at 30 MeV was measured at the variable energy AVF cyclotron of the Kernfysisch Versneller Instituut (KVI) at

Groningen. The deuteron beam was produced internally and transported to the experimental hall marked "D" in Figure 2.1. The NaI spectrometer shown in the figure was freely moved around on air-pads. For this experiment it was positioned to view the small chamber just inside experimental hall "D". The beam was then dumped onto a carbon block just before the magnetic spectrograph. This beam dump was built up for the purpose of this experiment, and was highly shielded with lead, concrete, and paraffin. The target chamber was built of thin walled aluminum and housed a liquid nitrogen cooled gas cell which was also thin walled aluminum, three inches in diameter with three quarter inch diameter windows for the beam to enter and exit. The windows were covered with one mil Kapton. In addition to the beam windows, there was a small window at thirty degrees from the beam axis for a solid state detector to view a small region of the interior of the target. This window was $^{1}/_{16}$ inch wide and $^{3}/_{4}$ inch tall, and was also covered by Kapton. This produced a double collimated slit geometry where the detector viewed a region within the target through which all the beam had to pass. The angle from which this "monitor detector" viewed the target was thereby made independent of the exact position of the beam. The monitors in a previous run at KVI using a solid target had proven unreliable because of changes in the beam position, hence monitor angle. The slit collimated gas cell arrangement eliminated this problem, while providing a thicker target with a higher ratio of deuterium to other elements. This cell was pressurized to four atmospheres, for a thickness of 40 $^{mg}/_{cm^2}$ D_2, and a Kapton window thickness of 11 $^{mg}/_{cm^2}$.

A discriminator on the gamma-ray energy defined events. For each event, gamma-ray energy, time relative to the cy-

clotron RF, and a shield coincidence bit were written to tape. The events were sorted at KVI, and the spectrum tables that were produced were sent to TUNL via the academic computer network Bitnet.

Figure 2.1. The layout of KVI; (the Kernfysisch Versneller Instituut) at Groningen.The NaI spectrometer was set up facing the small chamber in Hall "D". It is represented by the small black square in this figure. The beam was dumped on a carbon block at the entrance to the spectrograph. This beam dump was built up for the purpose of this experiment, and was highly shielded with lead, concrete, and paraffin. The target chamber was built of thin walled aluminum and housed a liquid nitrogen cooled gas cell which was also thin walled aluminum.

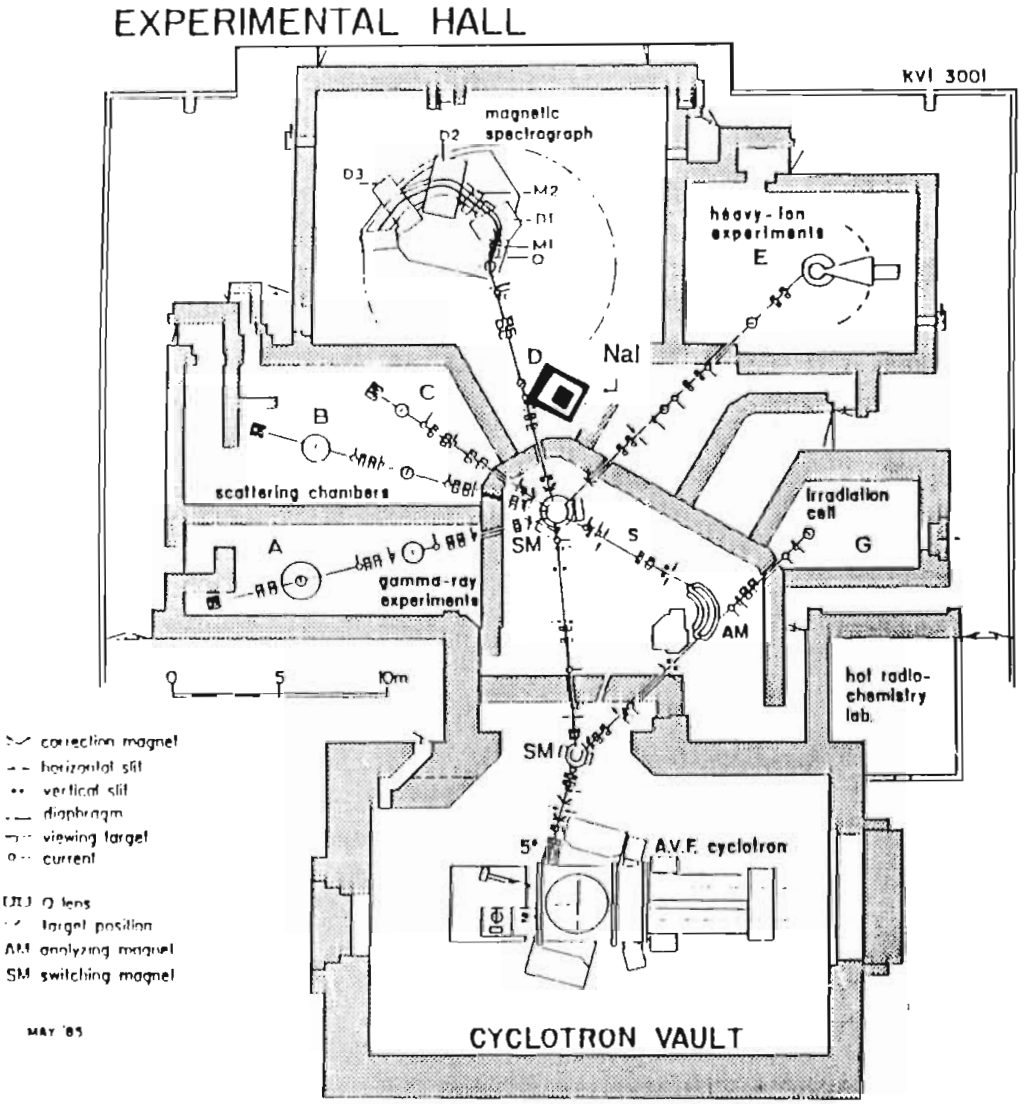

Figure 3.1 Layout of the cyclotron vault and the experimental hall at the KVI.

2.3. The Setup at LBL

2.3.a. Overview

The radiative capture setup in cave 4C at the 88-inch Cyclotron was first begun in the summer of 1985, and has been developed primarily with the $^{2}H(\vec{d},\gamma)^{4}He$ experiment in mind. Although development evolved continuously, most of what will be described applies to all of the data taken there for this experiment.

The important ingredients in this setup included two NaI spectrometers with active and passive shielding, gain stabilization and anti-pileup circuitry. The active shielding consisted of five inches of fast plastic scintillator surrounding the NaI crystals and viewed by an array of photomultiplier tubes. This was surrounded by lead shielding three to five inches thick. Outside of the lead was eight to twenty inches of neutron shielding consisting primarily of 1500 boric acid bricks, but also included ^{6}Li hydride, lithium carbonate, concrete, and water in various configurations depending on the run. Good neutron shielding is vital in almost any experiment involving either a deuteron beam or target.

Every effort was made to provide a well shielded, background free beam dump. The beam dump consisted of a carbon block at the end of an eight inch pipe buried about eight feet back into the hillside. This provided a very low target out count rate.

The runs at 50 MeV required detection of the recoiling 4He nuclei. For these runs a large extension had to be added to the scattering chamber to provide a flight path for these particles, see Figure 2.2. This was a wedge

shaped box that could be evacuated or let up to air independently from the chamber that contained the liquid nitrogen cooled gas target cell. This was necessary because of the difficulty that would be involved in warming up the target in order to gain access to the 4He detectors. Retractable apertures and viewers at the target position and recoil detection plane were used extensively to optimize the tuning of the beam.

Figure 2.2. Details of the Berkeley setupincluding shielding, and the time of flight chamber for the recoiling ^{4}He nuclei.

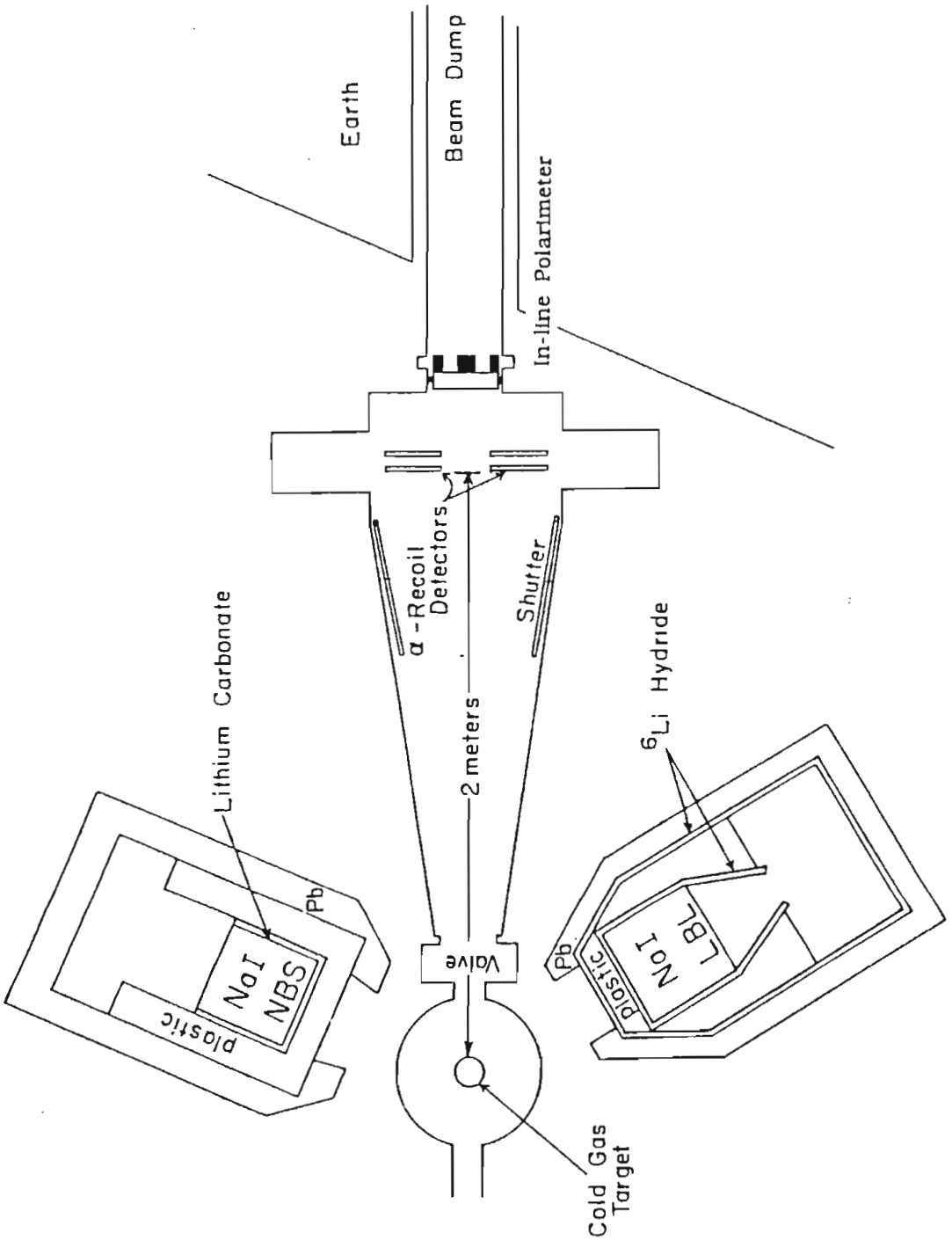
Earth
Beam Dump
In-line Polarimeter
α-Recoil Detectors
Shutter
2 meters
Lithium Carbonate
Pb
NaI
NBS
plastic
Valve
^{6}Li Hydride
Pb
plastic
NaI
LBL
Cold Gas Target

2.3.b. The Polarized Ion Source at Berkeley

The polarized deuteron beam at the 88 inch cyclotron (Clark, 1971) was produced using the atomic beam method (Glavish, 1970). This technique involves separation of hyperfine states in a neutral atomic beam, followed by induced transitions between populated and unpopulated states, before ionization and injection into the cyclotron.

Hydrogen atoms are formed in a dissociator tube by a radio frequency discharge. They then pass through a region of inhomogeneous magnetic field produced by a six pole magnet. The atoms tend to move towards the region of lowest potential energy, so that those with magnetic moment opposite to the field ($m_j = +1/2$) are driven toward the region of weaker magnetic field near the axis of the magnet while atoms in the $m_j = -1/2$ states are deflected away from the axis and are removed from the beam. This is similar to the familiar Stern-Gerlach experiment.

The atomic beam, containing only states 1, 2, and 3, of the original six hyperfine substates, then passes into a region of radio frequency transitions. The method of inducing the transitions is known as the adiabatic passage method, and was originally proposed by Abragam and Winter (1958). The Berkeley source employs three regions for inducing RF transitions; a so called weak field and two so called intermediate field regions. The radio frequency oscillators driving these regions are turned on and off in various combinations to achieve the desired exchanges in populations to produce different states of polarization in the beam. This method of changing states has the advantage that polarization changes are brought about by radio fre-

quency oscillations acting on a neutral atomic beam. Changing the polarization state therefore has no chance of changing the beam current or position on the target.

All the transition regions employ a static magnetic field to split the hyperfine states (see Figure 2.3). The weak field transition operates where the total angular momentum F is a good quantum number, and substates 1 through 4 are equally spaced. The rf corresponds to the energy difference between neighboring m_f components, and has the effect of interchanging the m_f and $-m_f$ populations through a multilevel transition. The mixture of states 1, 2, and 3, that were left after the separation magnet, becomes 4, 3, and 2. Operation of this transition alone would produce a beam with a pure vector polarization after ionization in a strong field ($P_z = -2/3$, $P_{zz} = 0$).

The intermediate field transitions are used to produce tensor polarization and to change the sign of the vector polarization. They operate with a magnetic field strong enough that F is no longer a good quantum number. Two such regions are employed, one exchanges the population of state 3 with the unpopulated state 5, the other exchanges state 3 with the empty state 6. These populations are not pure in nature, and the polarization produced by various combinations of transitions employed by the Berkeley ion source are any combination of p_z = +/- 2/3, and p_{zz} = +/- 1. A source that can select pure states can have maximum polarizations p_z = +/- 1, p_{zz} = 1,-2. The new atomic beam source being installed at TUNL is such a source by virtue of its second sextupole separation magnet after an intermediate field transition.

After the appropriate selection of substates and exchange of populations, the beam is ionized by electron

bombardment in a strong solenoidal magnetic field. The ionizer employed now is an upgrade from the original, and is described in detail in (Glavish, 1970). The ionization of deuterium gas that is not part of the atomic beam is the primary source of unpolarized background, pumping efficiency is therefore essential. Typical polarization of the beam was 70 to 80 percent of the maximum physically allowed value.

Tuning the source parameters requires acceleration of the beam to a polarimeter. The polarimeters are described in Section 2.3. The valid counts in the various detectors in the polarimeter are counted, and the scaler outputs are interfaced to the online data acquisition computer. A program is executed to calculate the beam polarization, and the result goes to an output register to be read on a remote meter at the source. In this way the tuning of the ion source can be optimized.

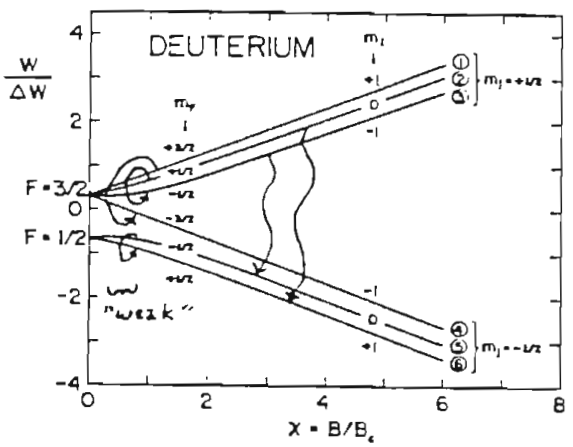

Configuration of Rf-transitions

2 → 6	3 → 5	weak-field	$\tilde{t}_{10}$	$\tilde{t}_{20}$
off	off	off	0	0
off	on	on	$-1/\sqrt{6}$	$+1/\sqrt{2}$
off	on	off	$+1/\sqrt{6}$	$-1/\sqrt{2}$
on	on	off	$+\sqrt{2}/3$	0
off	off	on	$-\sqrt{2}/3$	0

Figure 2.3. The hyperfine splitting in deuterium. The arrows indicate the radio-frequency transitions used to produce the desired polarizations.

2.3.c. The Solenoid

The tensor analyzing power A_{zz} at 50 MeV was measured early in 1988. As mentioned in Section 1.4, the simple model calculations that have done well to fit the A_{yy} data have failed to fit A_{zz} at tandem energies. The effects of S-wave capture have often been taken to be the cause. The usual explanation of the failure of the model to fit A_{zz} is that the S-wave scattering state is highly distorted. The D-state of the deuteron can also play a stronger role in S-wave capture (see Section 1.4). S-wave capture to the D-state of ^{4}He contributes in first order to A_{zz} but not to A_{yy}. This higher energy region was probed in hope of unraveling these effects. It is interesting to note that the most recent calculations which are described in Section 4.2.a. are also least successful at predicting A_{zz}.

The measurement of A_{zz} required that the spin axis not be perpendicular to the scattering plane, as it is when measuring A_{yy}, and as defined by the magnetic field of the cyclotron. A large solenoid was installed in the capture beam-line at Berkeley for the purpose of precessing the spin axis about the beam axis in order to measure A_{zz} (see Figure 1.1). This device consisted of a coil with 1096 turns and was 2.36 meters long. It was driven with a current of 1000 Amperes, for an internal field of 5.5 kG, and an integrated field of 13.1 kG-meters. A special beam dump polarimeter was built to verify the angle of precession, and the measured and calculated values for this were in agreement.

2.3.d. Polarimeters

Two polarimeters were used in this work. One utilized elastic scattering of deuterium from ^{4}He, and the other one used elastic scattering off of ^{12}C. The 4He polarimeter was taken from another beam line at the 88- inch cyclotron, and installed in the new capture leg at the beginning of our project. This position a few meters upstream from our chamber was convenient in that there was little retuning of the beam between measuring the polarization and taking data. When the spin precession solenoid was also moved to the radiative capture leg, this polarimeter had to be moved to the next beam leg over because of space considerations. There was still relatively little retuning required to measure the polarization. The polarization was measured every eight to twelve hours with this device.

The ^{4}He polarimeter consisted of a gas cell with Havar windows, viewed by two E-ΔE type charged particle telescopes. The telescopes were free to rotate to angles where previous measurements of the analyzing power were available. The thickness of the detectors was chosen such that most reaction products did not pass through the first plane. Typically a slow coincidence requirement between the two planes of a telescope was all that was required to produce a clean sum peak. This peak was simply counted in a single channel analyzer to measure the polarization.

When the spin precession solenoid was installed in our leg, the second polarimeter was built and installed in the beam dump, just downstream of the particle detectors. The target for this polarimeter was a carbon foil that was left in the beam at all times. This arrangement was intended to provide full time monitoring of the polarization, but this

turned out to be impossible because there was no set of beam tuning parameters compatible with both the polarimeter and the experiment itself. This device was similar to the 4He polarimeter except that the detector angle was fixed, and it included a second pair of telescopes in the vertical plane. With detectors in two scattering planes the precession of the symmetry axis of polarization could be measured. The calculated and measured values were in agreement.

There was not as much data available for the ^{12}C analyzer as for the ^{4}He, and the angles for this device were fixed, so it wasn't optimal to use it for the overall determination of the polarization. The polarization was always measured in the ^{4}He polarimeter as well.

2.3.e. NaI Spectrometers

The primary tool in this and most other studies of radiative capture is the large shielded sodium iodide spectrometer (Paul,1974). The commonly used alternatives are lithium drifted germanium with ultra-high resolution, or lead glass which detects gamma rays via Cherenkov radiation from the e^+, e^- pairs and hence is insensitive to neutrons except via nuclear reactions. These types of detectors would not have been as useful as the NaI used in this work, because of the low efficiency of GeLi, or poor energy resolution of Pb Glass. Three different NaI spectrometers were used in taking these data, one at KVI, and two at Berkeley (two more were used extensively at TUNL in preparation and testing). The specific details of each of these units differ slightly due to their time of manufacture and subsequent history. In this description, the minor differences will be overlooked but the aspects that are common to all three spectrometers and the most important differences will be discussed. One of the detectors is described minute detail in (Dietrich,1978)

The capture gamma rays in this energy region (35 to 50 MeV) interact with the NaI crystal primarily through the process of pair production, in which an electron-positron pair is created. These are charged particles, and they radiate away their energy primarily through bremsstrahlung and atomic ionization. The NaI is uniformly doped with thallium iodide, a compound that is present at the level of around a quarter of a percent to shift the wavelength of the radiation down into the optical region. The crystal is more transparent there (less self absorption), and the efficiency of the photomultiplier tubes peaks in the upper end of the visible spectrum. When the positron has slowed

to a low energy, the annihilation cross-section becomes significant. The positron and an electron annihilate to produce a pair of 0.511 MeV gamma rays with roughly opposite momentum. One or both of these may escape the crystal undetected.

Anti-coincidence shields of fast plastic scintillator surrounded the NaI crystals, and typically could be used to reject around 99% of the events produced by cosmic radiation passing through the NaI crystals and shields. The cosmic ray background count rate was greater than the radiative capture gamma ray count rate, and could obscure the peak of interest. While these spectrometers have a high intrinsic efficiency for the gamma rays that were produced in this reaction, the anti-coincidence requirement also rejects a large fraction of the gamma ray events due to escaping radiation being detected in the shield. While this sharpens the resolution of the system by throwing away gamma rays that don't deposit all their energy in the crystal, it reduces the efficiency and introduces uncertainty in measuring absolute yields.

Four or more inches of lead shielding surrounded the detectors for the purpose of excluding radiation that does not come from the region of the target. This shielding was open in front to allow the full crystal to be illuminated by the gamma rays coming from the target. The lead shielding was surrounded by six or more inches of neutron shielding that included lithium carbonate, lithium hydride, paraffin, boron loaded water, polyethylene, and concrete in various combinations and configurations, depending upon the circumstances of the measurement. This type of shielding also covered the fronts of the spectrometers attenuating another large fraction of the gamma rays

of interest. The uncertainty of this attenuation factor for the various configurations used is the main source of uncertainty in measuring the gamma ray yields. It should be noted that this only affects the analyzing power measurements through the reduction of the counting statistics.

Since NaI is hygroscopic, it must be housed in a hermetically sealed container with transparent windows for the photomultiplier tubes to view the interior of the crystal. All blind surfaces of the NaI crystal are coated to reflect light back into the detector, and these surfaces are compensated in such a way that the light being reflected from all regions produces the most uniform response in the photomultipliers possible. The techniques for manufacturing uniform crystals and the methods of surface compensation have been improved through the years, hence the differences in the resolution of the three spectrometers used in this study.

All three NaI crystals were ten inches in diameter. The two used at Berkeley were ten inches deep, while the KVI spectrometer was twelve inches deep. The KVI spectrometer was the newest, just being completed in 1985, and exhibited the best resolution. This crystal was manufactured by Harshaw of the Netherlands, and had an intrinsic resolution of around two percent for gamma rays in the 35 to 50 MeV region. The two spectrometers that were installed at Berkeley for this experiment were somewhat older, both having been previously at other laboratories that were no longer actively using them for nuclear physics. One was brought from Livermore National Laboratory and could be described as a first generation large NaI spectrometer having only one nine inch photomultiplier tube, and a res-

olution of about nine percent at 4.4 MeV, and about five percent at the energies of this study. The detector that was moved from the National Bureau of Standards was a more modern one, built by Bicron Co. of Ohio, and had performance intermediate between the two just described. This spectrometer was modified to include an LED light source for gain stabilization, while the other two had been built with this capability. While the resolution of the oldest crystal would make it impossible to distinguish closely spaced transitions, it was adequate for the purposes of this experiment, owing to the lack of excited states in ^{4}He.

2.4. The Coincidence Technique

2.4.a. Overview

Because of the large Q-value of this reaction, it is relatively easy to obtain quality data at energies that are available at the tandem accelerator laboratories where most of the previous work has been done. It is easy to see that this advantage is lost as the energy is increased. The energy of the capture gamma ray is roughly equal to the center of mass (COM) energy, plus the Q-value, since the gamma, and hence also the alpha, don't carry much momentum in this frame. Because the target and projectile are the same in this case, the COM energy is just half the beam energy. As the energy is increased the difference between the COM energy plus the Q-value becomes smaller compared to the beam energy (e.g. at a beam energy of 50 MeV, the gamma ray that is produced is actually at a slightly lower energy than the beam. It is therefore possible to have much beam induced background in the same region of

the spectrum, but with a 10 MeV beam, the gamma ray is near thirty MeV, usually a clean region of the spectrum because it is difficult to produce any other radiation at three times the beam energy). At tandem Van de Graaff energies the use of heavy materials has some advantage because of the Coulomb barrier. Metal foils used there as target windows produce little significant gamma ray background. At the higher energies of this work this advantage is also lost, and gamma rays emanating from the target windows must be somehow separated from the events of interest.

Overcoming the problems with background radiation at 50 MeV beam energy necessitated detecting the recoiling ^{4}He nuclei in coincidence with the gamma rays in order to unambiguously identify the $^2H(\vec{d},\gamma)^4He$ events. Requiring the appropriate timing and particle information in sorting the sodium iodide spectrometer events produced very clean gamma ray spectra.

2.4.b. The Use of Time-Of-Flight

The difficulty associated with the necessity of detecting the gamma rays in coincidence with the recoiling 4He nuclei lies in the fact that the recoils aren't cleanly separated from the beam. The component of the momentum carried by the gamma ray perpendicular to the beam axis is sufficient to separate the trajectory of the recoils from the beam by from three to seven degrees, depending on the angle of the gamma ray. Unfortunately, for a reasonable target thickness and a detector geometry that doesn't limit solid angle, the rate of scattered deuterons in this forward angle region is around ten MHz. The solution was

to separate the alphas from the deuterons by time of flight. This doesn't effect the high rate of deuterons, which is essentially one per beam burst, but with sufficiently fast electronics, it was possible to ignore the deuterons and wait for the ^{4}He nuclei, as they were slower, and thus arrived at the detection plane later.

For a variety of reasons including space and cost considerations, a flight path of two meters was chosen. It was of course necessary to build an extension to the vacuum chamber to accommodate this flight path, as these are charged particles, see Figure 2.2 for a diagram. The two meter flight path separated the ^{4}He recoil from the deuteron flash by twenty nanoseconds or more, depending on energy and angle. See Figure 2.4 for a time of flight spectrum.

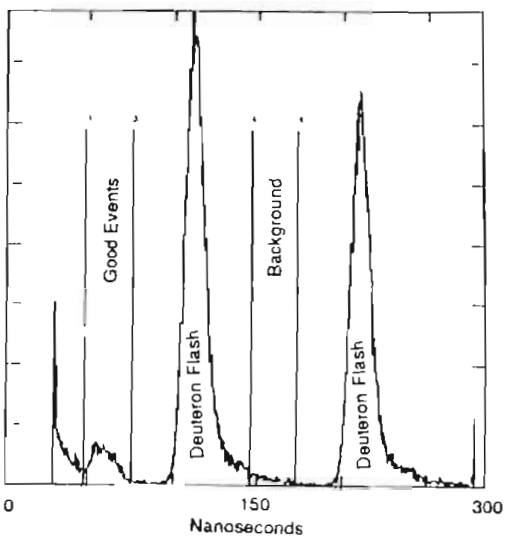

Figure 2.4. Particle Time of Flight Spectrum. The recoiling ^{4}He nuclei are clearly separated from the periodic deuteron flashes associated with the beam bursts.

2.4.c. Target Design Considerations

Because the differential cross section for this reaction is on the order of ten nanobarns per steradian, it is important to have the thickest target that is practical, taking certain other factors into consideration. Clearly the areal density of the deuterium for a given window thickness, and hence pressure, scales linearly with the geometric length of the cell. The limiting factors on cell dimensions are the angular averaging of the observables, and the smearing out of the charged particle time of flight spectrum; after all, the length of the cell is the uncertainty in the flight path. The cell was built in the shape of a cylindrical can four inches in diameter, with a vertical axis of symmetry. Taking into consideration a quarter to a half inch bulge for each window, the target was about 4.5 to 5 inches in length along the beam axis.

This length increases the angular averaging of the ten inch NaI spectrometers by roughly 25%, depending on the angle. The angular averaging due to the large spectrometers and the extended target was estimated using the method of the attenuation coefficients (Q_k) (Rose, 1953) and by a Monte Carlo method (see Section 3.4.). The uncertainty in the flight path is the effect that would account for the width of the recoil alpha peak in the time of flight spectra if there were no other smearing due to effects such as energy loss. Since the background included in the gate is proportional to the width of the gate, it was important to minimize the width of the TOF peak. The width due to target geometry was unimportant compared to that due to energy loss of the alphas in the target.

The widening due to these effects is the cause of the roughly rectangular shape of the peak in the TOF spectrum. The sloping top of this distribution is due to a combination of effects; particles having the greatest flight path also endure the most energy loss. This distorts the rectangular distribution into something of a rhombus. The TOF spectrum was simulated using the Monte Carlo procedure described in Section 2.4.e. The simulated spectrum is shown along with an actual one in Figure 2.5, and it can be seen that the shape of the recoil spectrum is well understood. The energy loss of the recoiling ^4He nuclei was the limiting factor in the target thickness.

In order to maximize the ratio of target deuterium to foil window thickness, the whole cell was kept at liquid nitrogen temperature. This improves this ratio by a factor of around three. Because the tuning of the beam was critical to the quality of these data, the target dewar assembly was built suspended from a bellows in such a way that it could be raised out of the beam without breaking the vacuum or warming the target above the liquid nitrogen temperature. A variety of apertures and a viewer for beam diagnostics were suspended below the target. (See Figure 2.6).

The foil window thickness and target pressure were determined by the energy loss of the alphas. Most of the data were taken with one mil Kapton windows and a pressure of three atmospheres, for a thickness of 40 $^{mg}/_{cm^2}$ D_2, and 11 $^{mg}/_{cm^2}$ Kapton. Some data were taken with twice these thicknesses, but they were more difficult to analyze due to the broadening of the time of flight peak, and some of these were retaken in the original configuration.

Figure 2.5. The Monte Carlo simulated particle time of flight spectrum (bottom), along with an actual one. The sloping top of this distribution is due to a combination of effects, where particles having the greatest flight path also endure the most energy loss, distorting the rectangular distribution into something of a rhombus. It can be seen that the shape of the recoil spectrum is well understood.

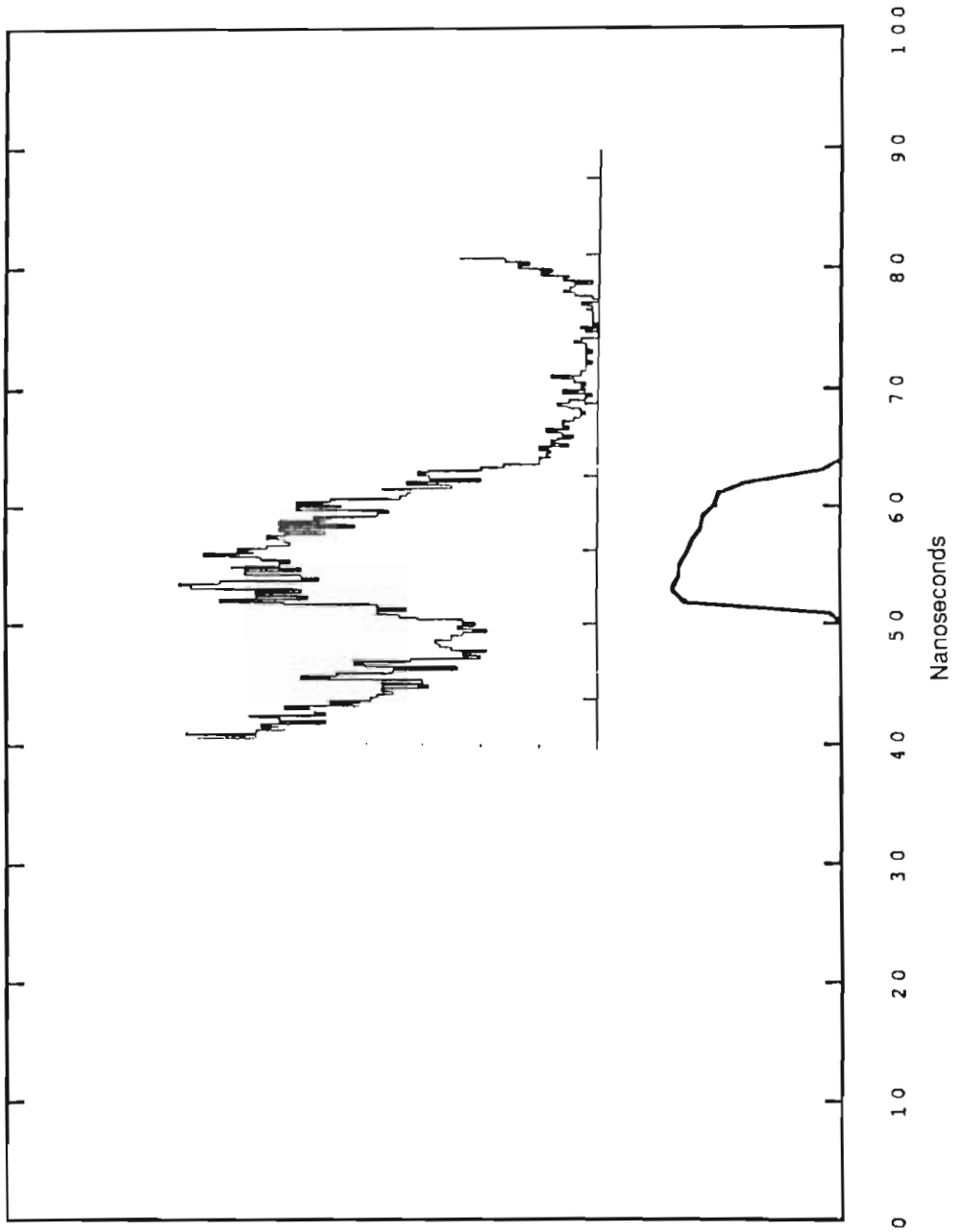
0
10
20
30
40
50
60
70
80
90
100
Nanoseconds

Figure 2.6. Details of the target assembly which consisted of a liquid nitrogen cooled gas cell 4 inches in diameter with 1 or 2 mil Kapton windows. Viewers and apertures for beam diagnostics were attached to the bottom of the cell for beam diagnostics. These could be positioned in the beam without breaking the vacuum. This assembly was built at the National Bureau of Standards, now called the National Institute of Science and Technology.

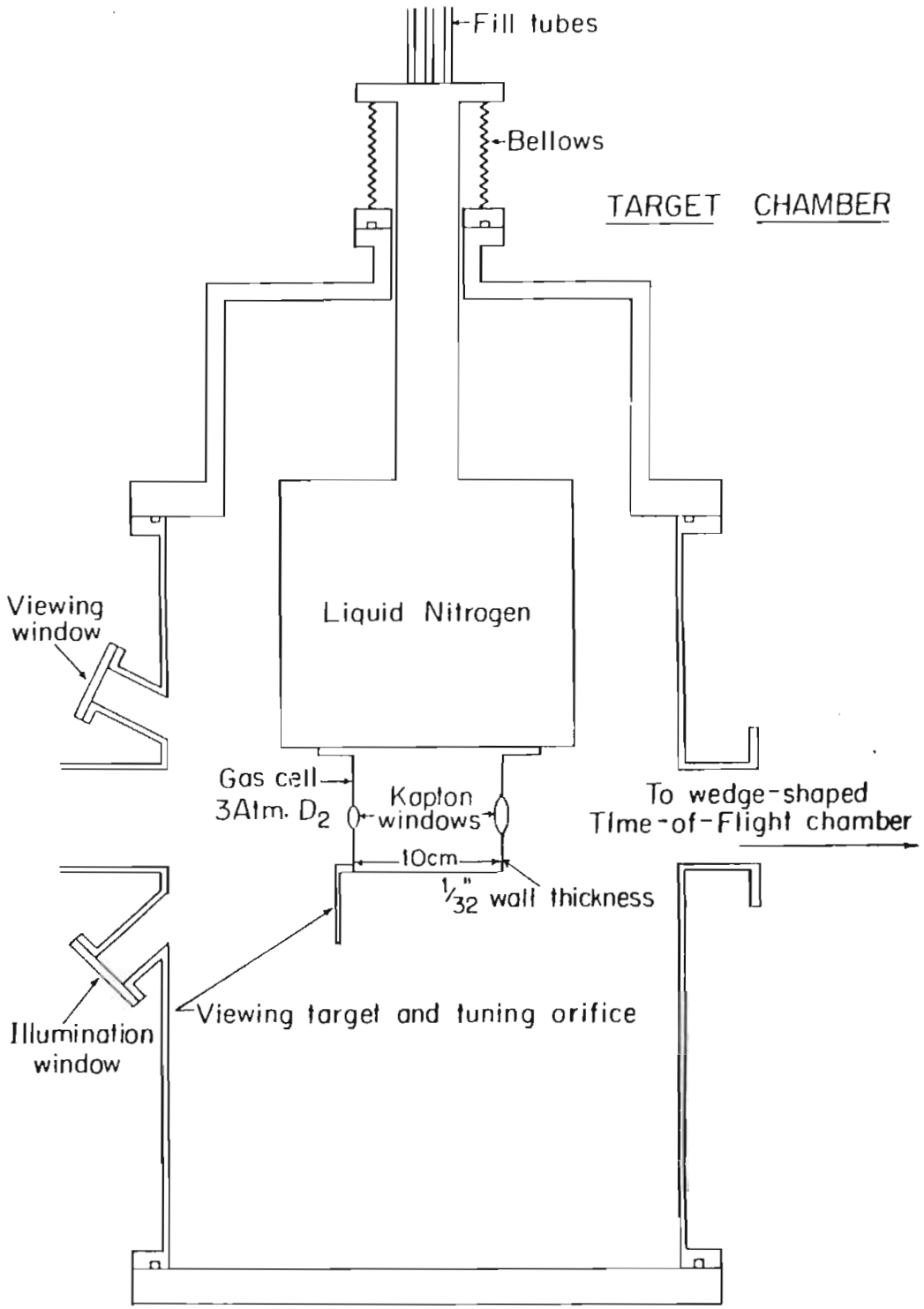
Fill tubes
Bellows
TARGET CHAMBER
Liquid Nitrogen
Viewing window
Gas cell
3Atm. D_2
Kapton windows
10cm
$\frac{1}{32}$" wall thickness
To wedge-shaped Time-of-Flight chamber
Viewing target and tuning orifice
Illumination window

2.4.d. The Particle Detectors

The ^{4}He recoil detectors themselves were planes of BC418 plastic scintillator. This particular type was chosen because it had the fastest time response without much sacrifice of light output or attenuation length. It was desired to have the best possible energy resolution for the recoils, while at the same time we wanted to minimize the light loading in the photomultiplier tubes due to the high count rate arising from deuterons hitting these detectors. The thickness was therefore chosen to be the minimum required to stop the 4He nuclei of interest.

Two identical planes were used on both sides of the beam, the rear plane used as a fast veto for the deuterons, which passed through both, depositing only around 20 percent of their energy. The fast veto was used to reduce the rate of signal processing in some of the slower components of the electronics.

It was desirable to minimize the area of the recoil detectors in order to minimize the count rate of scattered deuterons. The overall dimensions were chosen to catch all the alpha particles for the configuration of the gamma ray detector that would produce the largest locus of recoils at the detection plane, with an additional margin included to accommodate the combined effects of multiple scattering and beam divergence of a quarter of a degree. A Monte Carlo simulation was carried out to better understand these effects (see Section 2.4.e). The overall dimensions of the scintillators was 0.30" x 2.75" x 4.5".

The scintillators were coupled to Lucite light pipes that were polished to a brilliant surface. These light

pipes and the scintillators themselves use total internal reflection to transfer light to the photomultiplier tubes. The light pipes merged the dimensions of the longest edge of the scintillator smoothly to a two inch circle, at which point the light pipe became cylindrical and passed through an O-ring seal out of the vacuum chamber, see Figure 2.6. These were viewed by two-inch Hamamatsu R329 photomultiplier tubes. These tubes were chosen for their fast timing characteristics. The scintillators were glued to the light pipes with a common commercial quick setting epoxy while the tubes were coupled with an optical coupling grease.

The scintillator/light-pipe assemblies were loosely wrapped with 0.3 mil aluminized Mylar to protect against any stray scintillation light emanating from the target, or light from the viewing windows in the chamber. Light emitting diodes were installed in each of the light pipes for setup purposes and gain monitoring.

The detector assemblies could be moved in and away from the beam axis, in order to optimize their position for a given gamma ray detector angle. See Section 2.4.e. for a discussion of the Monte Carlo method that was used to optimize the position of the particle detectors.

Figure 2.7. The charged particle detectors and their physical arrangement. The assemblies slid in and out within a cylindrical attachment to the chamber in order to position them relative to the beam axis. The light guides passed through O-ring vacuum seals within this sliding arrangement, which was also sealed with an O-ring which is visible in this view.

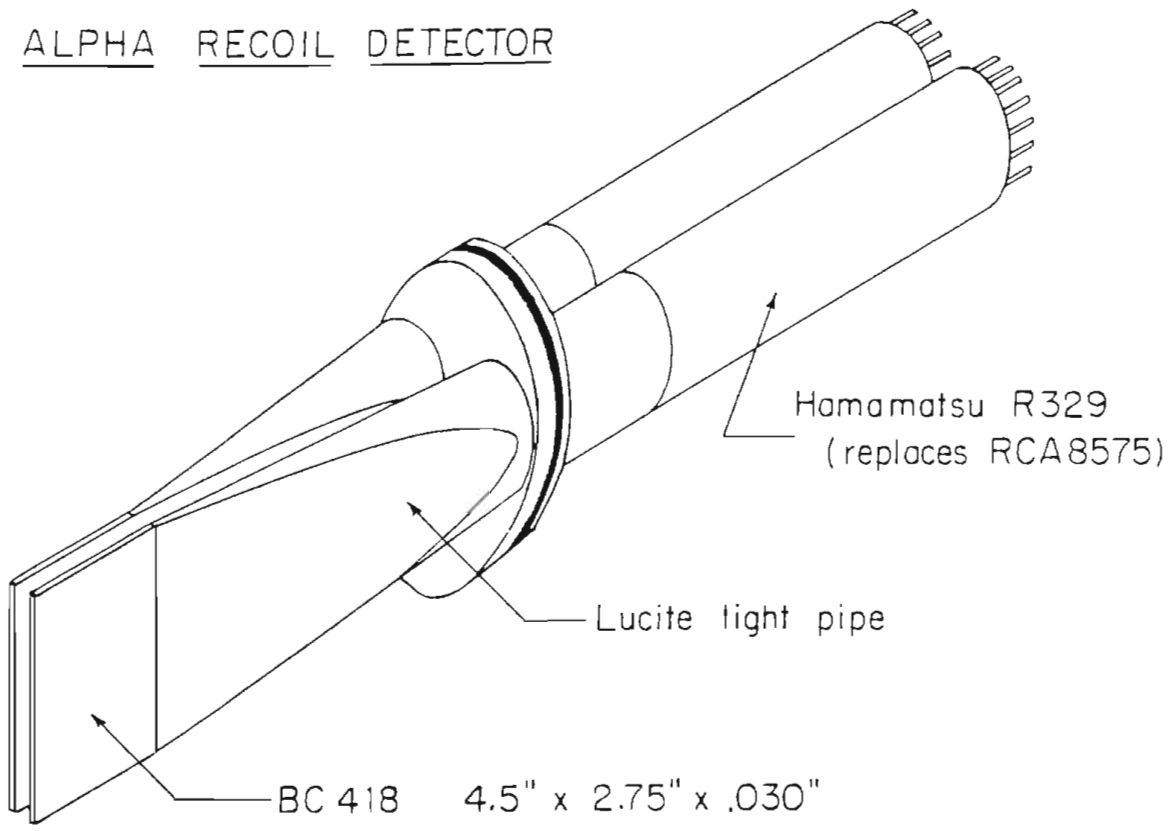
ALPHA RECOIL DETECTOR
Hamamatsu R329
(replaces RCA8575)
Lucite light pipe
BC 418 4.5" x 2.75" x .030"

2.4.e. The Monte Carlo Simulation of The Recoils

Radiative capture events take place at all points within the target through which the beam passes. When the recoiling ^{4}He nuclei are produced, their momentum and energy are uniquely determined by that of the gamma ray. This is why it is possible to detect the two reaction products in coincidence with high efficiency. The recoiling nuclei are kinematically restricted to small forward angles within about seven degrees of the beam.

Unfortunately, once they are created, the recoiling nuclei are subjected to scattering from the other atoms in the target. The amount of multiple scattering a given nucleus is expected to be subjected to, of course, depends on the point in the target where it is created. The uncertainty in the location of where the particle is expected to strike a detector is hence a function of where the particle is created in the target, which of course can't be known. This uncertainty is also increased dramatically by the large geometry of the gamma ray detectors and of the target. In other words the angle of the gamma ray is very uncertain due to large geometry, hence the trajectory of the alpha is also uncertain. Uncertainty in the angle of the incident deuteron beam is also a major effect in where the alpha particles can be expected to be detected.

The region where the ^{4}He nuclei can be expected in the plane two meters downstream of the beam of course had to be estimated in designing a detector for them, and to have a good idea of the efficiency of this geometry. Obviously, some fraction will be scattered away from any detector unless it could subtend 4π. Because of the many sources of uncertainty, an analytical estimate for all angles and en-

ergies was impractical, but a Monte Carlo simulation of these effects was relatively simple. This was important both in positioning the detectors for the highest efficiency, and for estimating the efficiency as a correction to the yields as a function of angle. These corrections were always less than ten percent and in some cases, less than one percent.

The basic idea of the program is to select five numbers at random. These numbers are between zero and one. They are then scaled to the size of the random variable that they are simulating. The first two represent the position on the face of the NaI spectrometer where the gamma ray is detected. The third simulates the position along the beam axis at which the trial capture event takes place. All kinematics can then be calculated.

It is then possible to calculate the characteristic multiple scattering angle for the thickness of target through which the simulated recoiling nucleus passes. The parametrization of Marion and Young (1968) was used in calculating this width, along with the corrections of Morrill et.al. (1987) for thick targets. The energy loss experienced by the trial particle was calculated according to the parametrization of Marion and Young, and this information was used to produce the simulated time of flight spectrum of Figure 2.5. The spreading angle of the beam is simply added in quadrature to the multiple scattering angle since both the multiple scattering distribution and the beam profile are approximated by Gaussian functions (the width of the product of Gaussian functions is equal to the square root of the sum of their squares). The other two random numbers are used to sample a Gaussian of this width. These two angles are added to the vertical and hor-

izontal angles which describe the trajectory of the recoiling ^4He nucleus. The position of the simulated alpha at the detection plane is checked to see if it strikes the detector in a given geometry. Through a sampling of many trial events in this way, the efficiency of any given geometry is estimated, with the effects of the beam spreading,the extended target and the large acceptance angle of the spectrometers, as well as multiple scattering taken into account.

Graphic outputs of this program can be seen in Figure 2.8. for two different NaI spectrometer angles. A printout of the code is included in Appendix D.

Figure 2.8. Simulation of the position of the recoiling ^4He nuclei for two different NaI spectrometer angles. The figures represent images of the recoil detection plane, with the beam axis at the centers of the left-hand edge. The rectangle represents the margin of the particle detector at its optimized distance from the beam axis. The scattered dots represent 1000 trial events. The closed curves in each figure define the kinematically allowed region for the recoils, if there were no multiple scattering or beam divergence. The closed curve in the center is for a point target, and the larger one surrounding it (and tangent at the top and bottom) is for the 5 inch long extended geometry of the target.

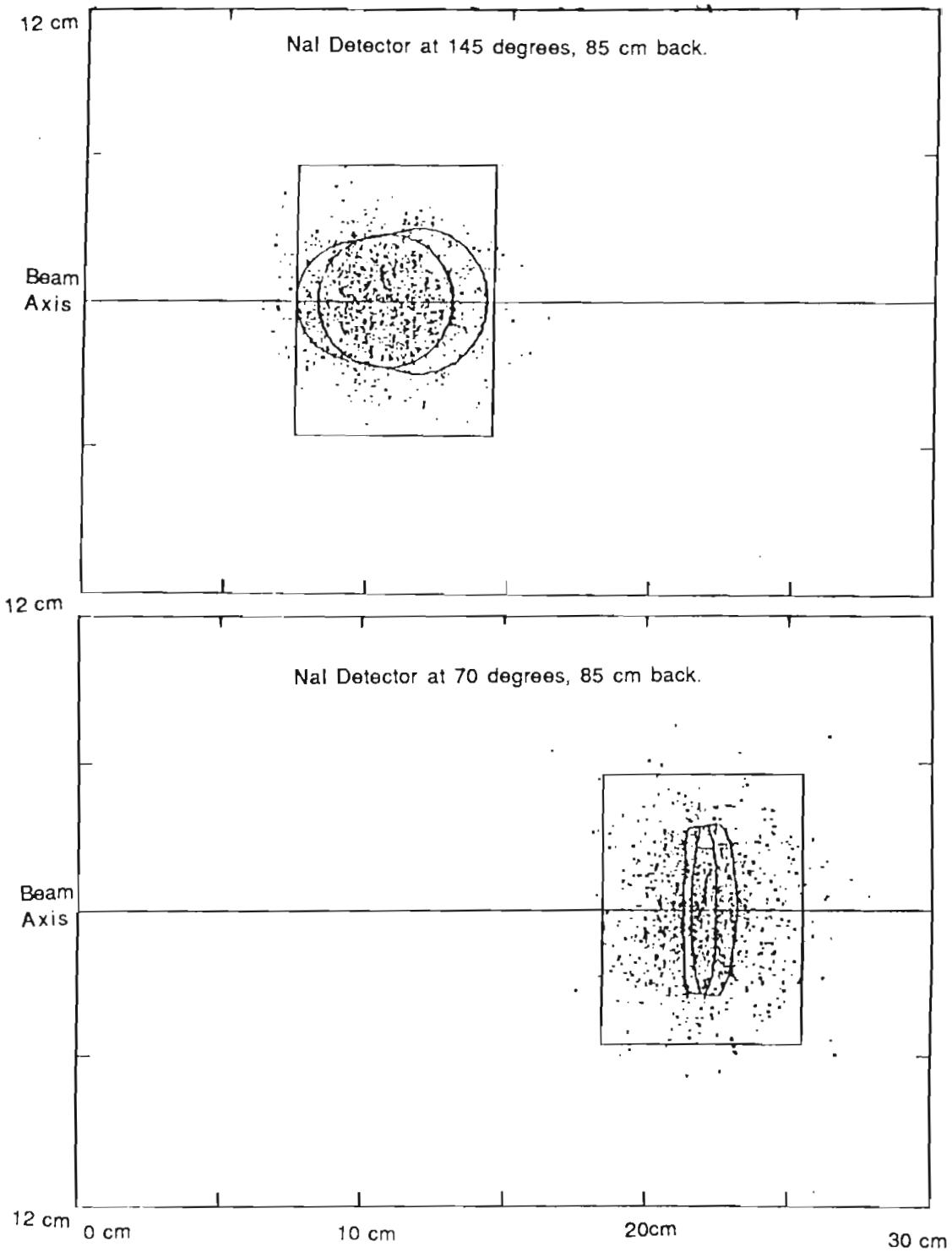
12 cm
NaI Detector at 145 degrees, 85 cm back.
Beam
Axis
12 cm
NaI Detector at 70 degrees, 85 cm back.
Beam
Axis
12 cm
0 cm
10 cm
20cm
30 cm
Distance From The Beam Axis

2.5. Fast Electronics

2.5.a. NaI Spectrometer Electronics

Because of the nature of this experiment, done in the user mode with several different collaborators, many minor features of the setup differed between the three sodium iodide detectors that were used. For that reason, this section will only attempt to cover the logic common to all three circuits.

The photomultiplier tubes were biased at negative high voltage and the part of the circuit that carried the energy signal was d.c. coupled at ground potential. This eliminates capacitive coupling for more stability at high count rates and gives better timing. This signal was clipped to a length of ~350 nanoseconds by reflection down and back an almost shorted cable, with the terminating resistance adjusted to give the best baseline restoration. It was determined that clipping the pulse to this length causes no appreciable loss of energy resolution. (The preceding part of this paragraph doesn't apply to the detector that was brought to Berkeley from the NBS, and it was usually kept at back angles in order to minimize the count rate.) This pulse could then pass completely through a fast linear gate of the same width. The gate was subsequently held closed for the signal processing time (~10 μsec.), thus eliminating the possibility of pulse pile-up for signals differing in time by more than 350 nsec. Keeping the pulse completely within the gate eliminates gain shifts due to timing changes between the linear and logic branches of the circuit. After the gate, the linear signal is amplified, shaped and digitized.

The logic branch of the circuit starts at the anode of the tube, as this has the best timing characteristics. After being shortened in a timing filter amplifier, this signal triggers a pair of simple leading edge discriminators. One discriminator is set at a high level somewhat below the gamma ray of interest. The other is set just above the noise level, to provide better timing information, with the minimum dependence on the pulse height. A coincidence is required between these in order to have both the timing and energy level information in this logic pulse. The output timing of this coincidence circuit was determined by the lower level (timing) discriminator.

The logic signal is used in several ways. It defines a valid NaI event which, along with gating the ADC, is the start signal for two time to amplitude converters; one stopped by the cyclotron RF signal, and the other stopped by the recoil particle detector. The valid NaI signal, along with a similar logic signal from the active shield, is used to produce a coincidence bit for cosmic ray and escape rejection. It is also counted and compared to the number of events that are actually digitized to calculate the dead time of the ADC, multiplexer and computer. This signal is also used to open the aforementioned fast linear gate through which the energy signal passes.

The purpose of the fast linear gate is to reduce pile-up. It is not desired that more than one pulse be digitized at a time, lest their amplitudes be summed. Since the time required for digitization is on the order of ten microseconds, the fast linear gate is held shut by an arrangement of gate generators for this period after each valid event. This eliminates high-high pile-up to the level of two pulses occurring at time differences greater

than ~350 nanoseconds. High-low pileup is inspected for using an arrangement of gate generators and a coincidence module. The valid NaI logic pulse is stretched to a length of ~400 nsecs, delayed about 250 nsecs, and fanned back together to form a pulse 850 nsec long, with a 50 nsec notch in the middle. This goes to a coincidence module with the corresponding low level discriminator pulse sandwiched within this notch. If the low level discriminator fires within ~400 nanoseconds before or after the valid firing, the coincidence module produces a pileup bit. This inspects for possible pileup to the 50 nanosecond level. Low-low pile-up is eliminated to the 20 nanosecond level by processing the branch of the anode signal that the discriminators see with an active amplifier (Timing Filter Amplifier). This module differentiates and integrates the signal in such a way that two small pulses must occur within 20nsec in order to add together significantly. This circuit reduces the chances for all types of pile-up.

A simplified schematic diagram follows in Figure 2.9 while complete circuit diagrams are included in Appendix C.

The sodium iodide spectrometers were actively stabilized against the gain shifts that could be caused by variations in the count rates in the photomultiplier tubes. A light pulse was produced in a light emitting diode optically coupled directly to the crystal. The amplitude of the pulse was chosen to be below the level of the NaI energy discriminator so that it wouldn't register as an event, or be stored in the computer. Because of this, some extra gate generators are required to open the fast linear gate to allow the LED pulse through. It is amplified and shaped as if it were a real gamma ray pulse, and then held at a

fixed amplitude by a stabilization module (a variable gain amplifier), built by Canberra Nucleonics Co. The pulser was run at a constant rate of 800 Hz. This rate was high enough to give good gain stabilization, while not so high as to cause significant pile-up. Fixing the position of the pulser peak stabilizes the rest of the spectrum.

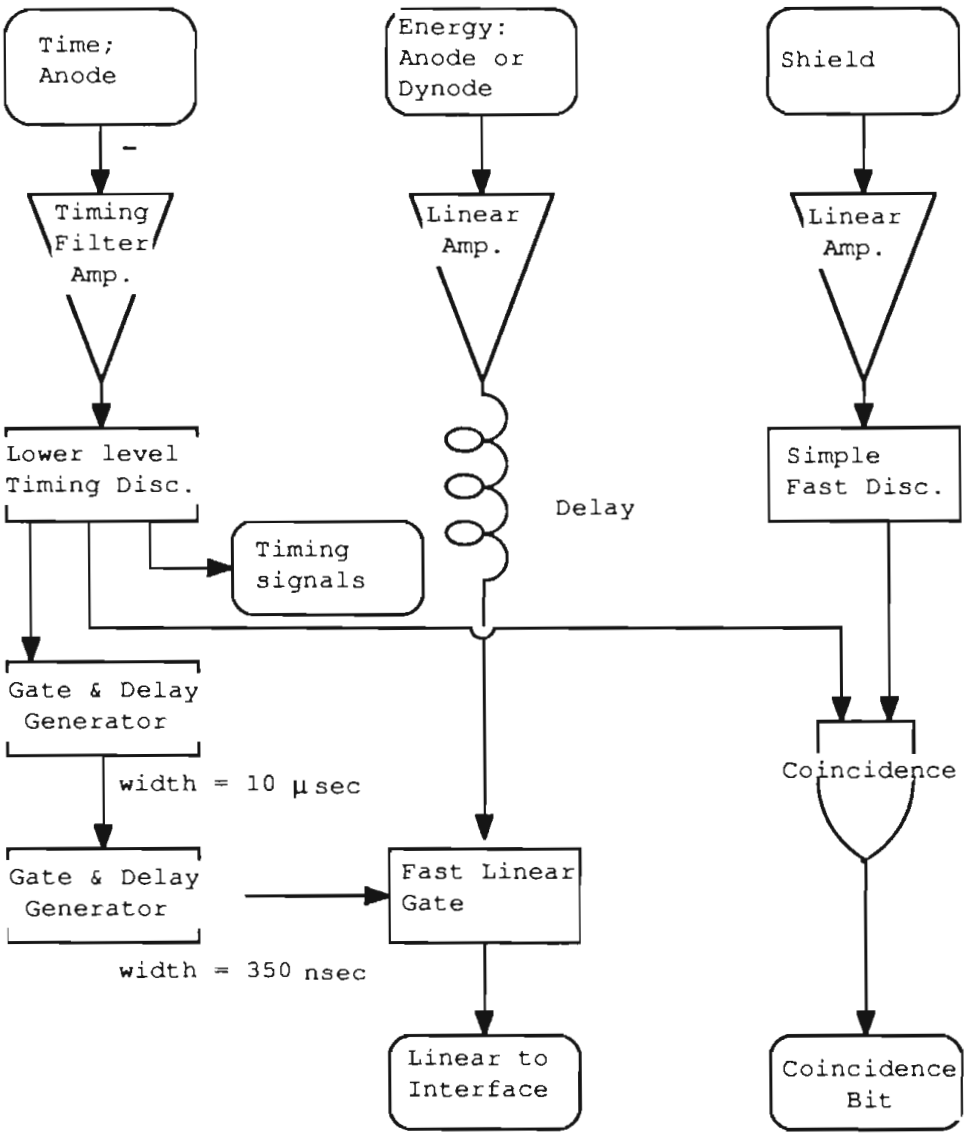

Figure 2.9. Simplified view of NaI electronics. See Appendix C for details.

2.5.b. Scintillator Electronics.

The recoil particle detectors were quite simple in concept and the only crucial aspect was the speed at which they could recover from the detection of a scattered deuteron and be ready to cleanly detect a recoiling alpha particle. The detectors themselves were fast plastic scintillators and the photomultiplier tubes used were chosen for their speed (see Section 2.4.c.). The electronics used to process the signals had to of course be capable of the same fast response. The high count rate is a matter of concern with regard to the time-to-amplitude converters (TACs) because of the probability of an accidental stop coming before the real event arrives. This problem was dealt with in two ways. First of all, the lengths of the cables were adjusted in such a way that the TAC stops that were associated with the alpha particles would arrive within 20 nsec of the start signal coming from a valid NaI count. The difference in the times of flight of scattered beam deuterons, and the ^{4}He nuclei of interest was always more than 20 nsec. The signal generated by the deuteron flash associated with the beam burst that produced the capture event would then arrive at the TAC before is was started, too early to produce a premature stop. In this way it was possible to push most of the huge deuteron peak off of the left side of the TAC spectrum. It was previously mentioned that the width of the beam bursts was inadequate to provide clean n-gamma separation in the NaI spectrometers. For the same reason, this timing method couldn't provide clean deuteron-alpha separation in the particle time of flight spectra, and a tail of the deuteron peak still would remain under the ^{4}He peak. The

second method of separating these ^{2}H nuclei from the ^{4}He recoils was by exploiting the difference in the range of the alphas and deuterons in matter. The first plane of scintillator was thick enough to stop the ^{4}He nuclei, but not thick enough to stop the deuterons. A second plane of scintillator was used to veto the deuterons to remove this background. It was possible to make this veto within a resolving time of less than ten nsec using discriminators and logic modules from the Phillips Co. line of 300 MHz electronics (A PS771 variable gain quad linear amplifier and a PS708 octal discriminator were used, see Appendix 3. These modules are designed with a flat response bandwidth, and a switching rate of 300 MHz, respectively. This very fast timing was necessary in order to minimize the possibility of a deuteron veto also overlapping the alpha particle signal (see Section 2.5.c. for a discussion of accidental vetos).

To be sure that the discriminator threshold was below the level of the alpha particles in the front scintillator electronics, the linear signal from this detector was digitized and stored. Recall that there was almost always one or more deuterons arriving in the scintillator around 20 nsecs before the alpha and again in the next beam burst about 50 nsecs after the alpha particle. Careful use of a fast linear gate was therefore required to prevent these deuteron pulses from piling up on the alpha energy signals. This gate was opened for about 40 nsecs by a coincidence between a valid NaI signal and a scintillator discriminator signal subject to the fast veto requirement. Care was taken to be certain that the cables that went to the coincidence module were exactly the same as those

starting and stopping the time of flight TAC. The overlap timing was about 30 nsecs. Therefore, if the alpha peak appeared in the first 30 nsecs of the time of flight spectrum, a coincidence was assured for each of these events and the fast linear gate was opened for them.

A simplified schematic diagram follows in Figure 2.10, while more complete circuit diagrams are included in Appendix C.

The coincidence timing between NaI and scintillator signals was set up prior to the run. A scintillation detector that was similar to the recoil particle detectors, but much larger in volume, was set up near the face of the NaI spectrometer, and cabled into the counting room with the cable that would be used for the recoil detector. The coincidence timing could then be set up using an Americium-Beryllium source which produces a neutron in coincidence with a 4.4 MeV gamma ray. When a delay that was equal to the alpha particle time of flight was added, and the cable returned to the front scintillator tube, the timing was set up. While a simple operation, once understood, this method of timing using a larger neutron detector and a coincidence radiation source, proved a crucial step in reliably setting up the coincidence circuitry. When the alpha peak was identified in the time of flight spectrum, some minor adjustment was usually necessary to place it as far to the left as possible.

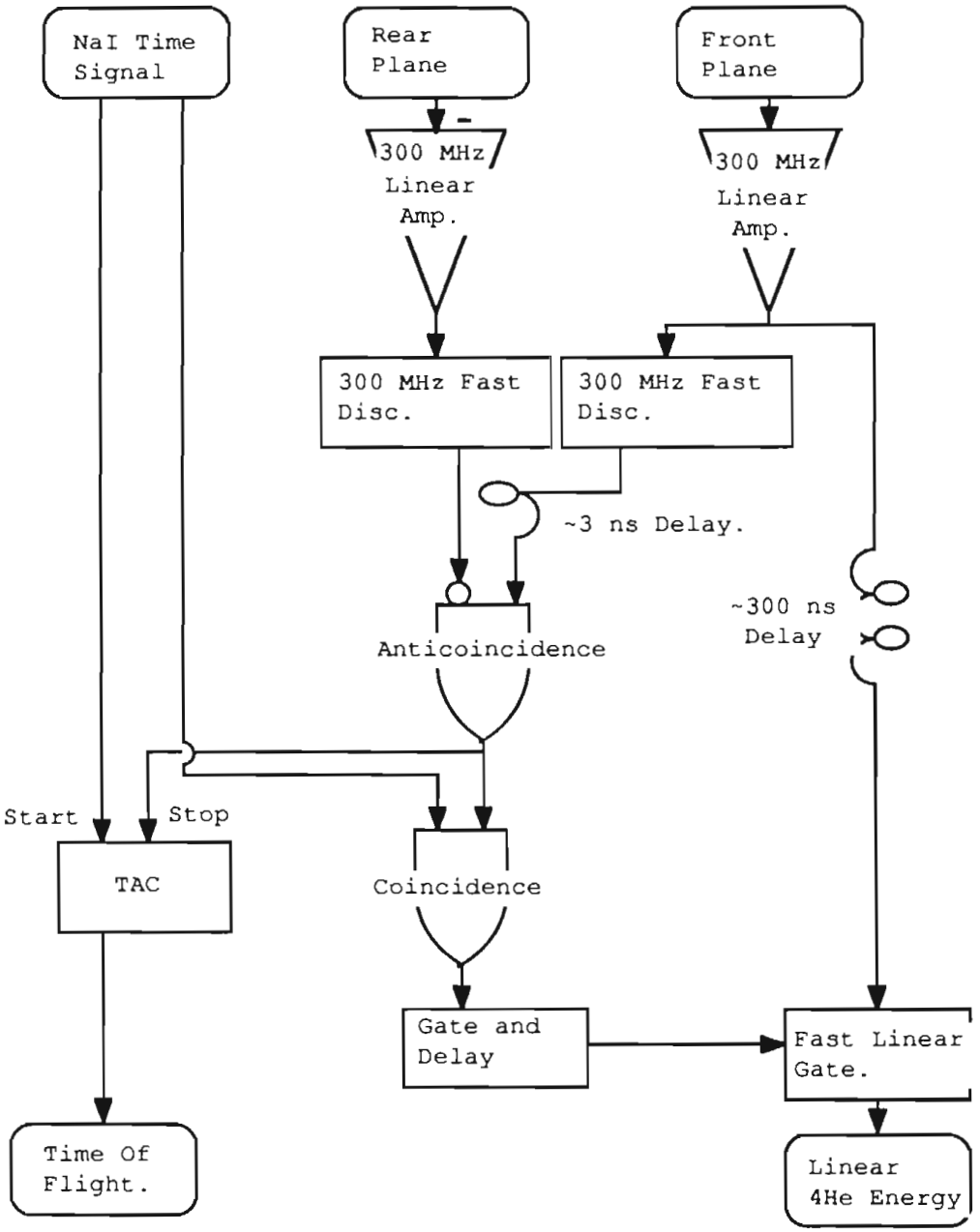

Figure 2.10. Fast scintillator electronics (Schematic). A more complete diagram including the part of the circuit for measuring the rate of accidental vetoing of the re-coiling ^{4}He nuclei due to the high rate of scattered deuterons is included in Appendix C.

2.5.c. Accidental Anticoincidence Considerations

Because of the high count rates and the poor energy resolution in the plastic anticoincidence shields that surrounded the NaI detectors, the energy information from these photomultiplier tubes wasn't normally stored. Instead, a bit was produced by a fast coincidence circuit, which corresponded to an event above an energy threshold in the shield in coincidence with an event in the NaI. The coincidence resolving time for this requirement was about 60 nanoseconds and was determined by the time jitter in the discriminators. Any time events are rejected on the basis of an anticoincidence requirement, the worry of accidental rejection arises. According to (Evans, 1955) the accidental rejection rate R_{ac} may be expressed as $R_{ac} = (R_1 - R_{tc})(R_2 - R_{tc})(t_1 + t_2)$, where R_1 is the count rate of one detector (e.g. the shield), R_2 is the count rate of the other detector (e.g. the NaI), and R_{tc} is the true coincidence rate between them. The length of time that a count in a detector defines an affirmative logic level is t. The shield and the NaI have different timing characteristics, so different lengths of logic pulses are associated with each of them, and the overall coincidence resolving time is $t_1 + t_2$. It is therefore advisable to limit both count rates and resolving time in a way compatible with the purpose of the coincidence requirement. The accidental rejection rate was monitored by counting the output of a similar coincidence circuit, where the logic signal corresponding to a valid NaI event was delayed by several hundred nanoseconds with respect to the shield signal. This delay removes all time correlation within the resolving time of the circuit so that any coincidences must be accidental. This rate was kept at

less than ten percent of the true NaI count rate, and was recorded as a possible correction to the cross section data. The need for this correction is evaluated and dismissed in Section 3.6 for the KVI data, but is not a factor at all for data taken with the alpha particle coincidence requirement. The narrow time window in the particle time of flight spectrum, as well as the background subtraction technique used (see Section 3.3.c.), eliminated the need for the anticoincidence shield requirement to reject cosmic rays, thus eliminating the worry of correcting for accidental shield coincidences.

Similar consideration had to be made of accidental vetoing of the ^{4}He recoils. A circuit was configured (see Appendix C.) in which the accidental vetoing could be checked as a function of the relative timing with respect to the beam bursts. The discriminator signals from the front and rear planes were fanned out to an additional anticoincidence module. Fast pulses at a known rate and phase relative to the beam bursts were obtained by prescaling a signal from the cyclotron RF circuit, and these were fanned together with the discriminator pulses associated with the front plane. The phase relative to the cyclotron was varied by changing a delay cable. This rate could then be inspected after the anticoincidence to see how many were lost, as a function of timing relative to the cyclotron. This provided a good estimate of the accidental veto rate (a), throughout the time region where the alpha particles were expected. Three rates had to be known to make this measurement; the rate of pulses that were produced artificially simply by scaling down a signal from the cyclotron RF circuit (N_1), the rate of real anticoincidences coming from particles (N_2), and the rate of real and artificial anticoincidences less those lost to acci-

dental vetos ($N_3 = N_2 + N_1 - a\ N_1$). See appendix 3 for a diagram of this circuit.The accidental ^{4}He veto rate (a) is then approximately $((N_1 + N_2 - N_3) / N_1)$ and is plotted in Figure 2.11 as a function of relative timing of the fast logic signal from the cyclotron RF. The word "approximate" is used because a number of the prescaled cyclotron RF pulses overlap the signal from the front plane and are not counted separately as they emerge in the count rate N_3, even though they weren't vetoed by the rear plane. Since more than 80 percent of the pulses from the front plane are vetoed by the rear plane, it is assumed that the RF pulses which are essentially in coincidence with the front plane would, with the same probability, be vetoed. The inaccuracy due to this effect is therefore small, and a represents an upper bound on the rate of events lost to accidental vetos.

Five percent accidental vetos was the typical measured upper bound for this effect. This is small compared to the statistical accuracy of this work, and due to rapid state changing, has no effect on analyzing power measurement except in reducing counting statistics.

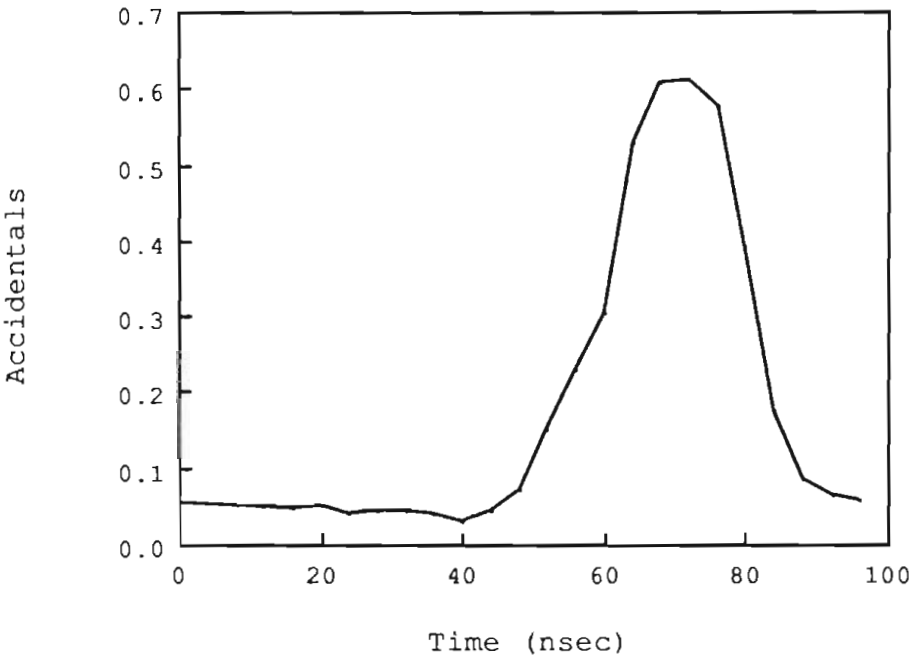

Figure 2.11. The accidental vetoes of pulses in the front veto plane due to the high rate in the rear plane (typical measurement). The time scale is with respect to the cyclotron RF, with zero corresponding to the expected time of arrival of a recoiling ^{4}He nucleus. The large bump at 45 to 85 nsec corresponds to deuterons from the next beam burst.

2.6. Computers Used

The data taken at KVI were written to magnetic tape and disk by the online Vax 11-750 at that laboratory using the software package PAX that is in common usage there. It was written to tape event by event, and reduced to spectrum tables using the KVI Vax 11-850. It was then transferred to the TUNL Vax 11-780 through the research computer network Bitnet. It was then summed, corrected for solid geometry effects and accidental rejections due to shield coincidences. Finally it was then fitted to Legendre polynomials with modified versions of the usual TUNL capture group software (see Chapter 5).

The data taken at Berkeley were written to tape by the online NSD ModComp "Classic" computers in use there, using the software package Chaos (Maples, 1985). The event tapes were then shipped to TUNL to be sorted and summed using the software package WC (Countryman, 1984) that was developed at LBL to analyze data written in the Chaos format (see Section 3.1.a.).

3. Offline Analysis

3.1. Introduction

The coincidence data taken at Berkeley included for each event, the energy information from the NaI spectrometer, the energy information from the recoil detection scintillator, the time information between the NaI spectrometer and the cyclotron radio frequency signal, and the time information between the NaI and the recoil detector. In actual practice, it was sometimes necessary to place software gates in the spectra of at least two of these quantities in order to identify the capture peaks in the spectra of the remaining ones. Since in these cases an iterative process of gating was necessary even to identify the capture peaks, the data were written to tape event by event so that the gate positions for this three-fold coincidence could be optimized offline.

3.2. Polarization Observables.

In all polarization studies, one must extract physically meaningful quantities from count rates. In measurements involving a spin 1/2 polarized beam one could identify the beam state as having a direction (up or down) by somehow making a comparison of the way it "looks" from the left and from the right. It therefore may be easy to visualize the physical observable, the analyzing power of the target nucleus, producing a left right asymmetry in the count rates. The case of a spin one beam, whose polarization is characterized by an ensemble of states m_s = 1, 0, and -1, is "polarized" with respect to some axis so long as there is some difference in the population over the purely ran-

dom case where the population is equal in the three states. In this case, it is sometimes much more difficult to imagine the effect that such polarizations can have on count rates. This may be due to the fact that some relative population distributions, for example the case where all particles are in the $m_s = 0$ substate, has no definable "up" or "down" and looks the same from the left and right. This is a case of a pure tensor polarization, and as so is notable as having no identifiable direction. The physical observables, in the case of tensor analyzing powers, are normally extracted by comparison of yields from beams prepared with different substate populations. The methods and formulas can be found in the literature (Haeberli, 1974; Ohlsen, 1973).

Some familiarization with the subject is in order for the specific cases of this experiment. First we define a coordinate system in what is known as the Madison convention (Haeberli, 1974), (see Figure 3.1). The direction of the incident momentum (k_{in}) defines the Z axis, the Y axis is defined by the cross product $K_{in} * K_{out}$, and X is defined to create a right-handed coordinate system. The Y axis is thus up or down in the lab, depending on whether we are referring to the left or right detector respectively.

The description of the polarization state of spin one particles is rather complicated, but due to the symmetry of most experimental arrangements, simplifications are possible. For more general discussions see Darden (1971) and Goldfarb (1958). Because the spin system is symmetric about the magnetic field at the point of ionization, the polarization state can be described by the fractional populations with N_+ having spin projection 1, N_0 having pro-

jection 0 and N_- having projection -1. Two numbers are adequate to describe the relative populations: $p_z = N_+ - N_-$ is commonly referred to as the vector polarization of the beam, and $p_{zz} = (1 - 3 N_0)$ is commonly called the tensor polarization or sometimes the alignment. It must be emphasized that these definitions rely on the fact that the axis of quantization is along the magnetic field at the point of ionization, which is defined as the Z axis.

These definitions are sensible. Note that if $N_+ = N_0 = N_- = 1/3$, we have zero vector and tensor polarization. In the case first mentioned, where $N_+ = N_- = 0$, and $N_0 = 1$, we have p_{zz} equal to a maximum negative value of -2, and p_z equal to zero, in accordance with no identifiable direction.

For this simplified, but common case of axial symmetry, the other elements of the second rank tensor p_{ij} representing expectation values of the cartesian spin operator S_{ij} are $p_{xx} = p_{yy} = -1/2(1-3N_0)$, and $p_{xy} = p_{xz} = p_{yz} = 0$.

Given a beam with the desired polarization properties, one must extract the observables associated with the reaction from count rates. In the case of a vector analyzing power a left right asymmetry is sufficient, but most researchers choose to reverse the spin direction as well, to reduce systematic error (Hanna,1966). When one measures analyzing powers and has use of an ion source that selects pure m_s substates with some constant unpolarized background (such as the TUNL lamb shift source), one can simply measure the count rate in all three substates and use the formulas for the specific observables:

$$A_y = \frac{1}{P}\frac{Y_1 - Y_{-1}}{Y_{-1} + Y_0 + Y_1}$$

$$A_{yy} = \frac{1}{P}\frac{Y_{-1} + Y_1 - 2Y_0}{Y_{-1} + Y_0 + Y_1}$$

where P is the constant polarization, and the Y's are the yields in the substates denoted by the subscripts, and with the polarization axis in the Y direction as defined in accordance with the Madison convention defined above.

Spherical tensors T_{kq} are often used instead of the cartesian tensors described above. This is because the Legendre functions transform as spherical tensors and thereby provide a convenient method of expression of one's results. The transformation between the cartesian tensors measured in this project and the spherical tensors are

$$A_y = \frac{2}{\sqrt{3}}\mathrm{Re}(iT_{11})$$

$$A_{yy} = -\sqrt{3}T_{22} - \frac{T_{20}}{\sqrt{2}}$$

$$A_{zz} = \frac{T_{20}}{\sqrt{2}}$$

While the spherical representation is elegant in that it possesses the transformation properties that allow convenient expression in terms of the Legendre functions, there are two reasons that most of the work of this thesis is better expressed in terms of cartesian tensors. First of all the magnetic field of the 88 inch cyclotron (and all others that I know of) is perpendicular to the scattering plane. That is therefore the most natural axis of symmetry. The spin axis of the beam would precess, due to the magnetic moment of the particles, about this field. The beam is however, ionized in a strong magnetic field

along this axis so no such precession occurs. This axis perpendicular to the scattering plane is not a natural axis in spherical coordinates, which have one axis already defined as the beam direction. It can however be a natural axis in the cartesian representation, and is referred to as the Y axis in accordance with the Madison convention. The spin axis is allowed to remain symmetric about the Y axis in measurements of A_{yy}.

The second reason that most of this work has been done with an axis of symmetry perpendicular to the scattering plane has been mentioned earlier. The model calculations that have fit the A_{yy} data at tandem energies fairly well (see Section 4.1.a.) have failed to fit the A_{zz} (T_{20}) data. S-wave capture to the D-state of ^{4}He contributes in first order to T_{20} but not to A_{yy}. The accepted explanation of the failure of the model to fit the spherical tensor analyzing powers is that the S-wave scattering state is highly distorted (Santos, 1986). The D-state of the deuteron can also play a stronger role in S-wave capture (see Section 4.1.a.). It seems to be a rare kindness of nature that the most easily measurable tensor analyzing power, A_{yy}, is also the most easily interpretable.

A measurement of $A_{zz} = 1/\sqrt{2}\ T_{20}$ was also made, in hopes that a more complete data set would help unravel the importance of S-wave distortions in comparison to deuteron D-state effects.

In the case of the Berkeley atomic beam type polarized ion source, there is never a pure polarization state, whose signs can simply be reversed. What is done in this case is to run with three or four known and different combinations of weak and strong field transitions producing

the same number of independent beam polarizations P_y and P_{yy}, typically P_y ~ +/- 0.2, and P_{yy} ~ +/- 0.7. With the polarization axis in the direction of the Y axis, the cross section is expressed in terms of polarizations as

$$\sigma^i = \sigma_u(\theta,\phi)\left[1 + \frac{3}{2} p_y^i A_y(\theta) + \frac{1}{2} p_{yy}^i A_{yy}(\theta)\right]$$
$$i = 1,4$$

where σ_u is the unpolarized cross section. Three or four equations in the three unknowns; σ, A_y and A_{yy} are produced. These are simply solved following the method of the program "Regres" (Bevington,1963) which makes a multilinear regression fit and takes statistical errors in count-rates and polarizations into account.

Although it seems more complicated than the case with pure polarization states, the use of the fitting program to extract values of the observables from the count-rates did not produce much inconvenience. The only real drawback is that it was sometimes difficult to extract the observables online, while collecting the data, as a diagnostic.

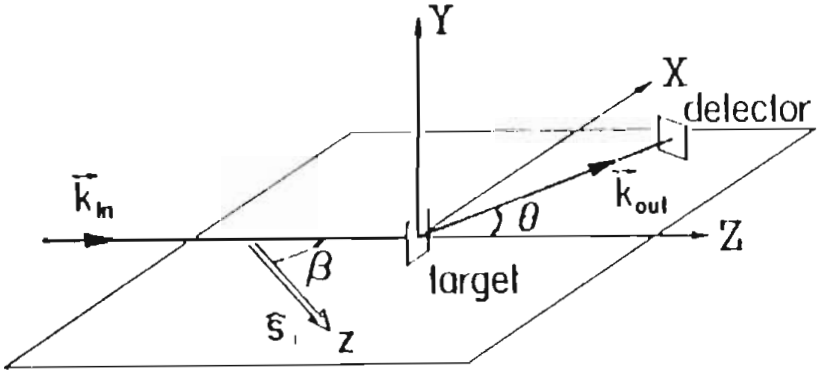

Figure 3.1. The Madison Convention.

3.3. The Event Sorting

3.3.a. Software

The majority of the data that were taken at Berkeley were sorted using the data analysis software package "WC" that was developed at LBL by (Wald and Countryman, 1984). This is a Fortran package that is designed to read data tapes that are written by the Berkeley Modcomp computers using the software package "Chaos", that was also developed in house. Since WC is a Fortran code it was easily installed on the TUNL Vax 11-780, and the data tapes could be sorted at home at Duke University.

3.3.b. Setting Gates

In this experiment the emphasis was placed on measuring relative cross sections. Since all of the NaI spectrometer systems that were used were newly installed, and an absolute efficiency calibration would have represented a major investment, absolute cross sections had to be ruled out as a goal in this work. In measuring analyzing powers, the widths and positions of the gates were chosen to produce the cleanest spectra without loosing a significant number of counts. In the runs that were also analyzed for the differential cross section, including all of the KVI runs, and selected runs at Berkeley, the energy gate in the NaI spectrum had to be carefully moved in a way that is consistent with the kinematic shift of the gamma ray energy. The coincidence system provided a convenient way to measure backgrounds simply by taking an equivalent time of flight window that corresponded to the wrong beam burst

(see Figure 3.4 and the next section for a discussion of background subtraction).

3.3.c. Sorting and Summing the Events

The coincidence gating proved very effective in producing clean spectra especially at back angles, and there was often no need to be extremely careful in positioning the gates when sorting for analyzing powers. At these angles the mere constraint that a particle was detected at the plane two meters downstream of the target often enabled the gamma spectrum to be summed over a large region including those gamma rays that don't deposit up to ~1/3 of their energy in the spectrometer. The measurements at forward angles were much more problematic because of the intense flux of neutrons from the $^{2}H(d,n)^{3}He$ reaction being detected in the NaI spectrometers. For these runs clean gamma spectra were obtained by subtracting a background spectrum. The background spectra were produced by placing a gate in the particle time of flight spectrum at a time that corresponds to one beam burst later than the "foreground" gate (see Figure 3.4).

Because accidental stops occur in the time to amplitude converter at high count rates of the particle detectors, the background spectra sometimes had to be normalized to compensate for this effect. The effect of accidental stops can be qualitatively understood by thinking that for a given start of the time to amplitude converter (TAC), the probability of a stop occurring at a given time later (dN/dt), without one having already occurred, is inversely proportional to the time that has elapsed since the TAC

was started (t), and proportional to the frequency of stops, with proportionality constant ($-\lambda$).

$$\frac{dN}{dt} = -\frac{\lambda f}{t}$$

The solution is $N = N_0 e^{-\lambda f t}$, with N_0 = the original stop rate without the effect of the accidental stops. In reality the stop rate (and hence f) wasn't a constant, but was much higher at times associated with beam bursts. It is still true that because of the periodic nature of the stop rate, the effect at points constant in phase with respect to the beam bursts follows the above exponential expression. To normalize the background spectrum to compensate for accidental stops, equal width regions of the ungated TAC spectrum were integrated, and the ratio taken. These regions were associated with different beam bursts than the capture events so that they would truly represent accidental stops. The regions were equal in width, and one cyclotron RF period apart in the TAC spectrum, hence represented rates at the same phase with respect to the beam bursts. This ratio was always within 25 percent of unity and most often within 5 percent. This ratio was used to normalize the background spectrum to compensate for accidental stops, and the normalized background spectrum was subtracted from the "foreground" spectrum, to produce a very clean gamma-ray spectrum.

This technique also subtracts out a sample of cosmic rays that is statistically equal to the number in the foreground gate, and therefore eliminates the need to use the anticoincidence shield requirement. This in turn elim-

inates the need to consider a correction factor due to accidental rejections caused by the high count rate in the shield. (this was discussed in Section 2.5.c.). The effect of background subtraction produced spectra that were much more pleasing to the eye but the overall effect on the sums was less than 30 percent in the worst cases, and was usually only a few percent. This was usually within the statistical uncertainty of the sum, hence not necessary in most cases.

3.4. Finite Geometry in the Apparatus; Compensating for the Effects

Thus far this chapter has been concerned with how raw data were reduced to correct net sums. However, these sums are not physically meaningful observables. The aim of the experiment was to measure angular distributions of analyzing powers and cross sections of the $^{2}H(\vec{d},\gamma)^{4}He$ reaction. Due to finite sizes of the target cell and detector, the measured count-rate of the detector must be correctly interpreted in order to extract the result for point geometry. The effects that must be accounted for are deuteron flux averaging over the volume of the target and gamma-ray flux averaging over the area of the detector.

A Monte Carlo program, FIXER (Jensen, 1981), existed to calculate the effects of multiple scattering and solid geometry in neutron capture experiments. It originated as an adaptation of a program used in neutron scattering experiments. It was relatively simple to remove the multiple scattering and neutron production parts of the code, for use in estimating the effects of the solid geometry in this

experiment. A correction factor, $R = \sigma_{obs}./\sigma_{true}$, relating the observed differential cross section to the true differential cross section was calculated.

The logic of the program is as follows. The procedure begins with the random selection of two points: one within the target ($^2H(\vec{d},\gamma)^4He$ reaction point); and one on the detector face (γ-ray detection point). This defines the path travelled by the γ-ray. Employing an assumed $^2H(d,\gamma)^4He$ differential cross section (σ_{guess}), FIXER proceeds to calculate a probability associated with the chosen path.

The procedure just described (i.e. select a set of random points and calculate a probability associated with the defined paths) is carried out repeatedly. This repetition effectively averages the calculated probability over the target volume and detector area. Convergence to what shall be called the predicted $^2H(d,\gamma)^4He$ differential cross section (σ_{pred}) occurs within 5000 histories. The prediction is compared with the observed cross section and a new guess is obtained according to

$$\sigma_{guess}^{(i+1)} = \frac{\sigma_{obs}}{\sigma_{pred}^{(i)}} \sigma_{guess}^{(i)}$$

The initial guess $\left(\sigma_{guess}^{(1)}\right)$ was taken to be the observed $^2H(d,\gamma)^4He$ γ-ray cross section (σ_{obs}). In practice, only one iteration was necessary to obtain R since $\sigma_{obs}-\sigma_{pred}$ was small. Hence the correction factor is given by $R = \sigma_{obs}/\sigma_{pred}$.

3.5. Spectra

Figure 3.2. Gamma-ray spectra from the run at E_{beam} = 30 MeV, taken at KVI. They are for ϑ_{cm} = 140 degrees and 90 degrees respectively. The summing region is shown. Note that while the 140 degree data appear to be free of background, the yield at 90 degrees is so diminished that the summing region is affected by background counts.

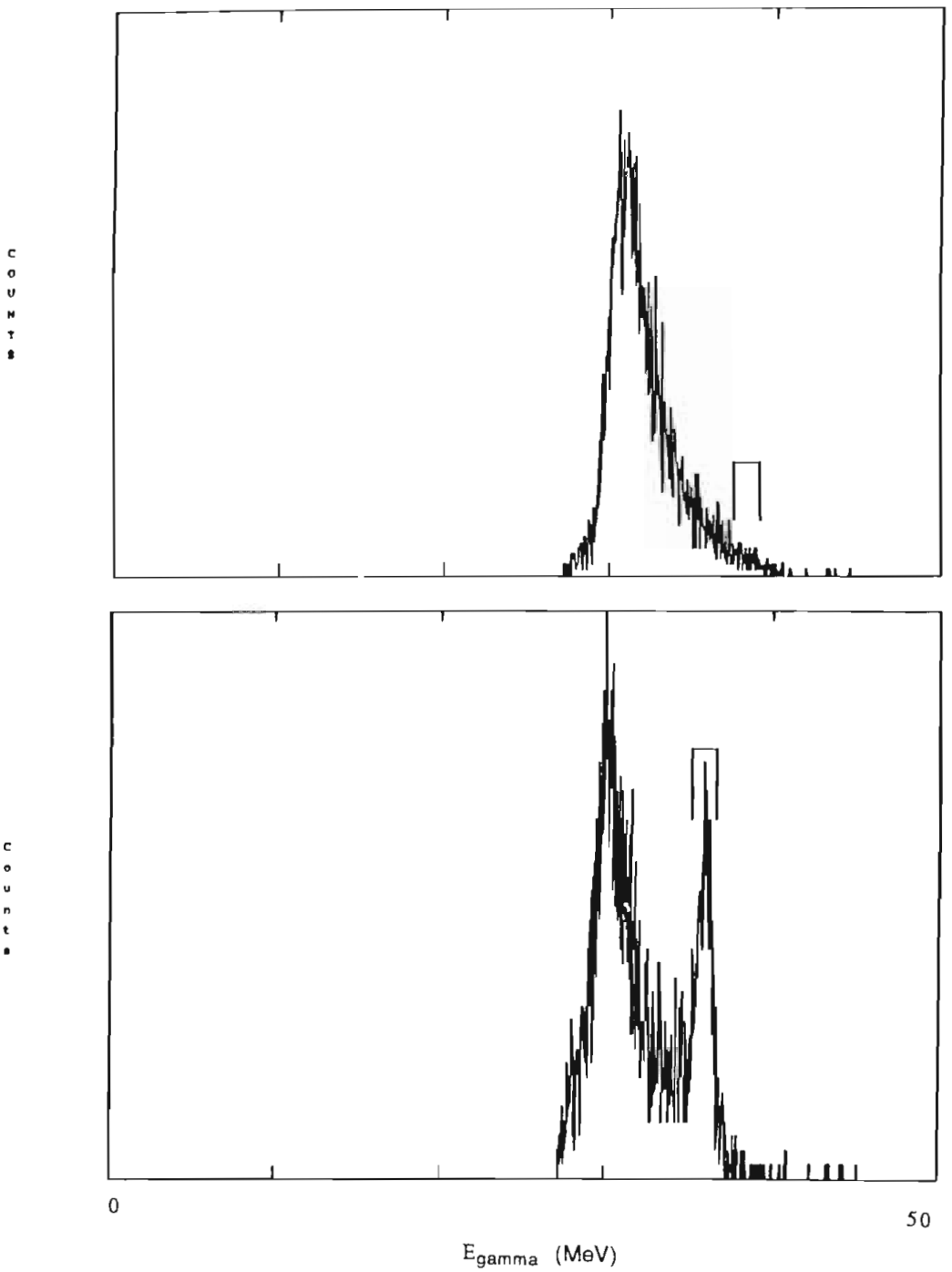
COUNTS
COUNTS
0
50
E_{gamma} (MeV)

Figure 3.3. Gamma-ray spectra from LBL, E_{beam} = 50 MeV, ϑ_{cm} = 140 degrees. The four spectra show four different levels of gating. #1 is a raw spectrum, #2 is gated by time relative to the cyclotron timing, #3 is fully gated including the particle time of flight, and #4 is similar but with the particle gating at a time of flight corresponding to one cyclotron period later than the beam burst that produced the trigger. This provides a measure of the background. The scale on the two fully gated spectra is enhanced by a factor of ten.

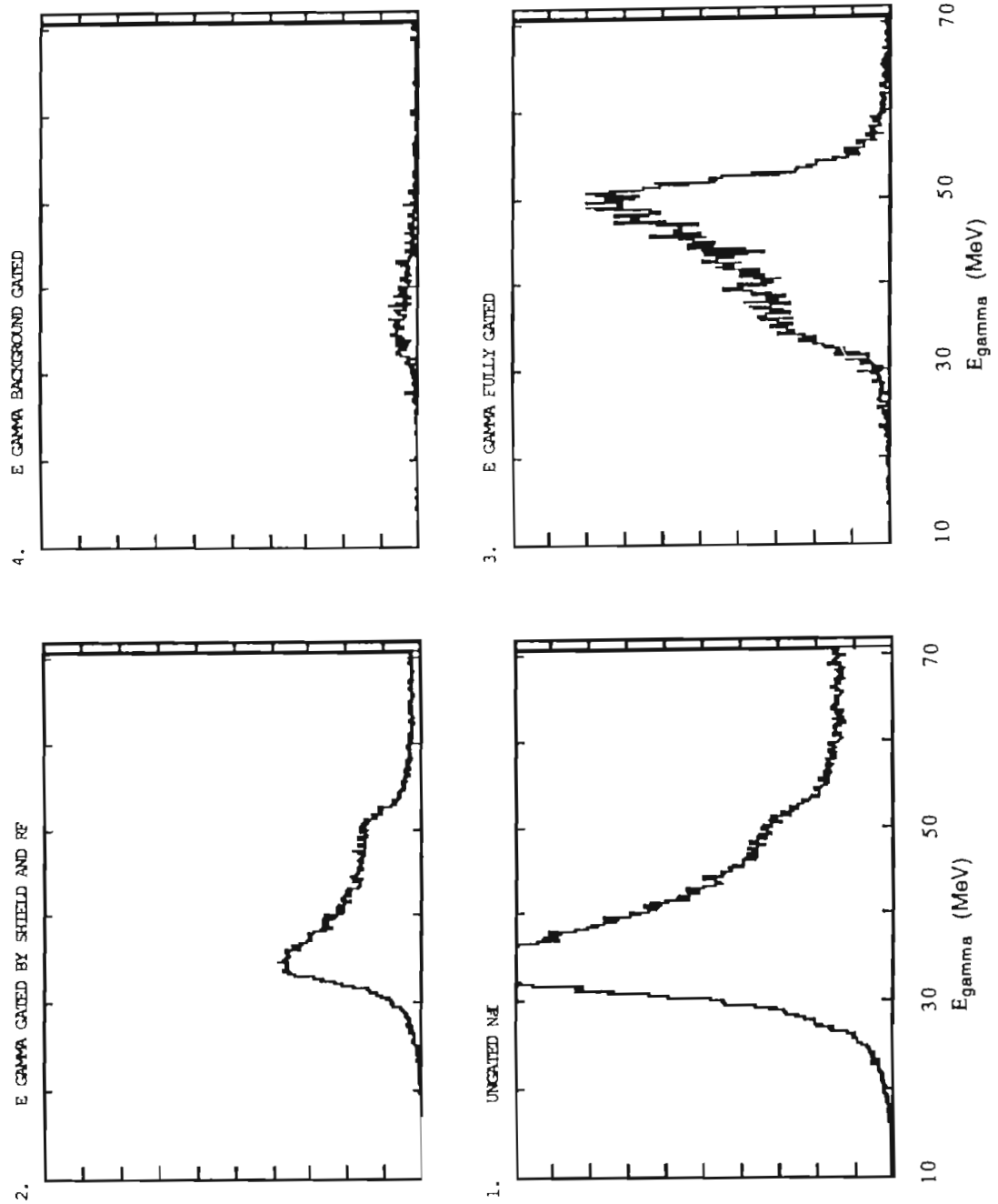
4.
E GAMMA BACKGROUND GATED
3.
E GAMMA FULLY GATED
2.
E GAMMA GATED BY SHIELD AND RF
1.
UNGATED NaI
10
30
50
70
E_{gamma} (MeV)

Figure 3.4. The two time spectra and the particle energy spectrum. The version at the bottom is ungated, while the version at the top is gated by conditions in the other time spectrum, (or both, in the case of the particle spectrum) as well as an energy condition in the the gamma-ray spectrum of the preceding figure. The clean event identification should be noted. The particle spectrum was stored as a diagnostic concerning the discriminator level, but was not used for gating. The gates are shown in the time spectra, gate four being for the background.

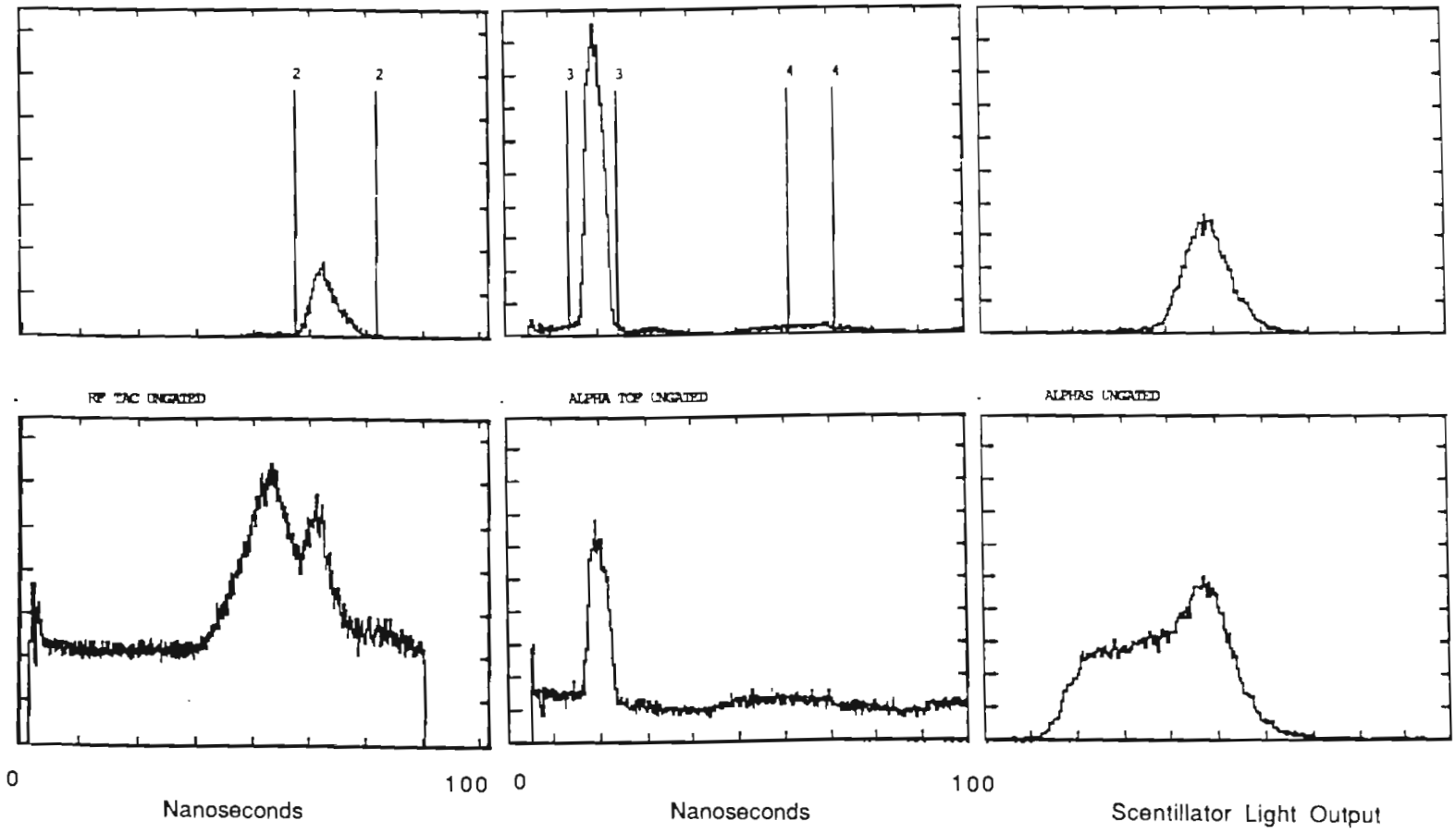
2
2
3
3
4
4
RF TAC UNGATED
ALPHA TOF UNGATED
ALPHAS UNGATED
0
100
Nanoseconds
0
100
Nanoseconds
Scentillator Light Output

3.6. Summary of Errors and Corrections

3.6.a. Analyzing Power Error

Due to the previously mentioned nature of the atomic beam type polarized ion source, there was little systematic error associated with the polarization of the beam. The changes between polarization states occur at a point where the beam is neutral in charge, and thus the steering is unaffected by any changes in the homogeneous magnetic field associated with the transition regions. Slow fluctuations in the beam position and current, etc. are averaged over all states by fast spin flip, as are effects of changing target thickness and detector efficiency. For these reasons the systematic errors associated with the analyzing power measurements are diminishingly small compared to statistical errors associated with the polarimetry, and the gamma ray statistics. Propagation of these statistics as well as the uncertainty in the analyzing power of the polarimeter are handled within the multilinear regression program used to calculate observables (Section 3.2, and Bevington, 1963).

The other possible source of error in the analyzing powers is associated with the finite geometry of the target and the detectors. There was not sufficient angular structure in these observables that this was a significant effect. The errors associated with a Monte Carlo correction procedure would have been on the order of the errors due to finite geometry, and so such a procedure was not applied. The errors quoted on all analyzing powers therefore arise purely from counting statistics and polarimetry.

3.6.b. Error in the Differential Cross Section

The angular distributions of the cross-section are unfortunately not nearly so free of systematics. Possible sources of systematic error in the 50 MeV measurement include the beam integration, coincidence efficiency, accidental ^{4}He vetos, and electronics dead time. The sources of systematic error in the 30 MeV (singles) experiment included a difficult to determine background and accidental gamma ray rejection due to the anticoincidence shield. The finite geometry effects both measurements due to the angular structure of the cross section.

Some background had to be subtracted from the sums at 30 MeV, see Figure 3.2. This could only be done by an interpolation between the backgrounds on both sides of the gamma ray peak, and this subtraction was taken to have an accuracy of 50 %. This makes a small contribution to the quoted errors.

Beam integration error was assumed to be constant with angle, is not included in the quoted errors at 50 MeV. The counting statistics in the beam monitor at 30 MeV were such that this didn't contribute as a significant source of error.

Electronics dead time was compensated for naturally by the used of a monitor at 30 MeV, and was found to always have a measured value of less than 1% in the 50 MeV experiment. As such, it was not considered in the analysis.

Accidental rejections due to the shield were measured to be less than 10% at all times in the 30 MeV measurement. They are taken to be constant within 20 %, and so contribute an error of +/- 2% added in quadrature to the other

sources of error. The anticoincidence shield requirement was not used in sorting the 50 MeV events, and so that measurement is free of this effect. Precisely the same bounds can be placed on the effects of accidental vetos in the 50 MeV measurement. When 2% is added in quadrature to the ~ 5 % errors associated with other sources, it contributes less than 0.5% additional error, and as such is unimportant.

The 50 MeV data can be affected by the loss of coincidence efficiency associated with alpha particles not being detected in the scintillators. A Monte Carlo procedure was used to estimate the effects of the placement of the particle detectors, the multiple scattering in the target, and the beam divergence, (see Section 2.4.e. and Appendix D). While the placement of the detectors and the target thickness were known, the divergence of the beam was unknown, and was the primary source of uncertainty in this correction factor. The beam divergence was estimated at being less than 0.35 degrees, based on tuning aperture sizes. This amount of divergence reduced the calculated coincidence efficiency by 4.4 to 6.8 percent, depending on the angle. One half of the difference between the calculation with no beam divergence and that with .035 degrees divergence was taken as the uncertainty in this correction. The correction factor that was used was the average of those two situations. It must again be emphasized that this correction was also on the order of 5%, and as such did not contribute significantly to the overall uncertainty.

By far the largest source of systematic uncertainty in the cross section measurements at both 30 and 50 MeV is due to the large finite geometry of the apparatus, and the rapid change with angle in the physical observable. The method of correction through a Monte Carlo procedure is de-

scribed in Section 3.4. These corrections depend on an accurate guess of the physical cross section as a starting point, and makes the approximation that the NaI spectrometer detects all gamma-rays that impinge on its face with equal probability. The error in this procedure was estimated to be 10% of the difference between the correction factor and unity . This estimate may be realistic when the correction is small but at some angles these corrections were large, and the error bars at these points (near ninety degrees) must be viewed with caution. Where the corrections were small however, this estimated error does not contribute significantly to the total error.

While there are several corrections that could be made to the overall sums, only two were angle dependent in these measurements. Since it was not possible to extract an absolute cross section, only the corrections with angle dependance needed to be made. (In some cases the accidental rejection ratio is much higher at more forward angles, but that did not appear to be the case in 30 MeV measurement. This is because the count rates in the shield were low, since the detector was not placed forward of 90 degrees in the laboratory. Forward angle yields are deduced from symmetry.) The corrections to the cross section data are tabulated in Table 3.1, while the level at which each effect contributed to the overall uncertainty is tabulated in Table 3.2. The sources of error in the analyzing powers are not tabulated, as they were entirely statistical.

Table 3.1 Correction Factors to the Cross Section

CM Angle	Coinc. effic.	Solid geometry
30 MeV		
85.1, 95.1	-	0.4 +/- 0.06
50.6, 129.1	-	1.1 +/-0.001
37.0, 143.2	-	1.02 +/-0.002
50 MeV		
89.6, 90.6	1.340 +/- .034	0.22 +/- 0.08
69.0, 111.2	1.044 +/- .024	0.79 +/- 0.02
59.5, 120.8	1.043 +/- .024	1.03 +/-0.003
42.2, 137.6	1.081 +/- .022	1.07 +/-0.007

Table 3.2. Fractional Sources of Error
(% each source squared contributed to the total squared)

CM Angle	Coinc. effic.	Solid geometry	Backgnd. estimate	Stat-istcal
30 MeV				
85.1, 95.1	-	17	8	75
50.6, 129.1	-	0	1	98
37.0, 143.2	-	0	1	98
50 MeV				
89.6, 90.6	0	≈85	-	≈15
69.0, 111.2	1	28	-	71
59.5, 120.8	1	0	-	99
42.2, 137.6	1	0	-	99

Table3.3. Reduced and Corrected Values of the Measured Observables

CM Angle	A_y at E_{beam}=20MeV	Error[1]
42.8	-0.07	0.20
74.0	-0.08	0.38
118.7	-0.15	0.35
133.1	0.02	0.11

CM Angle	A_{yy} at E_{beam}=20MeV	Error[1]
42.8	-0.02	0.10
74.0	0.10	0.18
118.7	0.30	0.20
133.1	0.18	0.06

CM Angle	σ/A_0[(2)] at E_{beam}=30MeV	Error[3]
36.97	1.71	0.094
50.86	1.89	0.155
85.07	0.049	0.027
95.11	0.049	0.027
129.08	1.88	0.152
143.18	1.71	0.094

CM Angle	A_y at E_{beam}=30MeV	Error[1]
44 8	-0.08	0.10
64.5	-0.03	0.13
95.1	-0.19	0.14
119.8	-0.05	0.05
138.0	-0.05	0.07

CM Angle	A_{yy} at E_{beam}=30MeV	Error[1]
44.2	0.22	0.13
64.5	0.33	0.12
95.1	0.39	0.17
119.8	0.25	0.06
138.0	0.23	0.08

CM Angle	σ/A_0[2] at E_{beam}=50MeV	Error[4]
42.25	1.604	0.077
59.52	1.015	0.075
69.03	0.391	0.044
89.58	0.064	0.026
90.588	0.064	0.026
111.27	0.391	0.044
120.83	1.015	0.075
137.64	1.604	0.077

CM Angle	A_y at E_{beam}=50MeV	Error[1]
55.2	0.059	0.071
71.1	-0.087	0.090
111.3	-0.061	0.078
120.8	0.150	0.087
138.6	0.069	0.036
148.6	0.155	0.119

CM Angle	A_{yy} at E_{beam}=50MeV	Error[1]
55.2	0.244	0.081
71.1	0.351	0.097
111.3	0.352	0.040
120.8	0.361	0.063
138.6	0.217	0.024
148.6	0.215	0.061

CM Angle	T_{20} at E_{beam}=50MeV	Error[1]
55.2	-0.69	0.24
71.5	-1.1	0.4
120.1	-0.59	0.15
138.8	-0.67	0.14

[1]Due to counting statistics, both in the in the gamma-ray spectrometers, and in the polarimeter.

[2]A_0 From a fit constrained by selected amplitudes, see Chapter 5.

[3]Due to the combination of counting statistics in the gamma-ray spectrometers, an uncertainty in the estimated background, and an uncertainty associated with the Monte Carlo correction for the effects of the solid geometry, see section above.

[4]Due to the combination of counting statistics in the gamma ray spectrometers and polarimeter, and uncertainties associated with the Monte Carlo corrections for the effects of the solid geometry and multiple scattering of the He nuclei, see section above.

4. Discussion of Recent Data and Calculations

4.1. Recent attempts to extract D-state Information; from the Data

4.1.a. Polarization Work at Tandem Accelerator Energies

The first polarization work on the $^2H(\vec{d},\gamma)^4He$ reaction was done at TUNL and reported in Weller et. al., (1984). Following the arguments of that reference and many that came later, it will be shown that because of the special symmetries of this reaction, many reasonable simplifications can be made to facilitate at least a qualitative understanding of the results. As the theoretical understanding has improved, it has been often pointed out that these simplifying arguments are only approximations, and much of the physics may be swept under the rug. An attempt will be made to address these concerns more or less chronologically as they have arisen in the course of the research.

Mandel and Flowers (1950) have pointed out that, to the extent that the magnetic multipole operator depends only upon the spin coordinates, and the electric operators only on the spatial coordinates of the nucleon,the reaction $^2H(\vec{d},\gamma)^4He$ should be dominated by E2 radiation. Furthermore, because the incident deuterons are identical bosons, only scattering states with L+S even are allowed. In the case of E1 radiation, this requirement is met only by (L=1,S=1) 1^- [i.e., the $\langle\ ^1S_0\ |E1|\ ^3P_1\ \rangle$ and $\langle\ ^5D_0\ |E1|\ ^3P_1\ \rangle$ transition matrix elements (labeled as $\langle$ ^{4}He Component | Multipolarity |Initial State $\rangle$ and with notation $^{2S+1}L_J$)]. These are zero for the normal spin independent part of the E1 operator, so transitions to the ground state (S = 0 or S = 2) will be diminished because they have $\Delta S = 1$.

Besides this, E1 is further inhibited by the isospin selection rule in self conjugate nuclei ($\Delta T = \pm 1$).

There is only one possible M1 capture amplitude, the $\langle {}^5D_0 \; |M1| \; {}^5D_1 \rangle$ and note that this term is a transition to the small D-state component in the ^{4}He ground state. The isospin selection rule should give a considerable inhibition of this $\Delta T=0$ transition (Warburton, 1969); M1 strength is thus expected to be small.

In addition to the selection rule, the magnetic part of the electromagnetic operator is reduced by a factor of $\hbar\sqrt{10} / (McR) \approx 1/20$ compared to the electric part, where M is the projectile mass, and R is the radius of the nucleus (deBenedetti, 1964).

There are three possible M2 amplitudes, but it was noted in the early work that they would manifest themselves as an odd order Legendre function (and hence an asymmetry) in the tensor analyzing power T_{20} as a result of interference with the dominant E2. M2 could not therefore be the source of the large and isotropic value of the tensor analyzing power that was observed. There was no evidence for M2 in the data of (Weller et. al. 1984, 1986).

Based on the above arguments, and on the fact that the differential cross section displayed a $\sin^2 2\vartheta$ angular distribution, Weller et. al. concluded that to a very good approximation this reaction could be considered pure E2. With this simplification they followed equations (11) and (23) through (25) of (Seyler and Weller, 1979), to write out the observables in terms of amplitudes and phases. They then made the following approximation. It was noted that some terms involved the product of two transition matrix elements that lead to the D-state. Since the D-state

admixture is small compared to the S-state, these terms are then second order to the terms that involve an interference with the S-state, and were dropped. The result of these approximations is that the tensor analyzing powers T_{20} and T_{22} are independent of angle (and hence also A_{yy}, being a linear combination of these two tensor analyzing powers), and all tensor analyzing powers are proportional to the $S = 2$ transition matrix elements, which are in turn proportional to the D-state admixture in the ground state of ^{4}He (this has been mentioned with reference to the Racah coefficient $W(x\ S\ x\ S';\ a\ 2)$ in Section 1.2). The tensor analyzing powers that were reported in this work indeed supported this prediction of isotropy, and attracted a good deal of attention to the $^2H(\vec{d},\gamma)^4He$ reaction as an excellent source of information on the D-state component in the ^{4}He ground state.

This original reference included the results of a calculation aimed at extracting a D-state probability. In this calculation the ground state and continuum wave function were constructed from two Wood-Saxon potentials which bound two point-like deuterons at 23.84 MeV with $L = 0$ (V_0 = 54.6 MeV, r_0 = 2.0 fm, a = 1.0 fm), and $L = 2$ (V_0 = 120.8 MeV, r_0 = 2.0 fm, a = 1.0 fm). Using these wavefunctions and Siegert's form of the E2 operator, the four relevant transition matrix elements were constructed, and it was found that a D-state probability of 5% produced a value of $T_{20} = -0.22$, which best fit their data.

The Lisbon group (Santos et. al., 1985) made a calculation which also included only E2 strength, but the scattering wave functions were constructed from phase shifts obtained from resonating group calculations which describe the elastic scattering data very well (Santos, 1985).

These authors used a comparison of the results of their calculation with the T_{20} data of (Weller et.al., 1984) to extract a value for the ratio ρ of the D-to-S state asymptotic normalization constants, $-0.5 < \rho < -0.4$.

The following year, (Aug '85) Mellema et. al. reported work that cast the first doubt on the validity of the assumption of a pure E2 transition (Mellema, 1985). Their work was of sufficient quality that it could be seen that A_{yy} differed slightly from isotropy, and moreover, they measured the vector analyzing power A_y and found it to be approximately the same magnitude as A_{yy}. This is significant because in a pure E2 model, a finite vector analyzing power can only arise as a result of the interference of two s =2 amplitudes and should be extremely small, and furthermore this mechanism would produce values of A_y which are asymmetric in sign with respect to 90 degrees. This was not the case, and was therefore strong evidence that non-E2 radiation contributed significantly to this reaction, at least in the region of E_d(lab) = 10 MeV. (Weller et.al. had also already reported a measurement of A_y (Weller, 1986; Osaka Conf.), and the data agree but the emphasis of Mellema's work was on the non-E2 nature of the reaction.)

All the E1 and M2 transition matrix elements have s = 1 in the continuum and, due to the aforementioned Racah coefficient, cannot effect the tensor analyzing power by interference with the dominant s = 0 E2 going to the predominant S-state in ^{4}He. They could however produce the large vector analyzing power in this way. The authors of the original reference pointed out that the existence of a vector analyzing power certainly does not invalidate their

analysis of the tensor analyzing power with regard to the D-state (Weller, 1987).

The quality of the data set, and the sophistication of the calculations has gradually improved over time. Mellema has taken enough data to have made an S-matrix decomposition at 10 and 4 MeV, indicating the existence of both E1 and M2 radiations (Mellema, 1986). Tostevin made a calculation similar to that of Santos but included these additional multipoles and used a more realistic variational calculation for the ground state which included three body force effects (Tostevin, 1986). This calculation was fairly successful in fitting the observables A_y and A_{yy}, but less successful in the T_{20} analyzing powers. Recall, as a possible explanation, that the $\langle\ ^5D_0\ |E2|\ ^5S_2\ \rangle$ and $\langle\ ^1S_0\ |E2|\ ^5S_2\ \rangle$ amplitudes are known to be highly problematic, and do not contribute to A_{yy} as they do to T_{20}.

4.1.b. Low Energy Effects

It was thought that the energy region near or below 1 MeV would be a reliable place to study the ^{4}He D-state. This was based on the assumption that the angular momentum barrier would suppress the normally dominant D wave capture to the S-state, so that the effects of the S wave capture to the D-state would be enhanced. It was also supposed that at low energies the capture reaction would only be sensitive to the asymptotic part of the wave function, providing a more reliable determination of ρ, the model independent ratio of the D-to-S state asymptotic normalization constants (Weller et.al., 1986). Wilkinson and Cecil (1985) reported the results of measurements of the Γ_g / Γ_p branching ratio for the d + d reactions for labora-

tory deuteron energies of from 50 to 150 keV. These authors found that this branching ratio was seven orders of magnitude larger than that predicted when the $^2H(\vec{d},\gamma)^4He$ cross section is computed as an E2 transition with no D-state in ^4He. Since the ratio of the penetrabilities for D-waves to S-waves at this energy is on the order of 10^{-7}, S-wave capture to the D-state has been taken as a likely explanation (Weller, 1987) (Wilkinson and Cecil actually suggested M1 may be responsible for the enhancement of the cross-section, but that comes from a D-wave scattering state, which is suppressed by the angular momentum barrier).

Noting that S-wave capture will show up in the gamma ray yield at ninety degrees, the TUNL group undertook to measure the differential cross section, at energies in the few MeV region (Weller, 1986). A calculation was made that followed along the lines of (Santos et.al., 1985) and since Coulomb effects are important at lower energies, they were included in this calculation. The Coulomb effect was estimated using an energy dependent Coulomb penetration factor P_C for each E2 amplitude. P_C was assumed to be given as the square of the ratio between the E2 amplitude calculated with a distorted wave generated by representing each deuteron as a uniform charge distribution with a radius equal to the deuteron rms radius, and the E2 calculated from a plane wave of the same energy. The data of (Weller, 1986) clearly showed increasing yield at ninety degrees relative to 135 degrees, as the energy is decreased. The ratio $R = \sigma(\pi / 2)/\sigma(3\pi /4)$ is shown in Figure 4.1 along with the curves from their calculation using various values for ρ. The results of this same calculation along with the measured integrated cross section is shown in Figure 4.2. This work illustrated both the

change in the magnitude of the cross section and the change in shape of the differential cross section as function of energy. In this work the authors deduced a value of $-0.25 < \rho < -0.15$, and made a good qualitative description of the behavior of this reaction at low energies based on S-wave capture to the D-state.

The low energy work continued at TUNL with polarization measurements that are reported in (Weller et.al.,1986; Langenbrunner et.al. 1988). In this reference however the authors compare their data to the results of a new calculation from the Erlangen group (Wachter, 1988) and as a result dismiss the effects of S-wave capture to the D-state in ^{4}He. This calculation will be discussed in more length in the next section, but briefly, it is a resonating group calculation but with the p-^{3}H, and n-^{3}He channels included in the scattering wave-function. This calculation was published in the context of explaining the 10 MeV data of (Mellema et.al., 1986), but these authors applied it to their 1.2 MeV data, and found it successful there as well. This calculation implied, in stark contrast to the conclusions of (Weller et.al. 1986), that S-wave capture to the D-state of ^{4}He contributed to the 1.2 MeV cross section at less than the one percent level. The enhancement to the cross section and to the ninety degree yield at low energy was, in part, the result of P-wave M2 and E1 capture to broad 1^- and 2^- resonances that were reported in refs (Gruebler, 1981; Friarman, 1973). Presumably the phase shifts from these resonances were included in the construction of their RGM scattering states, and manifest themselves in the capture channel through the enhancement of the P-wave capture amplitudes in this way.

In conclusion, two startling low energy effects have been reported: (1) the total cross section is enhanced and (2) the shape of the differential cross section is different. This has been interpreted in two contrasting ways, one as a D-state effect and the other as a resonance effect. The D-state interpretation is a simple result of the angular momentum barrier not affecting the S-wave capture. S-wave capture is difficult to interpret because the S-wave scattering state is known to be highly distorted, and the $\langle\ ^1S_0\ |E2|\ ^5S_2\ \rangle$ amplitude involves the deuteron D-state. None the less, reference (Weller et.al., 1986) made a convincing argument that low energy capture provided a powerful amplifier of D-state effects. S-wave capture must involve a D-state, either in ^4He or ^2H. One must conclude however that these arguments are too simplistic, based on the more recent article (some of the authors are the same), and other recent theoretical work (Bluge, 1987). The more sophisticated calculation showed that the data could certainly be described with very little S-wave capture, and the D-state playing only a minor role at 1.2 MeV.

4.1. Table of Amplitudes

Multipole	Allowed Amplitude	Comments
E1	$\langle\ ^1S_0\ \|E1\|\ ^3P_1\ \rangle$	Inhibited due to spin* and isospin
	$\langle\ ^5D_0\ \|E1\|\ ^3P_1\ \rangle$	" "
E2	$\langle\ ^1S_0\ \|E2\|\ ^1D_2\ \rangle$	Dominant.
	$\langle\ ^1S_0\ \|E2\|\ ^5S_2\ \rangle$	Involves deuteron D-state.
	$\langle\ ^5D_0\ \|E2\|\ ^5S_2\ \rangle$	S-wave capture to D-state. Affected by distortion
	$\langle\ ^5D_0\ \|E2\|\ ^5D_2\ \rangle$	D wave capture to D-state.
	$\langle\ ^5D_0\ \|E2\|\ ^5G_2\ \rangle$	G wave capture to D-state.
M1	$\langle\ ^5D_0\ \|M1\|\ ^5D_1\ \rangle$	Inhibited by isospin.
M2	$\langle\ ^1S_0\ \|M2\|\ ^3P_2\ \rangle$	The magnetic operator is down by a factor of $\hbar\sqrt{10}/(McR) \approx 1/20$ from the electric operator of the same multipolarity.
	$\langle\ ^5D_0\ \|M2\|\ ^3P_2\ \rangle$	
	$\langle\ ^5D_0\ \|M2\|\ ^3F_2\ \rangle$	

Because the projectile and target are identical bosons, only amplitudes with L+S even are allowed. They are tabulated here labeled as ⟨4He Component | Multipolarity | Initial State⟩ and with notation $^{2S+1}L_J$.

* There are spin dependent parts of these operators and the comment about inhibition doesn't apply to these.

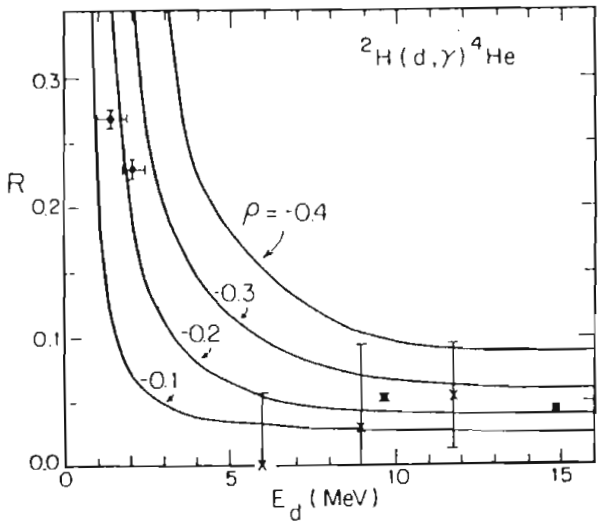

Figure 4.1. The ratio $R = \sigma(\pi / 2)/\sigma(3\pi /4)$ shown along with the curves from their calculation using various values for ρ. From (Weller et.al., 1986).

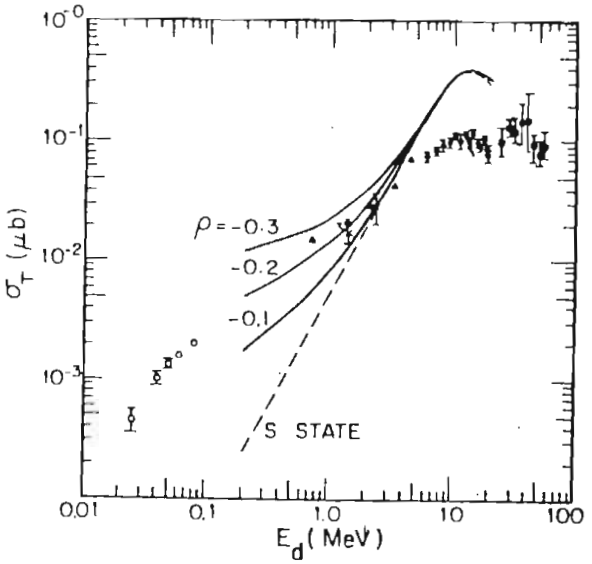

Figure 4.2. The measured integrated low energy cross-section shown along with the curves from a calculation using various values for ρ. From (Weller et.al., 1986).

4.2. Calculations of The ^{4}He D-state from Modern Nucleon-Nucleon Potentials

Modern theoretical nucleon-nucleon potentials include a tensor force, and will thereby produce D-states in nuclei built up of such potentials. One should be able to derive the ^{4}He D-state directly from such a potential, without recourse to data, except in the indirect sense that the potentials are derived from some data. Attempts have been made to do this. There is however, much technical difficulty in solving the four body equations using such potentials. Various methods have been employed, yielding unfortunately, various results. Along with the D-state probability, other fundamental properties of the system, such as binding energy, RMS radius, and excited states are usually obtained. The overall success of a potential and a calculational method must be judged on it's ability to reproduce all of these quantities.

Some insight into the question of the ^{4}He D-state probability is gained by thinking of the ^{4}He wave-function as being made up of a combination of deuteron wave-functions. There are six possible combinations of the four nucleons in ^{4}He and about half the time each pair is in a S = 1, T = 0 state that can be considered a deuteron (Chen, 1986). One therefore might expect to have around three times the deuteron's D-state in ^{4}He. Three times 4 to 7 percent is 12 to 21 percent.

Sakai et.al.(1974) found, with an ATMS calculation using the Hamada-Johnson potential that the 4He nucleus could have a 12.8 percent D-state probability, but only gave an upper bound on the ^{4}He binding energy.

Ballot (1983) calculated the ground state, and first excited 0+ state binding energies in 4He. He used the hyperspherical method (Ballot, 1981) for the Gogny-Pires-de Tourreil (GPDT) potential (Gogny, 1970), and for two super soft core potentials (SSC.B and SSC.C) constructed by Tourreil and Sprung (Tourreil, 1973). With neglect to the Coulomb effect, the ground state energies were found to be -30.1, -25.88, and -21.19 MeV respectively. The first two potentials produced a bound 0+ excited state, at energies 25.66 and 25.11 MeV above the ground state respectively. This calculation produced values of the D-state probability in the ground state of 7.83 percent for the GPDT, 12.99 percent for the SSC.B, and 12.98 percent for the SSC.C potentials. A D-state probability of 2.85 percent and 3.07 percent was predicted for the excited state by the GPDT, and SSC.B potential. All three potentials produce a slightly large value of the RMS radius, of 1.64, 1.55, and 1.61 fm, compared with the experimental value of 1.44 fm. In summary, this set of calculations over-binds the ^{4}He nucleus by 1.7 MeV for the GPDT potential, and under-binds it by around 3 MeV for the SSC potentials. The first two potentials produce a bound excited state that isn't observed. The GPDT gives 7.83 percent, while the SSC's predict nearly 13 percent D-state component in 4He.

Paul Goldhammer (1984) used a version of the Brillouin-Wigner perturbation method (1933; 1935) with the Paris potential, to perform a variational calculation of the binding energy, D-state probability and RMS radius of ^{4}He. The values obtained were -25.5 MeV, 5.36%, and 1.28 fm. A coulomb correction establishes an upper bound of -24.1 MeV on the binding energy. The calculation significantly under-binds, and produces too small a radius for 4He. Gold-

hammer also points out that the value of 5.36% D-state is surprisingly low, particularly in sight of the fact that the Paris potential predicts 5.77% in the deuteron. This he explains by noting that for the tensor interaction, the three body terms make a contribution opposite in sign to the two body terms. This effect is obviously absent in ^2H, and plays a minor role in ^3H, but is important in ^4He due to the increasing number of three body terms relative to two body terms. Moszkowski (1981) finds that the same effect plays a role in nuclear saturation.

Meder (1988) made a shell-model calculation of the ^3H and ^4He ground state wave functions using effective interactions derived from the Reid Soft Core (RSC) and Paris potentials. A $6-\hbar\omega$ model space was used and the results for ^3H are in close agreement with essentially exact Faddeev calculations. The binding energy and D-state probability in ^4He was found to be 23.5 MeV and 16.7 percent for the RSC, and 23.7 MeV and 14.2 percent for the Paris potential.

The RGM calculation that is described in more detail in the next section derived a ^4He D-state of only 2.2 percent. The authors failed to make it entirely clear however that is is only in the two deuteron part, and the D-state probability in the entire ^4He wave-function should be higher. It must also be pointed out that this is from a nucleon-nucleon interaction of their own construction that is described as semirealistic.

The results of a Green's function Monte Carlo (GFMC) calculation have been recently published (Carlson, 1988). This calculation differs from those just mentioned, in that it makes no approximation in the form of the potentials, and through the use of numerical sampling methods,

is able to solve the four nucleon problem to arbitrary accuracy(Friar, pr. com.). This is an improvement in that observables are related directly to the potential used, without the approximations made in the solution contributing to the confusion. In this work the ground state properties of ^{4}He are calculated using a Ried *V*8 potential with the GFMC method, and also with a variational method. Reasonable agreement is seen between the methods in all ground state properties. A value of 15.5% was obtained for the D-state probability, compared to 14.8% using the same potential, but with the variational method. In this same reference the result of variational calculations using a variety of potentials are also presented. The Argonne *V*14, Nijmegen, and Reid *V*8 interaction models all give variational binding energies of around 23 MeV, significantly less than the experimental value (28.3 MeV). These produce 13.7%, 12.7% and 14.8% D-state respectively. The Urbana model-7 three-body-interaction improves the binding energy result when added to the Argon and Nijmegen N-N interactions. This shouldn't be surprising because this three body interaction was designed to fit the binding energy when added to the Urbana potential. This addition increased the D-state probability predictions from 13.7% to 17.5%, and from 12.7% to 15.2% for these potentials.

If a conclusion can be drawn from the recent calculations, it is that calculation of the D-state probability is highly sensitive to the model and method used. A wide range of results have been attained, even with the same potential, for example Goldhammer attains 5.36 percent while Meder gets 14.2 percent ^{4}He D-state probability, both using the Paris potential, and being in relative agreement on the binding energy (although not in agreement with experiment). Goldhammer's statement about the low

value he has attained being a result of a cancelation due to the three-body tensor terms being opposite in sign to the two body terms, hints at a curious aspect of this work, but doesn't seem to agree with Carlson's result. Perhaps when complete four body calculations are done with more sophisticated potentials, the ^{4}He D-state will provide new information about the three-body force. Much remains to be done before any quantitative conclusion can be drawn from these calculations.

4.3. The RGM Calculation

The most recently published theoretical work on the $^2H(\vec{d},\gamma)^4He$ reaction is the coupled channel resonating group calculation of (Wachter, Mertelmeier, and Hofmann, 1988). This work treats the incoming channel in a much more sophisticated way, but still suffers from the use of only a semi-realistic nucleon-nucleon force, and doesn't include the deuteron D-state. In this publication, the authors show good agreement with the 10 MeV data (Mellema et.al., 1986), but as mentioned above, a later publication showed that the calculation worked well at 1.2 MeV as well. This calculation has also been compared to the data of this dissertation at energies up to fifty MeV. There is qualitative agreement in this region, despite the fact that the $\langle\ ^5D_0 \mid E2 \mid\ ^5G_2\ \rangle$ amplitude is not included in the calculation, but should contribute significantly in this energy region (Eiró, private communication).

These authors (Wachter et.al., 1988) state that because the incoming deuterons are large relative to ^{4}He wave-function, proper antisymmetrization of the wave-function destroys the identity of the deuterons. They therefore intro-

duce ^{3}H-p and ^{3}He-n components to the final-state wavefunctions. They start with a so-called "semi-realistic" nucleon-nucleon force derived in earlier work from that group (Mertelmeier, 1986), which contains Coulomb, central, spin-orbit, and tensor components. Angular momenta up to *l* =2 were included in the relative motion of the fragments in the scattering state. No internal angular momentum (D-state) was included in any of the fragments. The ground state was made up of these fragments as well, as a linear combination of $^1S_0$(^{3}H-p), $^1S_0$ (^{3}He-n), $^1S_0$(d-d), and $^5D_0$ (d-d) components, in the most tightly bound 0^+ configuration. This led to the coupled channel nature of the calculation. For example, calculation of the E2 included the seven coupled channels; $\langle ^1S_0(^3\text{H-p}) \; |E2| \; ^1D_2 \rangle$, $\langle ^1S_0(^3\text{H-p}) \; |E2| \; ^3D_2 \rangle$, $\langle ^1S_0 \; (^3\text{He-n}) \; |E2| \; ^1D_2 \rangle$, $\langle ^1S_0 \; (^3\text{He-n}) \; |E2| \; ^3D_2 \rangle$, $\langle ^1S_0(\text{d-d}) \; |E2| \; ^1D_2 \rangle$, $\langle ^1S_0(\text{d-d}) \; |E2| \; ^5D_2 \rangle$, and $\langle ^5D_0 \; (\text{d-d}) \; |E2| \; ^5S_2 \rangle$. E1, M1, and M2 transitions were also calculated in this way. Notably lacking is the $\langle ^1S_0 \; (\text{d-d}) \; |E2| \; ^5S_2 \rangle$ amplitude, as this is the transition that involves an internal D-state of the deuteron, which isn't included in this calculation. This amplitude could be important at low energy. Also note that the $\langle ^5D_0 \; (\text{d-d}) \; |E2| \; ^5G_2 \rangle$ amplitude is not included. According to Eiró the G-waves contribute at the ~ 7% level at fifty MeV (See Table 1.3).

The matrix elements were calculated over the range of energies from a few keV up to 50 MeV, but the authors of ref.(Wachter, 1988) only compared it to the the astrophysical s-factor as a function of energy, and to the data set at 10 MeV. Besides the fact that the most complete data set exists at 10 MeV, this is probably also the energy where this calculation is most appropriate, in light of the deficiencies at high and low energies, mentioned above. In (Langenbrunner, et.al.,1988) observables are compared to

this calculation at E_d = 1.2 MeV, and reasonable agreement is seen. The startling statement is made on the basis of this calculation that S-wave capture to the D-state of ^{4}He contributes to the cross section of this reaction at less than the one percent level at 1.2 MeV. Besides the lack of a deuteron D-state in this calculation, it is stated in (Wachter, et.al., 1988) that because of the simplistic nature of the n-n interaction used, the calculated d-d threshold is too low in energy, so the P-wave resonances may contribute more than they should at this energy. While shedding some light on this reaction, this calculation has raised many questions, and clearly should be improved. Use of a more realistic nucleon-nucleon force, inclusion of the deuteron D-state, and inclusion of higher partial waves (G-waves), would help to clarify the situation.

In addition to the lack of G-wave amplitudes in the RGM calculation of (Wachter, et.al., 1988), the calculation was not made with the energy range of thirty to fifty MeV in mind. These authors did calculate matrix elements in this energy region, but little care was taken with numerical stability (Hofmann, private communication). Despite the shortcomings of this calculation, it was compared to the present data in the energy region up to fifty MeV.

When the matrix elements of the Erlangen group were first used to calculate observables in this energy region, it was found that the values displayed some wild resonance-like structure, particularly at the high energy limit of this work (50 MeV). On close inspection of the individual matrix elements as a function of energy, it was noted that there were certain singular deviations from smooth curves. Following (Hofmann, pr. com.), the matrix elements were smoothed as a function of energy. Although it is difficult

to defend this approach on rigorous grounds, it isn't at all unreasonable, because the matrix elements did follow smooth curves in general, and the wild excursions were clearly the result of incomplete convergence of the calculation at certain energies. The matrix elements and the smoothing that was done are shown in Figure 4.3.

It should be pointed out that these matrix elements were calculated before this data existed (or any in this energy region). The authors of this calculation have promised (Hofmann, pr. com.) that the calculation is being redone with a more realistic N-N force. Though they are apparently unable to invest in the additional complexity of inclusion of G-waves, hopefully the numerical stability problem will not exist in the future calculation.

4.4. The RGM Calculation Compared to the Data

This calculation is in qualitative agreement with the data as a function of energy, from threshold up to fifty MeV. This is presumably a result of the extensive scattering data set that is included in the construction of the RGM continuum matrix elements. The observables are shown as functions of energy, along with the results of the calculation in Figures 4.4 - 4.5.

In conclusion, the coupled channel resonating group model with the particle channels included has some very impressive agreement with experiment over the entire energy range up to fifty MeV. The recent calculations of Wachter et.al.(1988) and the comparison to low energy data in Langenbrunner, et.al.(1988) draw some conclusions that are very specific, and are at odds with previous calculations (Santos, 1986; Weller, 1986; Tostevin, 1986). It is

the opinion of this author that the qualitative agreement at all energies is the result of the coupled channel nature of this problem, and that the particle information is included in the formation of the RGM wave functions. Clearly this isn't the simple pure E2 reaction, at all energies, but it is also unwise to accept the very specific predictions of this model insofar as resonance effects are concerned. At very low energy this model predicts that the entire magnitude of the tensor analyzing power arises as a result of E1-M2 interference. This model also predicts that at higher energies, the tensor analyzing power is coming from E2-E2 interference at a level more in agreement with the general wisdom for the last several years. This coupled channel RGM is clearly a more sophisticated approximation of nature than the work that has preceded it, but this particular calculation lacks the precision that would be needed to draw some of the conclusions that have been drawn from it.

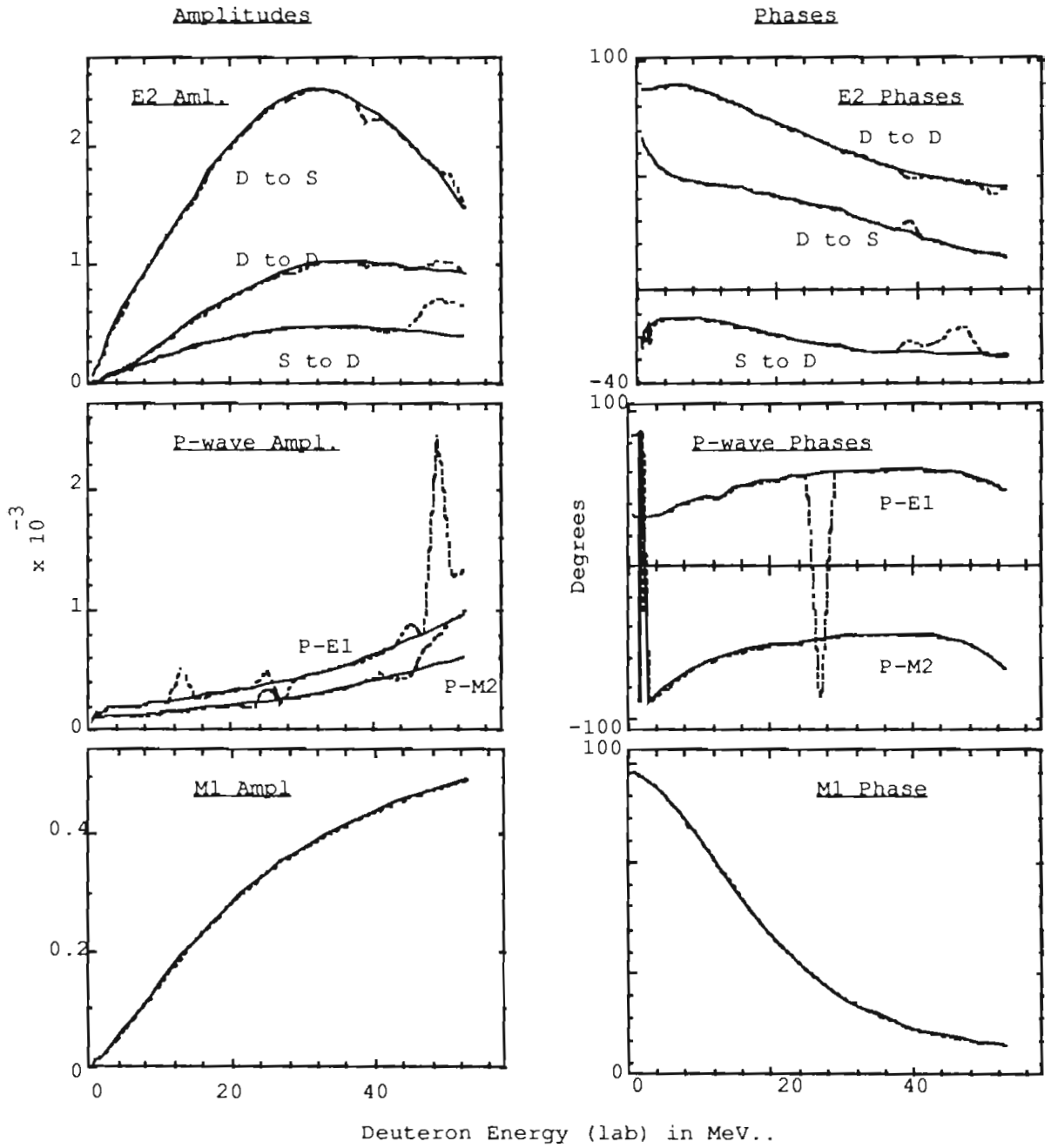

Figure 4.3. The RGM matrix elements from Hofmann et.al.,and the smoothing that was done.

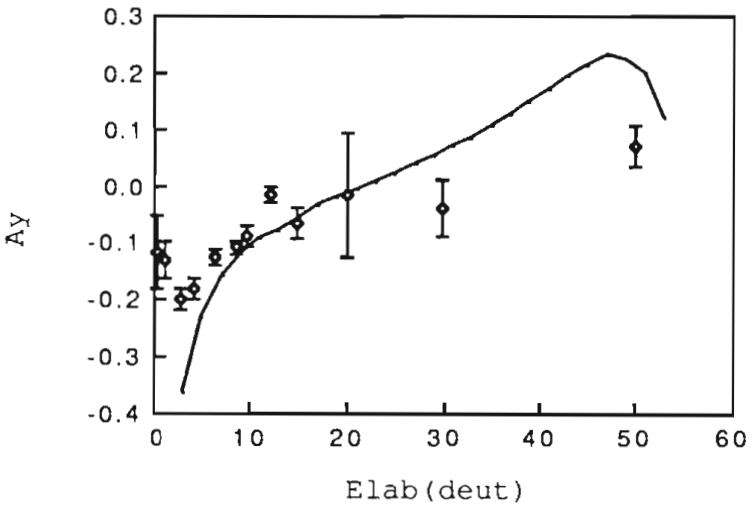

Figure 4.4. A_y ($\vartheta\gamma$= 130 degrees)as a function of energy. The curve is the calculated using energy smoothed RGM matrix elements from Hofmann (private com.).

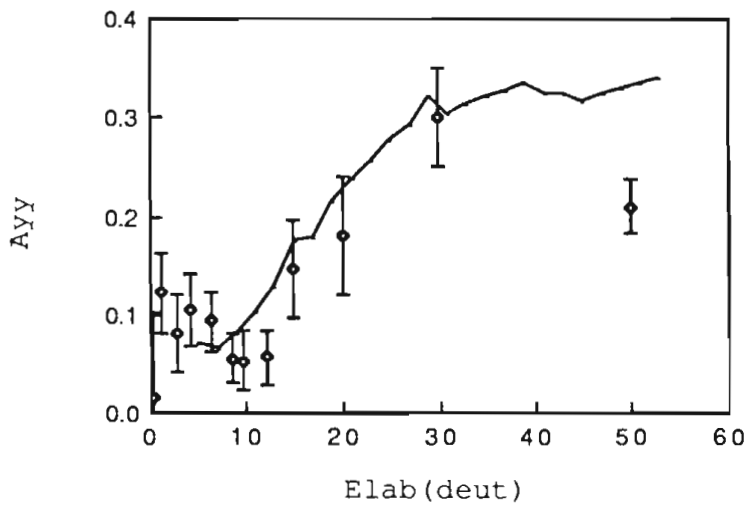

Figure 4.5. A_{yy} ($\vartheta\gamma$= 130 degrees) as a function of energy. The curve is calculated using energy smoothed RGM matrix elements from Hofmann (private com.).

4.5. A Direct Capture Calculation

A direct capture calculation was performed under the assumption of a pure E2 transition, as has been discussed. In this calculation, observable were computed from matrix elements of the form $\langle u | r^2 | \Psi \rangle$ where u is the bound state wave-function, Ψ is the continuum wave function and r^2 is the E2 operator in the long wavelength limit. These wavefunctions were constructed from potentials: The bound state potential was a Woods-Saxon well of Tostevin (1986) which is a parameterization of a microscopic potential of Schiavilla, (1986). The parameters are given in Table 4.2. The continuum potential was produced by an optical model fit to the $^2H(d,d)^2H$ elastic scattering data at 30 MeV (Nemets, 1985) and 50 MeV (Alderliesten, 1978). The parameters are also given in Table 4.2 and the fits are shown in Figure (4.6).

The value of Ayy predicted by this calculation is proportional to the amount of D-state included in the ground state of ^4He. This value was varied, and it was found that a 3.2 percent admixture best fit the data at 30 MeV. This seems to be a smaller number than predicted by most of the theories discussed in Section 4. It must however be noted that like the calculation of (Wachter,1988) this is only the $l = 2$ probability when ^4He nucleus is in a two deuteron configuration and isn't the entire D-state. This number is also similar to the 2.2 percent result of Wachter.

At 50 MeV, this calculation failed entirely to predict the data. The relative phase between the two D-wave capture amplitudes had passed though ninety degrees, contributing a negative value to A_{yy} in disagreement with the data. In addition, the model predicted that G-wave capture to the D-

state would be the dominant capture amplitude. G-waves were dominant even over the D-wave capture to the large S-state. This is an interesting prediction, because if it is true, the reaction mechanism at this energy will be dominated by a D-state effect. This calculation is presently at too crude a level for statements like that to be made with certainty, but it does suggest that the calculations of Hofmann that do not include G-wave capture at any level should not be applied at 50 MeV. The group of Santos et.al. has calculated that G-wave capture contributes at the 5 percent level at 50 MeV. Though that isn't in agreement with this result, it does corroborate the importance of G-wave capture at this energy.

The results of the direct capture calculation are included in Figures 4.8 - 4.10. The optical model fits to the elastic scattering data that were used to determine the scattering state potentials are shown in Figure 4.6. The. potential parameters are tabulated below.

Table 4.2. Table of Potential Parameters for the Direct Capture Calculation

Bound State Potentials

	V(MeV)	r_0(fm)	a(fm)
$^1S_0$	61.0	1.67	0.75
$^2D_0$	114.6	2.10	0.90

Optical Model Scattering Potentials

	30 MeV	50 MeV
V=	48.0 MeV	78.6 MeV
r_0=	1.67 fm	1.67 fm
a=	0.696 fm	0.696 fm
W_V=	0.02 Mev	0.010 MeV
r_V=	1.67 fm	1.67 fm
a_V=	0.75 fm	0.75 fm
W_D=	2.153 MeV	4.430 MeV
r_D=	1.67 fm	1.67 fm
a_D=	0.75 fm	0.75 fm

Figure 4.6. The elastic scattering data at 50 MeV (Alderliesten, 1978) (bottom), and at 30 MeV (Nemets, 1985) (top). The curves are the optical model fits that were used to produce the scattering state potentials that were employed in the direct capture calculation.

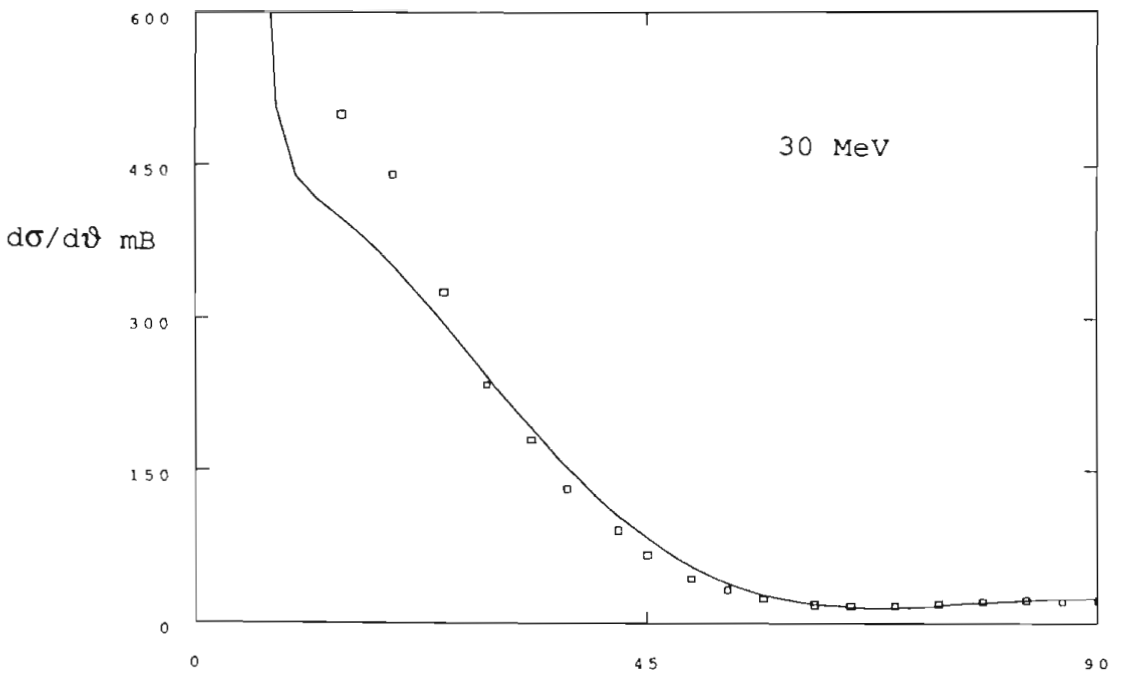

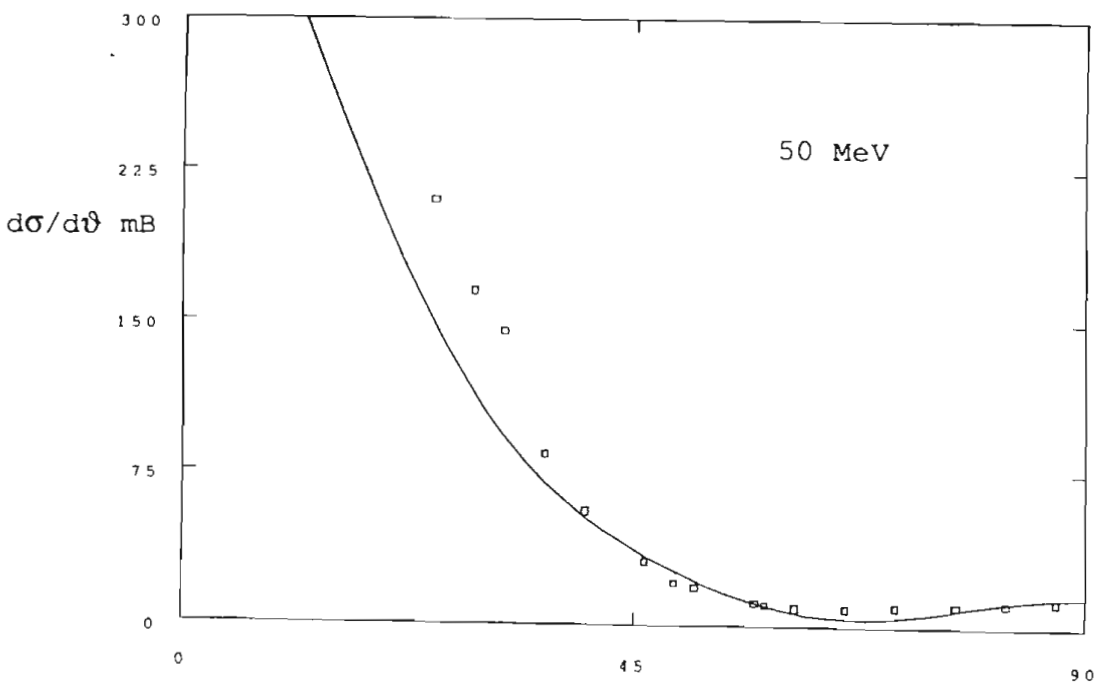

CM Angle (degrees)

Figure 4.7. A_y (ϑ_γ), and A_{yy} (ϑ_γ), (E_d = 20 MeV). The curve is from the RGM calculation (Wacher, 1988).

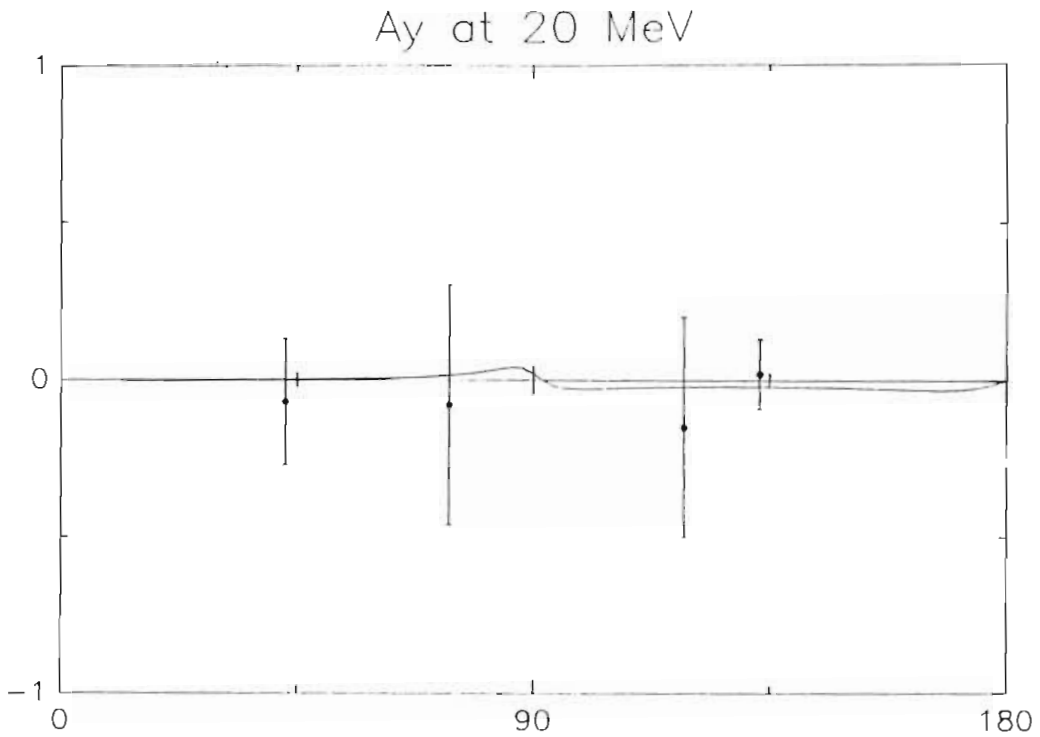
Ay at 20 MeV
1
0
−1
0
90
180

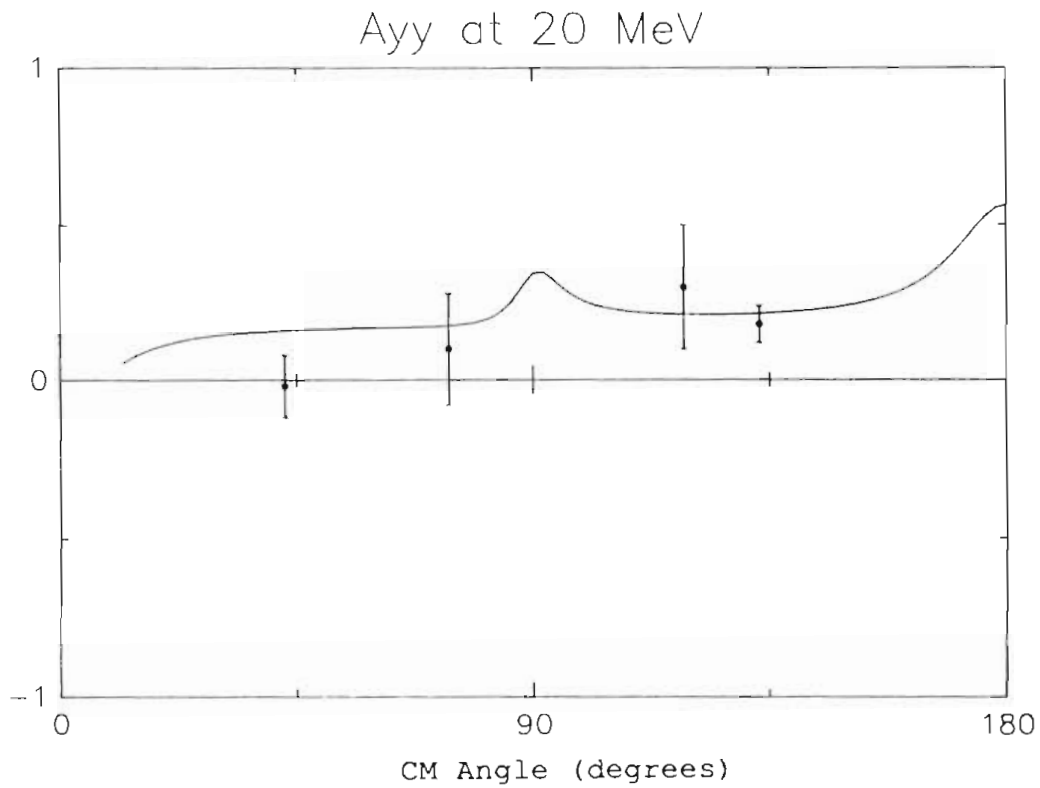
Ayy at 20 MeV
1
0
−1
0
90
180
CM Angle (degrees)

Figure 4.8. $\sigma(\vartheta_\gamma)$, $A_y(\vartheta_\gamma)$, and A_{yy} (ϑ_γ), (E_d = 30 MeV). The dashed curve is from the RGM calculation (Wacher,1988). The dot-dashed curve is from the direct capture calculation. The plain curve is from a fit to allowed amplitudes and phases, (see Section 5).

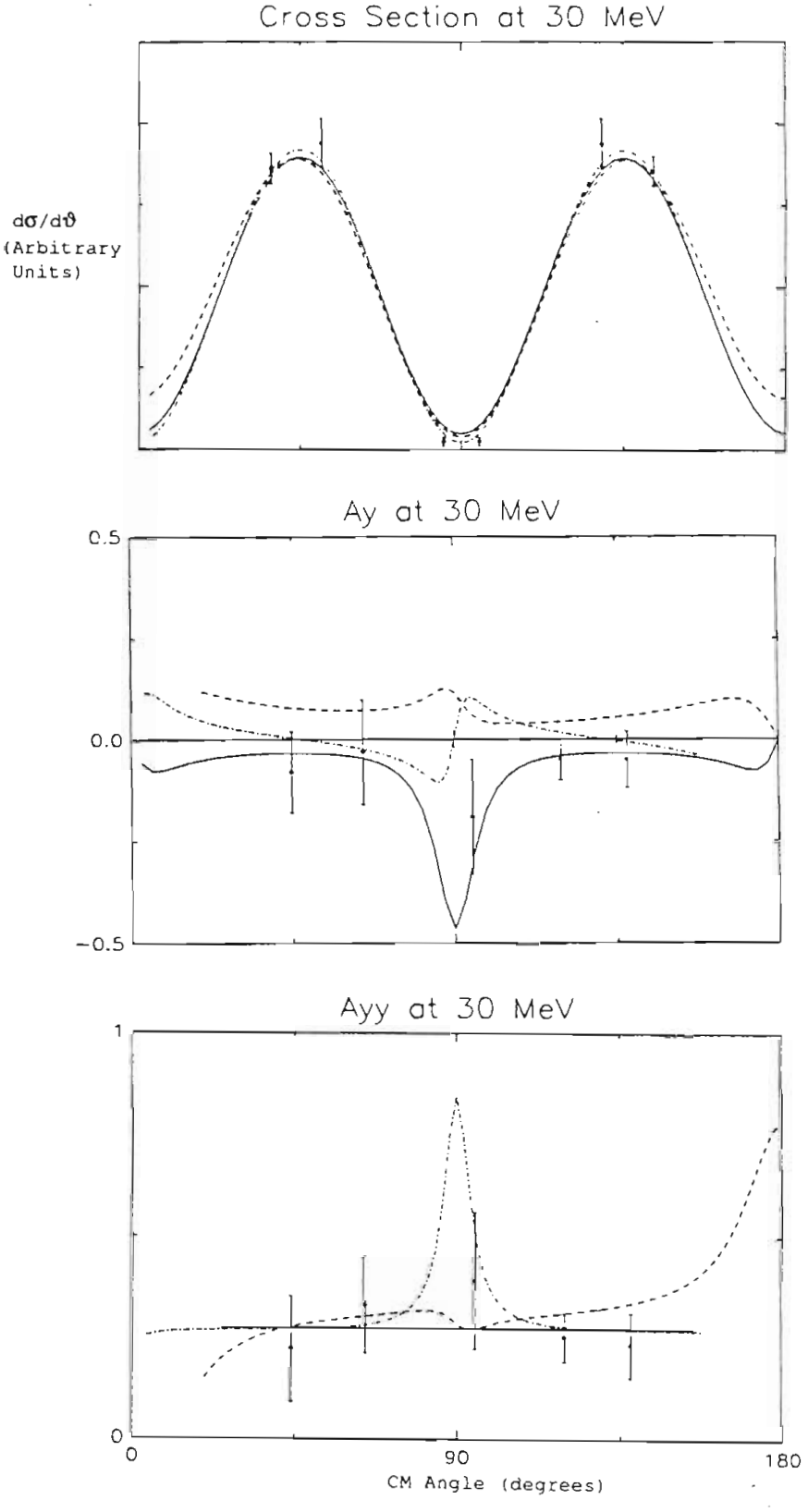
Cross Section at 30 MeV
dσ/dϑ
(Arbitrary
Units)
Ay at 30 MeV
0.5
0.0
−0.5
Ayy at 30 MeV
1
0
0
90
180
CM Angle (degrees)

Figure 4.9. $\sigma(\vartheta_\gamma)$ and A_y (ϑ_γ), $(E_d = 50$ MeV). The dashed curve is from the RGM calculation (Wacher,1988). The dot-dashed curve is from the direct capture calculation. The plain curve is from a fit to allowed amplitudes and phases, (see Section 5).

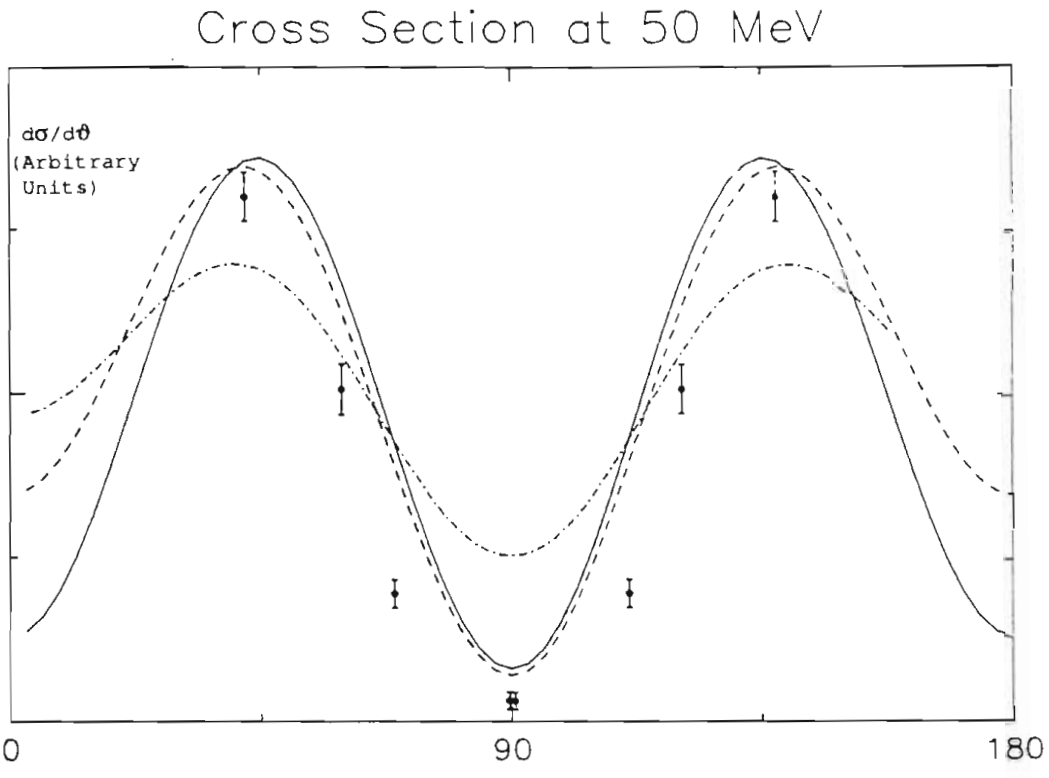
Cross Section at 50 MeV
dσ/dθ
(Arbitrary
Units)
0
90
180

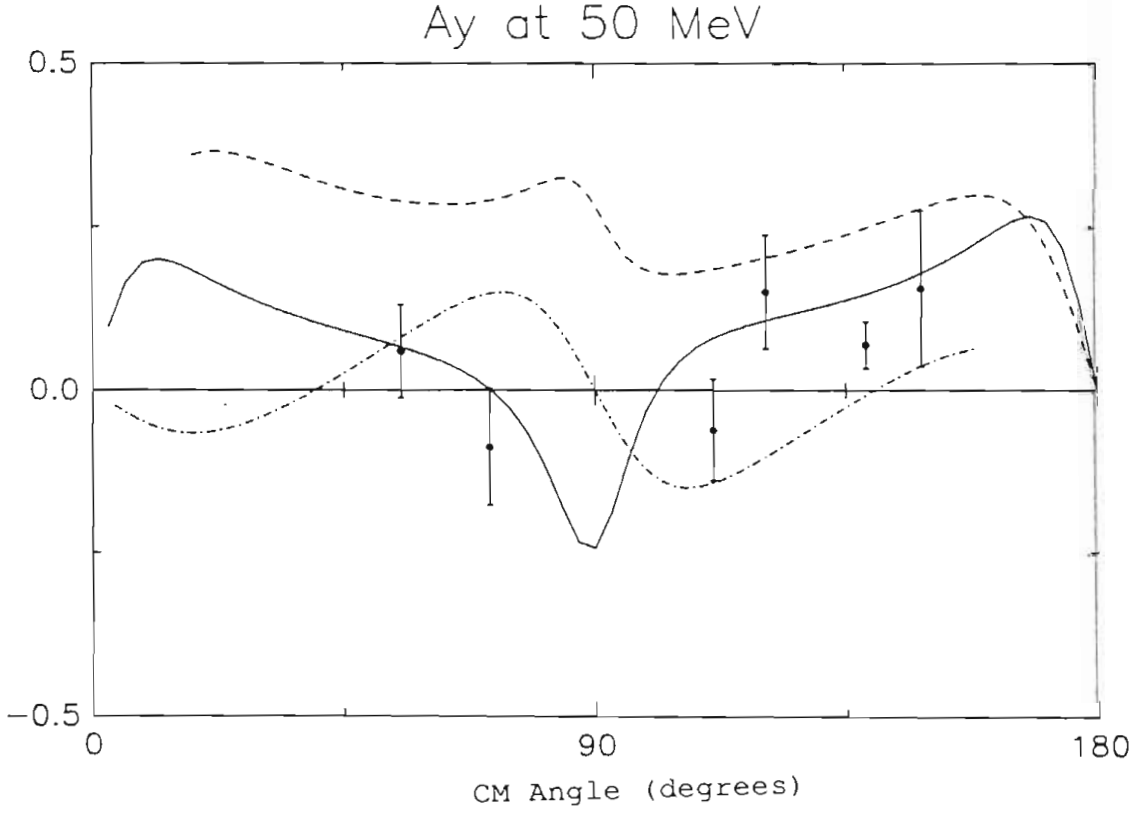
Ay at 50 MeV
0.5
0.0
−0.5
0
90
180
CM Angle (degrees)

Figure 4.10. A_{yy} (ϑ_γ) and T_{20} (ϑ_γ), (E_d = 50 MeV). The dashed curve is from the RGM calculation (Wacher,1988). The dot-dashed curve is from the direct capture calculation. The plain curve is from a fit to allowed amplitudes and phases, (see Section 5).

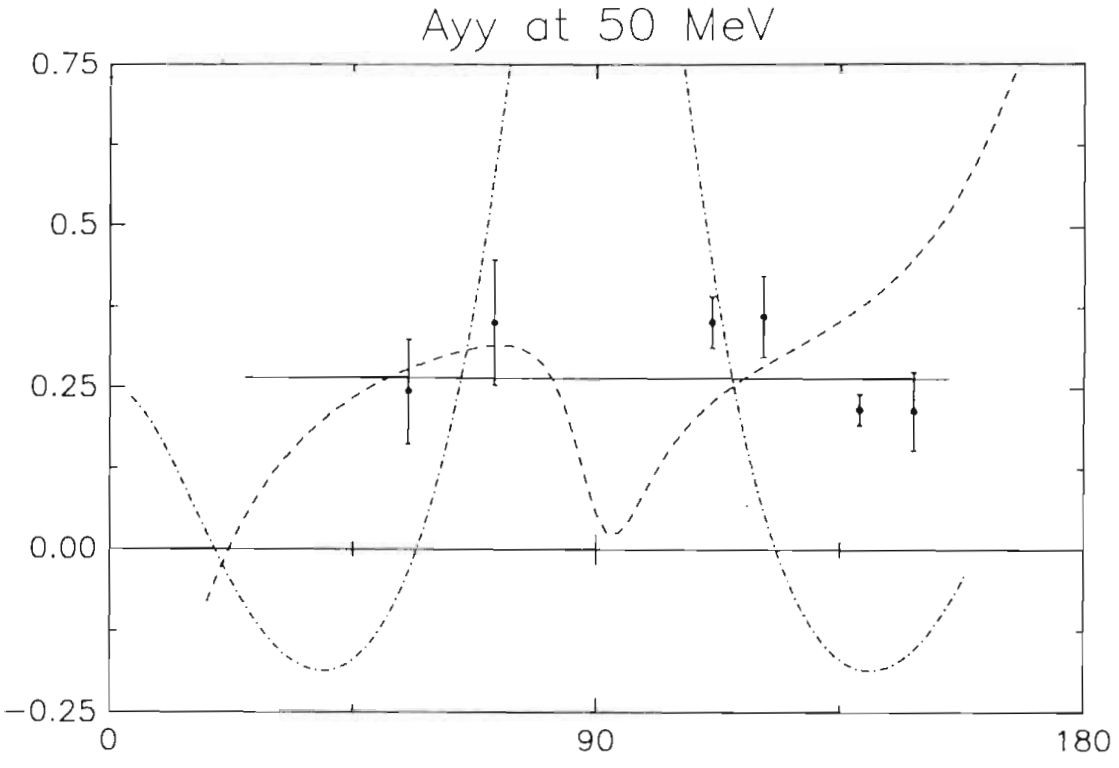
Ayy at 50 MeV
0.75
0.5
0.25
0.00
−0.25
0
90
180

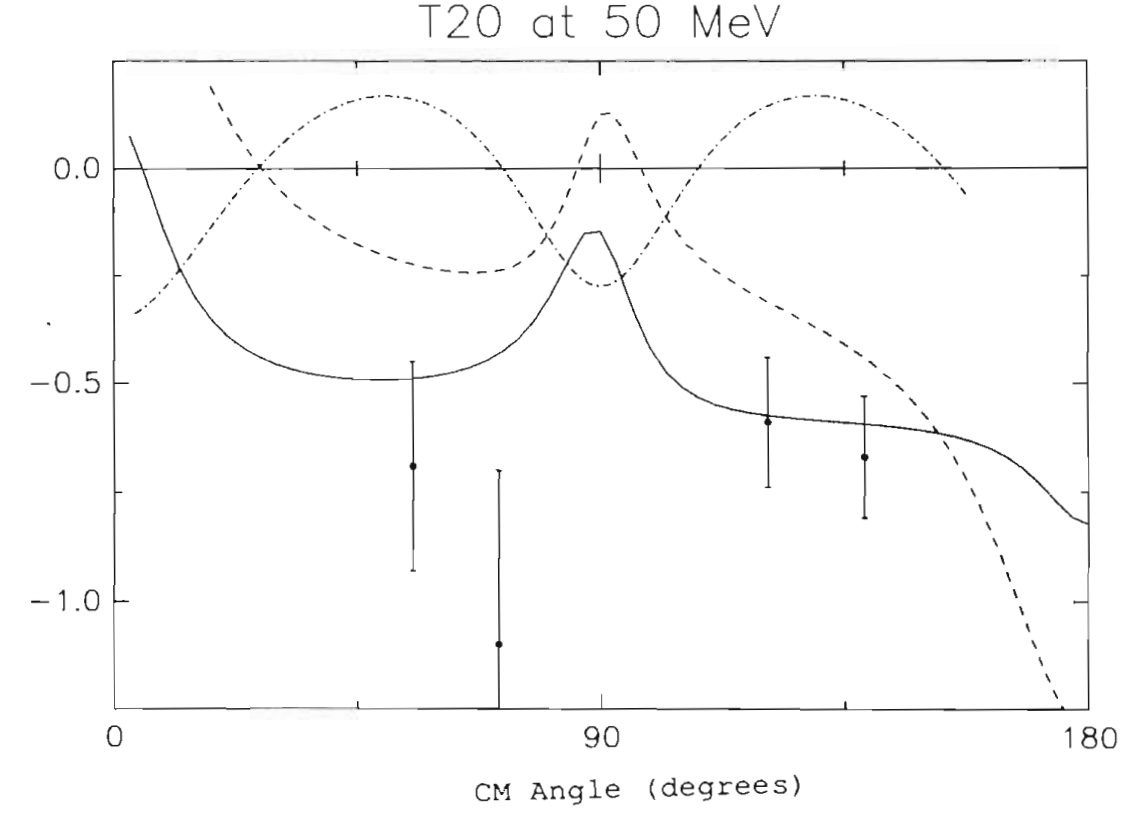
T20 at 50 MeV
0.0
−0.5
−1.0
0
90
180
CM Angle (degrees)

5. Transition Matrix Element Element Analysis and Legendre Fits

Transition amplitudes and phases can be determined from a transition matrix element analysis of data (Seyler, 1979). Because of the large number of amplitudes and phases consistent with angular momentum conservation in the $^{2}H(d,\gamma)^{4}He$, it was necessary to make some simplifying physical assumptions.

The symmetries of the spherical tensors, the Legendre functions and the rotation group imply that the observables can be expressed in the following way:

$$\sigma(\vartheta) = A_0\left(1 + \sum_{k=1} a_k P_k(\cos\vartheta)\right),$$

$$A_y(\vartheta)\sigma(\vartheta) = \frac{2}{3} A_0 \sum_{k=0} b_k P_k^1(\cos\vartheta),$$

$$T_{20}(\vartheta)\sigma(\vartheta) = A_0 \sum_{k=0} c_k P_k(\cos\vartheta) \quad .$$

The relationships between transition matrix elements and observables depend on the selected angular momentum coupling representation. The channel spin coupling scheme has been employed in the analysis of the data of this experiment. Let the angular momentum of the $^{2}H(d,\gamma)^{4}He$ reaction be specified as $\vec{a}(\vec{X},\vec{L})\vec{c}$, where $\vec{a}$ is the spin of the target, $\vec{X}$ the spin of the incident projectile, $\vec{L}$ the multipolarity of the emitted γ-ray and $\vec{c}$ the spin of the residual nucleus. Then

$$\vec{X}+\vec{a}=\vec{S}, \quad \vec{l}+\vec{S}=\vec{j}, \quad \text{and} \quad \vec{L}+\vec{c}-\vec{j},$$

where $\vec{S}$ is the channel spin of the reaction, $\vec{l}$ is the orbital angular momentum of the incident projectile and $\vec{j}$ is the total angular momentum of the system. With this

coupling scheme the a_k, b_k, and c_k coefficients are derived in equations 20-23 of (Seyler,1979) and are repeated here.

$$a_k = \sum_{tt'} (-1)^{s-c+1} [\,] \hat{l}\hat{l}'\hat{L}\hat{L}'\hat{b}^2 \hat{b}'^2 (l0, l'0|k0) W(lbl'b'; sk)(L1'L'-1|k0)$$
$$\times W(LbL'b'; ck)\delta_{ss} \mathrm{Re}(R_t R_{t'}^*),$$

$$b_k = \frac{3\sqrt{x}\,\hat{x}\hat{k}}{[(x+1)k(k+1)]^{1/2}} \sum_{tt'} [\,] s\hat{s}'\hat{l}\hat{l}'\hat{L}\hat{L}'\hat{b}^2 \hat{b}'^2 (-1)^{a-x+c-b+1} (l0, l'0|k0)$$
$$\times W(xsxs'; a1)(L1'L'-1|k_0)(L1'L'-1|k0) W(LbL'b'; ck)$$
$$\times X(lsb; l's'b'; k1k) \mathrm{Re}(iR_t R_{t'}^*)$$

$$c_k = \sum_{k_1} (k_1 0, 20|ko) F(k, k_1)$$

where

$$F(k, k_1) \equiv \hat{2}\hat{x}\hat{k}_1 \sum_{tt'} [\,] s\hat{s}'\hat{l}\hat{l}'\hat{L}\hat{L}'\hat{b}^2 \hat{b}'^2 (-1)^{a-x+c-b+1} (l0, l'0|k_1 0)$$
$$\times W(xsxs'; a2)(L1'L'-1|k_0)(L1'L'-1|k0) W(LbL'b'; ck)$$
$$\times X(lsb; l's'b'; k_1 2k) \mathrm{Re}(iR_t R_{t'}^*)$$

where R is the reduced transition matrix element. The sum over t represents sums over L, j, l, s and the two modes of radiation (electric and magnetic). The reduced transition matrix element is proportional to the radial matrix element, $R = \langle f \mid H_{int} \mid i \rangle$ where $|i\rangle$ represents the continuum initial state (two deuterons), $\langle f|$ represents the bound final state (^{4}He) and H_{int} is the electromagnetic operator. Since R is a complex number, it is common to decompose it into a real amplitude, $^{2s+1}l_j$, times the exponential of the corresponding real phase, $\exp(i\phi_{(^{2s+1}l_j)})$.

The electromagnetic transition operator which connects the initial and final states of the $^2H(d,\gamma)^4He$ reaction may be separated into an electric part and a magnetic part. The electric part of the operator reduces to a form proportional to $(kr)^L$ (Blatt, 1952) if one invokes Siegert's Theorem (Siegert, 1937) and the long wavelength approximation. The latter requires that for r ≅ nuclear size and k the wave number of the γ-ray , kr << 1. At the energies of this experiment kr ≅ 0.1 fm^{-1} x 2 fm = 0.2. Amplitudes of electric transition matrix elements rapidly diminish as the photon multipolarity increases because of the $(kr)^L$ factor. E4 amplitudes are therefore presumed to be negligibly small in the $^2H(\vec{d},\gamma)^4He$ reaction at these energies. Consequently, only electric quadrupole (E2) and electric dipole (E1) transitions have been considered in this analysis. The $\sin^2(2\vartheta)$ shape of the angular distribution of the cross section is indicative of predominantly E2 radiation, while the non-zero value of the vector analyzing power implies the presence of radiation of opposite parity, which is assumed to be E1.

The magnetic part of the electromagnetic operator similarly decreases with increasing multipolarity (Blatt, 1952). In addition, there exists an extra factor of $\sqrt{10}\,\hbar/(Mc^2R)$, where M is the projectile mass and R is the radius of the nucleus (deBenedetti, 1964). This factor is approximately $(hc)/(Mc^2R)$ = (200 MeV-fm/(2 x 10^3 MeV · 2 fm)=1/20. Magnetic transition amplitudes are therefore more than an order of magnitude smaller than electric amplitudes of the same L. The only allowed M1 amplitude is further suppressed by an isospin selection rule that forbids ΔT = 0 transitions (Warburton, 1969). Hence magnetic

multipoles are not expected to contribute significant transition strength.

All allowed amplitudes arising from E1, E2, M1 and M2 transitions in the $^{2}H(\vec{d},\gamma)^{4}He$ reaction are tabulated in Table 4.1. The extraction of amplitudes and phases from fits to the polarized data at E_d = 30 and 50 MeV has been restricted to simply E2 and E1 radiation.

Capture amplitudes with the same $^{2s+1}l_j$ are not treated separately in the channel spin representation. Considering only E1 and E2, there remain five amplitudes ($^{3}P_1$ and $^{5}S_2$ to the D and S-state, $^{1}D_2$ to the S-state, and $^{5}D_2$ and $^{5}G_2$ to the D-state component in the ground state of ^{4}He), with four relative phases among them - a total of nine unknowns. The data are not precise enough to determine this many unknowns.

Eleven equations were used (although not simultaneously) in fitting the data to a_2, a_4, b_1, b_2, b_4, b_4, c_0, c_1, c_2, c_4, and under a pure D-wave E2 assumption, an isotropic value for Ay (Seyler, 1985). The number of unknowns can be reduced by further approximations. In the limit of a plane wave approximation, the relative phase between amplitudes = l x $\pi/2$, on that basis, the phase between the $^{1}D_2$ and $^{5}S_2$ amplitudes was restricted to 180 degrees.

Under the restrictions outlined above, the data were fit to amplitudes and phases. As mentioned above, if the amplitudes are further restricted to the D-wave terms, and combining the equations for T_{20} and T_{22} to get A_{yy}, the resulting equation is reduced to a constant (Seyler, 1985). An isotropic value proportional to the two amplitudes times the cosines of their relative phase is thus expected. This relationship was used as a starting point in

getting a consistent fit. With the help of the proper software, the equations mentioned above relate Legendre coefficients to the transition amplitudes and phases.

Table5.1. Coefficients from Fits

20 MeV	A_{yy}(fit to constant)=	0.135	+/- 0.048
30 MeV	A_0** =	2.57 nb	+/- 0.47 nb
	a_2 =	0.651	+/- 0.206
	a_4 =	-1.555	+/- 0.140
	b_1 =	-0.090	+/- 0.418
	b_2 =	-0.000	+/- 0.099
	b_3 =	-0.016	+/- 0.045
	b_4 =	0.000	+/- 0.105
	Ayy(fit to constant)=	0.2218	+/- 0.0097
	C_0*=	0.256	+/- 0.031
	c_2*=	-0.337	+/- 0.283
50 MeV	A_0** =	1.67 nb	+/- 0.54 nb
	a_2 =	0.642	+/- 0.156
	a_4 =	-1.384	+/- 0.131
	b_1 =	0.132	+/- 0.045
	b_2 =	-0.041	+/- 0.084
	b_3 =	0.126	+/- 0.855
	b_4 =	0.000	+/- 0.054
	Ayy(fit to constant)=	0.262	+/- 0.018
	C_0*=	0.276	+/- 0.018
	c_2*=	-0.754	+/- 0.219
	c_0 =	-0.512	+/- 0.240
	c_2 =	-0.378	+/- 0.632
	c_4 =	0.799	+/- 0.875
	c_1 =	0.121	+/- 0.225

*These are simple fits of Ayy to Legendre functions as a parametrization, without assumptions about transition amplitudes ($A_{yy} = C_0(1+\Sigma c_k P_k)$.

**From the electro-disintegration data of Skopik et.al. (1983) converted to the radiative capture cross-section via detailed balancing. $A_0 = \sigma_{total} / 4\pi$.

5.1. Results of Transition Matrix Analysis

The transition matrix element analysis at 30 MeV indicates that the data we obtained at this energy can be explained if E2 radiation leading to the S and D state of ^{4}He dominates the reaction. The $A_{yy}(\vartheta)$ data indicate that the $^5D_2$ amplitude (going to the D-state in ^{4}He) accounts for 6 percent of the cross-section. This compares to 12.6 percent predicted by the RGM calculation of Hofmann et.al. The $A_y(\vartheta)$ data at 30 MeV required the presence of non - E2 radiation at the 5.0 ± 3.0 percent level. This is in agreement with the 2.5 percent predicted by the RGM calculation.

The 50 MeV data could be more fully analyzed since both $T_{20}(\vartheta)$ and $A_{yy}(\vartheta)$ data were taken. The $A_{yy}(\vartheta)$ data indicate a $^5D_2$ strength of 6.0 percent. The $T_{20}(\vartheta)$ require a 12% $^5S_2$(E2) capture strength. This analysis therefore indicates that at 50 MeV, 18.0 percent of the capture cross section is arising from E2 capture to the D-state of ^{4}He. Once again the $A_y(\vartheta)$ data can be accounted for by introducing E1 radiation. In the case of 50 MeV the results of the T-Matrix analysis indicate a $^3P_1$(E1) strength of 3.0 ± 1.0 percent, compared to 17.9 percent from the RGM model. Here too the model seems to predict entirely too much $^3P_1$(E1) strength.

Table 5.2. Transition Matrix Analysis Results and the Calculated Values from the RGM model

Amplitude	30 MeV Fit	30 MeV RGM	50 MeV Fit	50 MeV RGM
$^3P_1$	5 ± 3%	2.5%	3 ± 1%	14.3%
$^1D_2$	89 ± 4%	81.9%	79 ± 2%	64.2%
$^5D_2$	6 ± 2%	12.6%	6 ± 2%	17.9%
$^5S_2$	-	2.9%	12 ± 2%	3.5%
Phase rel. to $^1D_2$ Amplitude				
$^3P_1$	0° (Fixed)	24.7°	0° (Fixed)	39.3°
$^5D_2$	45° " "	26.0°	45° " "	28.4°
$^5S_2$	180° " "	-59.1°	-180° " "	-44.8°

6. Conclusions

The results of this experiment have demonstrated how the resources of several laboratories can be combined to produce results impossible for each individually. The success of the LBL venture speaks for itself in this regard. Besides the results of this dissertation, an active resource has been added to that laboratory. It is important to realize that the resources of TUNL, NBS, and LBL were all required to accomplish this.

The technique developed and used here: Studying few body capture reactions with simultaneous detection of γ - rays and the recoiling particle is clearly the most advantageous way to go in this field. The technique proved both manageable and effective in producing high quality data. It should be applicable to other critical few body capture reactions such as $^{1}H(d,\gamma)^{3}He$, and $^{4}He(d,\gamma)^{6}Li$ in future studies.

The qualitative aspects of this work as well as the lower energy work on this reaction are remarkably well explained by the calculations of Hofmann (Wachter, 1988) which predict a 2.2 % d+d D-state probability in the ground state of ^{4}He. While there is general agreement, there are important specific discrepancies which require further theoretical study. A calculation which uses a realistic two-body force, which includes D-states in the fragments (especially the deuteron), and which includes G-waves (at the higher energies) is sorely needed.

Both these calculations and the T-matrix element analysis at 50 MeV indicate that the D-state of ^{4}He is playing a significant roll in determining the cross section for this

reaction at these energies: about 15% of the E2 strength arises from capture to the D-state. We have also seen that non-E2 radiation is relatively insignificant at these energies.

Clearly future experimental work should be directed at obtaining precision data on all polarization observables. Such data should allow for precise determination of all E2, E1 and M2 transition matrix elements. A comparison of these with model predictions should provide further insight into both the reaction theory and the detailed role of the D-state of ^{4}He in this reaction.

References

A. Abragam and J.M. Winter
Phys. Rev. Lett. *1* 374 (1958)

C. Alderliesten, et.al.
Phys. Rev. *C18* 2001 (1978)

J. Arends, J,Eyink, T.Hegerath, H. Hartman, B. Mecking, G. Noeldeke, and H.Rost,
Phys. Lett. *62B* 411 (1976)

J.L. Ballot
Phys. Lett. *127B* 399-402 (1983)

Z. Phys. *A302* 347 (1981)

B.L. Berman, et.al.
Phys. Rev. *C22* 2273 (1980)

L. Brillouin
J. Phys. *4* 1 (1933)

B.D. Belt, et.al.,
Phys. Rev. Lett. *24* 1120-23 (1970)

Phillip R. Bevington
Data Reduction and Error Analysis for the Physical Sciences 290 (McGraw Hill New York, 1963)

G. Bluge, H.J. Assenbaum, and K. Langanke,
Phys. Rev. *C36* 21 (1987)

J.R. Calarco, B.L. Berman and T.W. Donnelly
Phys. Rev. *C27* 1866 (1983)

J. Carlson
Phys Rev C38 1879-85 (1988)

C.R. Chen, G.L. Payne, J.L. Friar, and B.F. Gibson
Phys Rev C33 1740 (1986) C31 *2266* (1985)

D.J. Clark, et.al.,
Proc. Fifth Cyclotron Conference 610
(Butterworths, London 1971)

P. Countryman and S. Wald,
WC - Users Guide (LBL internal pub-3038 1984)

R. de Tourreil and D.W.L. Sprung
Nucl.Phys A201 193 (1973)

S.E. Darden
Proc. Third Polarization Symposium (Univ. of
Wisconsin Press, 1970)

S. deBenedetti,
Nuclear Interactions 290 (John Wiley and Sons,
New York, 1964)

Frank S. Dietrich and Dale W. Heikkinen
Nucl. Inst. and Meth. 155 103-109 (1978)

T.E.O. Ericson and M.P. Locher,
Nucl. Phys. A148 1-68 (1970)

Nucl. Phys. A405 497-533 (1983)

Ann. Rev. Nucl. Part. Sci. 35 271-94 (1985)

R.D. Evans
The Atomic Nucleus 713, 791 (McGraw-Hill, New
York, 1955)

J.L. Friar and S. Fallieros
Phys. rev C *29* 1645 (1984)

J.L. Friar, et.al.,
Phys. Rev. *C37* 2859 (1988)

S.Fiarman and W.E. Meyerhof,
Nucl. Phys. *A206* 1 (1973)

H. Flowers and F. Mandl,
Proc. Roy. Soc. London, Ser. *A 206* 131 (1950)

M. Gari and H. Hebach
Photonuclear Reactions at Intermediate Energies *Phys. Rept.* *72* 1 (1981)

M.M. Giannini and G. Ricco,
La Rivista del Nuovo Cimento *8* n.4 (1985)

B.F. Gibson
Nucl. Phys. *A353* 85c (1981)

H.F. Glavish,
Proc. Third Polarization Symposium (Univ. of Wisconsin Press, 1970)

D. Gogny, P.Peres and R. de Tourreil
Phys. Lett. *b32* 591 (1970)

P. Goldhammer
Phys. Rev. *C29* 1444-49 (1984)

P. Goldfarb
Nucl. Phys. *7* 622 (1958)

W. Gruebler, V. Konig, P.A. Schmelzbach, B. Jenny, and J. Vybiral
Nucl. Phys. A369 381 (1981)

W. Haeberli
Nuclear Spectroscopy and Reactions, vol II
(Edited by Joseph Cerni, Academic press, New York, 1974)

R.C. Hanna
Proc. Second Polsrization Symposium 280
(Edited by Huber et.al. Birkhauser,Basel, 1966)

Evans Hayward
Photonuclear Reactions *National Bureau of Standards Monograph* 118 (1970)

S. Ishikawa and T. Sasakawa,
Phys. Rev. Lett. 56 317-19 (1986)

Few Body Systems 1 143-58 (1986)

J. Jourdan, et.al.,
Nucl. Phys. A453 220-40 (1986)

M.J. Jensen,
Ph.D. dissertation, North Carolina State University (1981) (unpublished)

J.M.B. Kellog, I. Rabi, N.F. Ramsey, J.R. Zacharias
Phys. Rev. 56 728-30 (1938)

D.J. Klepacki, Y. E. Kim and R.A. Brandenburg,
Phys. Rev. C38 (1988)

L.D. Knutson, et.al.
Phys. Rev. Lett. *35* 1570-73 (1975)

L.D. Knutson, P.C. Colby, and J.A. Bieszk,
Phys. Lett. *85B* 209-11 (1979)

L.D. Knutson, P.C. Colby, and B.P. Hichwa,
Phys. Rev. *C24* 411-19 (1981)

J.L. Langenbrunner, et.al.
Phys. Rev. *C38* 565-68 (1988)

Creve Maples, William Rathbun and Einor Potter
Beginning with Chaos (LBL internal pub-3024 1985)

M.R. Marion and F.C. Young
Nuclear Reaction Analysis 14,30 North Holland, Amsterdam (1968)

M.R. Meder, P. Chiang, and J.L. Purcell
Bull. Am. Phys. Soc. *Vol.33 No.4* 929 (1988)

S. Mellema, T.R. Wang and W. Heaberli,
Bull. Am. Phys. Soc. *30* 1268 (1985)

Phys. Lett. *166B* 282 (1986)

Phys. Rev. *C34* 2043 (1986)

T. Mertelmeier and H.M. Hofmann,
Nucl. Phys. 387 *A459* (1986)

Steven M. Morril, et.al.
Nucl. Instrum. and Methods *B23* 301-308 (1987)

S.A. Moszkowski
Recent Progress in Many Body Theories (Edited by J.G. Zabolitsky, et.al. Springer Berlin, 1981)

Gerald G. Ohlsen and P.W. Keaton,
Nucl. Instrum. and Methods 109 41 (1973)

P. Paul
Nuclear Spectroscopy and Reactions,part A. (ed. J. Cerny Academic Press, New York, 1974)

A.C. Phillips
Rep Prog. Phys. 4 905 (1977)

W.K. Pitts, et.al
Phys. Rev. C37 1-5 (1988)

PhD Dissertation, Indianna Univ.(1987)

G.R. Plattner, R.D.Viollier and K. Alder,
Phys. Rev. Lett. 34 830-33 (1975)

D.O. Riska and G.E. Brown,
Phys. Rev. Lett. 38B 193 (1972)

N.L. Rodning and L.D. Knutson
Phys Rev Lett 49 no.13 909 (1982)

M.E. Rose,
Phys. Rev. 91 610 (1953)

M. Sakai, et.al.
Prog. Theor. Phys. Suppl. 56 32 (1974)

F.D. Santos, A. Arriaga, A.M. Eiró and J.A. Tostevin,
Phys. Rev. C31 707 (1985); and F.D. Santos,
private communication.

F.D. Santos and A.M. Eiró
Portugaliae Phys. *15* 65-88 (1984)

F.D. Santos et.al.
Phys. Rev. *C25* 3243-46 (1982)

Leonard B. Schiff,
Quantum Mechanics 3rd. ed. (McGraw-Hill, New York, 1968)

M.E.Schulze, et.al.
Phys. Rev. Lett. *52* 597-600 (1984)

J. Schwinger
Phys Rev. *55* 235 (1939)

A.J.F. Seigert
Phys. Rev. *52* 787 (1937)

S.Sen and L.D. Knutson,
Phys. Rev. *C26* 257-59 (1982)

R.G.Seyler and H.R. Weller,
Phys Rev. *C20* 453-58 (1979)

Phys Rev. *C31* 1952-54 (1985)

B.H. Silverman, A, Boudard, W.J. Briscoe, G. Bruge, P.Couvert, L.Farvacque, D.H. Fitzgerald, C.Glashauser, J.C. Lugol, B.M.K. Nefkens,
*Phys. Rev.*C29 35 (1984)

D.M. Skopik, et.al.,
Phys. Rev. *C28* 52-56 (1983)

Phys. Rev. *C6* 43-55 (1972)

J.A. Tostevin,
Phys. Rev. C34 1497-1500 (1986)

M.C. Vetterli, et.al.,
Phys. Rev. Lett. 54 1129-31 (1985)

J.D. Welecka
Electron Scattering *Argon National Laboratory Report ANL-83-50* (1983)

B. Wachter, T. Mertelmeier and H. M. Hofmann,
Phys. Lett. B200 246-50 (1988)

E.K. Warburton and J. Weneser,
Isospin in Nuclear Physics 185 edited by D.K. Wilkinson (North-Holland, Amsterdam, 1969)

H.R. Weller and D.R. Lehman
Ann. Rev. Nucl. Part. Sci. 38 563-608 (1988)

H.R. Weller, et.al.,
Phys. Rev. C34 32-37 (1986)

H.R. Weller,
J. Phys. Soc. Jpn. 55 113-22 (1986)

Comments Nucl. Part. Phys. 17 25-37 (1987)

E.P. Wigner
Math. Naturw. Anz. Ungar. Akad. Wiss. 53 475 (1935)

E.J. Wilkinson III and F.E. Cecil,
Phys. Rev. C31 2036 (1985)

Appendices

A. Charge Polarization and the E1 Operator

The nature of the E1 operator is of some interest because, although never published there has been some theoretical discussion on the subject of charge symmetry breaking in ^{4}He. There is an ongoing controversy about the ratio of the photodisintegration cross sections $^4\mathrm{He}(\gamma,n)^3\mathrm{He}$ / $^4\mathrm{He}(\gamma,p)^3\mathrm{H}$. According to Berman(1980) and Calarco(1983) this ratio differs significantly from unity in the region of E_γ = 30 MeV. It has been speculated that charge polarization of the incoming deuterons may be a mechanism for this effect, and may also be the source of of E1 radiation in the $^2\mathrm{H}(d,\gamma)^4\mathrm{He}$ reaction, which in turn is evidenced in the large vector analyzing power at low energy (Mellema, 1986; Langenbrunner, 1988). Rodning(1982) has measured the polarization of the deuteron by scattering off of a heavy target at low energy. They have obtained a value of the polarization by comparing the difference from Rutherford scattering to a polarization potential. The same form of polarization potential is derived below, and it is shown that it cannot lead to electric dipole radiation, as a first or second order correction to the Hamiltonian in the case of the $^2\mathrm{H}(d,\gamma)^4\mathrm{He}$ reaction.

In this discussion, the E1 operator is treated as a perturbation to the Hamiltonian and the internal coordinates of the deuterons are retained. The part of the operator due to charge polarization is isolated, and it is shown to vanish as a perturbative correction in first and second order.

We start with the assumption that the Hamiltonian of the system can be written as $H = H_0 = H'$, where the perturbation H' is small compared to H_0. First and second order contributions to the transition matrix element $\langle \beta b|T|\alpha a\rangle$ due to H' are given by

$$\langle \beta b|T|\alpha a\rangle = \langle \beta b|H'|\alpha a\rangle + \int_{\gamma}\sum_{c} \frac{\langle \beta b|H'|\gamma c\rangle\langle \gamma c|H'|\alpha a\rangle}{E_{\alpha a} - E_{\gamma c} + i\varepsilon} \qquad (1)$$

furthermore, the transition probability per unit time can be written in terms of the matrix elements of H' as

$$W = \frac{2\pi}{\hbar}\left|H_{fi} + \sum_{c}\frac{H_{fc}H_{ci}}{E_i - E_c}\right|^2 \frac{dn}{dE}$$

Fermi's Golden Rule (perturbation theory).

where the integration is over the continuum and the summation is over the bound state solutions to the Schrodinger equation. (Schiff,1968)

The Hamiltonian can be defined as: $H = H_0 + H'$ where

$H_o = H_N + H_C^{CM}$, and $H' = H_C^{P} + H_{em}$ and where the unperturbed Hamiltonian is divided into a part due to the nuclear force, and a part due to motion of the charge relative to the center of mass. The Perturbation will be taken to have a part due to charge polarization of the deuterons, and an electromagnetic part due to charges and magnetic moments of the deuterons.

A set of relative coordinates for the ^{4}He nucleus is defined as in this diagram where $\vec{r}$ and $\vec{r}'$ are the internal coordinate of the deuterons, $\vec{S}$ is the distance between

the centers of mass of the deuterons, and $\vec{r}_j$ are the position vectors of the nucleons with respect to the ^{4}He center of mass. The relative position of one of the charges with respect to the other one (the protons) is $\vec{\rho}$. The distance from the center of mass of one deuteron to the proton in the other one is $\vec{d}$.

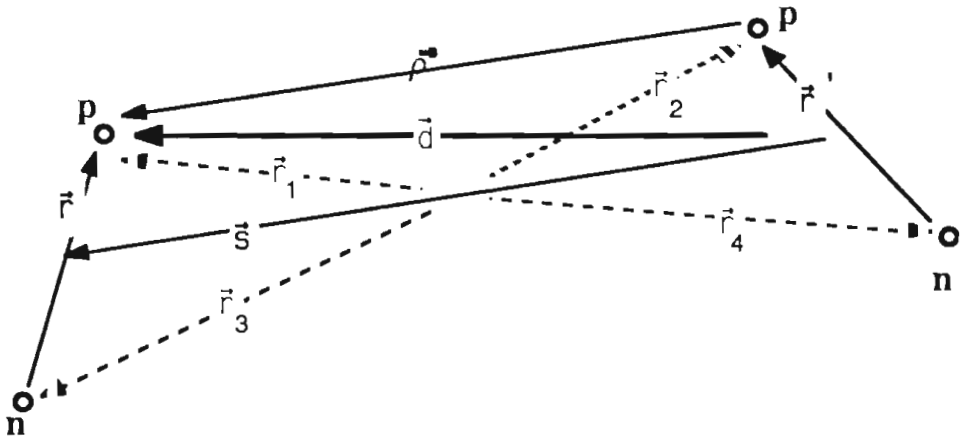

These position vectors can be related:

$$\vec{d} = \vec{s} + \frac{1}{2}\vec{r} = \vec{\rho} + \frac{1}{2}\vec{r}'$$

$$\vec{\rho} = \vec{s} + \frac{1}{2}(\vec{r} - \vec{r}')$$

The potential energy due to the Coulomb force is, in rationalized units, simply the proton charge squared divided by the distance between them:

$$\frac{e^2}{\rho} = \frac{e^2}{\sqrt{s^2 + \frac{1}{4}\left|(\vec{r} - \vec{r}')\right|^2 + \vec{s} \cdot \left((\vec{r} - \vec{r}')\right)}}$$

Expanding using the binomial theorem:

$$= \frac{e^2}{s} \frac{1}{\sqrt{1 + \frac{\hat{s} \cdot \left(\vec{r} - \vec{r}'\right)}{s} + \quad \ldots .}}$$

$$\approx \frac{e^2}{s}\left(1 - \frac{\hat{s} \cdot \left(\vec{r} - \vec{r}'\right)}{2s}\right)$$

This can be expressed in terms of the distance between the centers of mass of the deuterons, plus a term associated with the internal coordinates of the deuterons;

$$\approx \frac{e^2}{s} - \frac{e^2}{2s^2}\,\hat{s} \cdot \left(\vec{r} - \vec{r}'\right)$$

H_C^{CM} $\qquad$ H_C^{P}

giving the appropriate terms for the perturbative Hamiltonian.

The electric part of the electromagnetic operator is:

$$D_\ell = \frac{1}{\ell!}\sum_j e_j\left(\hat{\varepsilon}\cdot\vec{r}_j\right)\left(\hat{k}\cdot\vec{r}_j\right)^{\ell-1}$$

where e_j is the charge of the j^{th} particle, $\hat{\varepsilon}$ is the polarization vector, and $\hat{k}$ is a unit vector pointing in the direction of the momentum vector of the photon.

$$= \frac{1}{\ell!}\left[e\left(\hat{\varepsilon}\cdot\vec{r}_1\right)\left(\hat{k}\cdot\vec{r}_1\right)^{\ell-1} + e\left(\hat{\varepsilon}\cdot\vec{r}_2\right)\left(\hat{k}\cdot\vec{r}_2\right)^{\ell-1}\right]$$

$$\vec{r}_1 = \frac{1}{2}(\vec{r} + \vec{s})$$

$$\vec{r}_2 = \frac{1}{2}\left(\vec{r}' - \vec{s}\right)$$

($\vec{r}_1$ and $\vec{r}_2$ are position vectors of the two protons).

The electric dipole part of the operator is then;

$$D_1 = e\left[\hat{\varepsilon}\cdot\frac{1}{2}(\vec{r} - \vec{s}) + \hat{\varepsilon}\cdot\frac{1}{2}\left(\vec{r}' + \vec{s}\right)\right]$$

$$= \frac{e}{2}\ \hat{\varepsilon} \cdot \left(\vec{r} + \vec{r}'\right)$$

expressed in terms of the internal coordinates of the deuterons. This result verifies the fact that if we consider two point deuterons, r = r' = 0, and D1 = 0. Hence E1 radiation from 4He requires structured deuterons in order to be finite.

Putting the unperturbed part of the Hamiltonian into the Schrodinger equation defines the scattering $(|d\ d\rangle)$ and bound state $(|^4He\rangle)$ wave-functions;

$$(H_N + H_C^{CM})|d\ d\rangle = (E - 2B_d)|d\ d\rangle$$

$$(H_N + H_C^{CM})|^4He\rangle = -B_{He}|^4He\rangle$$

where E is the total energy of the system and B_d and B_{He} are the binding energies of the deuteron and ^{4}He respectively.

Lowest order Perturbation theory;

$$\langle^4He|H'|d\ d\rangle = \langle^4He|H_C^P + H_{em}|d\ d\rangle$$

$$H_C^P = \frac{-e^2}{2s^2}\ \hat{s} \cdot \left(\vec{r} - \vec{r}'\right)$$

$$H_{em} = c\sqrt{\frac{2\pi\hbar}{\omega}}\left[\frac{-i\omega}{c}(D_1 + M_1) - \frac{\omega^2}{c^2}(D_2 + M_2)\right]$$

Now, taking a look at symmetries;

The bound state solutions are $|^4He\rangle$ in a relative S-wave, in which case the deuteron spins are anti-aligned,

or in a relative D-wave, in which case the deuteron spins are aligned. L + S must be even, J = 0, so L and S = 0, or L and S = 2. The bound wave function $\Psi_{He}(\vec{r},\vec{r}';\vec{S})$ is an even function in $\vec{r}$ and $\vec{r}'$ because the deuterons have internal L = 0 or two, $\vec{r}$ and $\vec{r}'$ are their internal coordinates. It is also is even in $\vec{S}$ since the internal L of the ^{4}He is either 0 or 2. Since there is no spin term in the electric operator defined above, the continuum state $\Psi_{dd}(\vec{r},\vec{r}';\vec{S})$ can have only the same S as the ground state, S must be 0 or 2, so L in the continuum must be even as well. This implies that $\Psi_{dd}(\vec{r},\vec{r}';\vec{S})$ is even in $\vec{r}$, $\vec{r}'$ and $\vec{S}$ as well.

Writing the continuum state out more explicitly (for reference, though not really necessary for the argument presented here):

$$\Psi_{dd} = \varphi_{d_1}\varphi_{d_2}\mathcal{R}^{\bar{\kappa}}_{dd}(\vec{s})$$

$$= \varphi_{d_1}\varphi_{d_2}\,4\pi \sum_{\substack{JM\\ lm\\ SM_s}} i^l \mathcal{S}^J_{ls}(\kappa s)\, Y^{[l]\dagger}_m(\hat{\kappa}) \underbrace{\tfrac{1}{2}(1+(-)^{l+s})}_{\substack{\text{this factor insures}\\ l+s \text{ is even, for}\\ \text{the identical bosons}}} P_{l+s}$$

$$\langle lmSM_s | JM\rangle \left[Y^{[l]}(\hat{s}) \times \left[\varphi^{[l]} \times \varphi^{[l]}\right]^{[s]}\right]^{[J]}_M$$

It can then be seen immediately that the operator

$$H^P_c = \frac{-e^2}{2s^2}\,\hat{s}\cdot(\vec{r}-\vec{r}')$$

is odd in $\vec{r}$ and $\vec{r}'$ and is applied to the even wave-functions, hence the correction due to this part of the perturbation will result in an odd integrand which will integrate to zero. If we consider the electric part of H_{em},

$$D_1 = \frac{e}{2}\hat{\mathcal{E}} \cdot (\vec{r} + \vec{r}'),$$

we see that it is also odd in $\vec{r}$ and $\vec{r}'$, so that the matrix element above vanishes in the integration for this part of the perturbation as well. Hence we can conclude that $\left\langle {}^4He \left| H_C^P + H_{em} \right| d\,d \right\rangle \equiv 0$.

Looking at second order perturbation theory, the unperturbed bound and continuum states of the Hamiltonian;

$$H = \underbrace{H_0^{dd} + V^{dd} + H_C^{CM}}_{\mathcal{H}^{dd}} + \underbrace{H_1^d + H_2^d}_{\substack{\text{internal deuteron} \\ \text{Hamiltonians}}} + H' = H_0 + H'$$

and $H' = H_C^P + H_{em}$ (the perturbation)

with $H_C^P = \frac{-e^2}{2s^2}\hat{s} \cdot (\vec{r} - \vec{r}')$ as before.

The wave-functions are defined by the Schrodinger equation;

$$\mathcal{H}^{dd} \left| {}^4He \right\rangle = - B_{He}^{dd} \left| {}^4He \right\rangle$$

$$\mathcal{H}^{dd} \left| R_{dd}^{\bar{\kappa}} \right\rangle = E \left| R_{dd}^{\bar{\kappa}} \right\rangle \qquad E = \frac{\kappa^2}{2\mu_{dd}} > 0 \,,$$

represents the total center of mass energy of the two deuterons.

$$H_i^d \left| \varphi_{d_i} \right\rangle = - B_d \left| \varphi_{d_i} \right\rangle$$

$$H_i^d \left| \varphi_{np_i}^{\bar{\kappa}_d} \right\rangle = \frac{\kappa_d^2}{2\mu_{np}} \left| \varphi_{np_i}^{\bar{\kappa}_d} \right\rangle$$

Combining the two deuteron Hamiltonians with the cluster configuration Hamiltonian,

$$H_0 = \mathcal{H}^{dd} + H_1^d + H_2^d$$

produces unperturbed solutions;

$$H_0 \left| {}^4He \;\; \varphi_{d_1} \;\; \varphi_{d_2} \right\rangle = -\left(B_{He}^{dd} + 2B_d \right) \;\; \left| {}^4He \;\; \varphi_{d_1} \;\; \varphi_{d_2} \right\rangle$$

$$H_0 \left| R_{dd}^{\vec{\kappa}} \; \varphi_{d_1} \;\; \varphi_{d_2} \right\rangle = \left(E - 2B_d \right) \left| R_{dd}^{\vec{\kappa}} \; \varphi_{d_1} \;\; \varphi_{d_2} \right\rangle$$

$$H_0 \left| R_{dd}^{\vec{\kappa}} \;\; \varphi_{np_1}^{\vec{\kappa}_{d_1}} \; \varphi_{d_2} \right\rangle = \left(E + \frac{\kappa_{d_1}^2}{2\mu_{np}} - B_d \right) \;\; \left| R_{dd}^{\vec{\kappa}} \;\; \varphi_{np_1}^{\vec{\kappa}_{d_1}} \; \varphi_{d_2} \right\rangle$$

$$H_0 \left| R_{dd}^{\vec{\kappa}} \;\; \varphi_{np_1}^{\vec{\kappa}_{d_1}} \;\; \varphi_{np_2}^{\vec{\kappa}_{d_2}} \right\rangle = \left(E + \frac{\kappa_{d_1}^2}{2\mu_{np}} + \frac{\kappa_{d_2}^2}{2\mu_{np}} \right) \;\; \left| R_{dd}^{\vec{\kappa}} \;\; \varphi_{np_1}^{\vec{\kappa}_{d_1}} \;\; \varphi_{np_1}^{\vec{\kappa}_{d_2}} \right\rangle$$

And there are the completeness relations;

$$\left| {}^4He \right\rangle \left\langle {}^4He \right| + \int d^3\kappa \left| R_{dd}^{\vec{\kappa}} \right\rangle \left\langle R_{dd}^{\vec{\kappa}} \right| = 1$$

$$\left| \varphi_{d_i} \right\rangle \left\langle \varphi_{d_i} \right| + \int d^3\kappa_{d_i} \left| \varphi_{np_i}^{\vec{\kappa}_{d_i}} \right\rangle \left\langle \varphi_{np_i}^{\vec{\kappa}_{d_i}} \right| = 1$$

and the normalizations:

$$\left\langle {}^4He \middle| {}^4He \right\rangle = 1$$

$$\left\langle \varphi_{d_i} \middle| \varphi_{d_i} \right\rangle = 1$$

$$\left\langle R_{dd}^{\vec{\kappa}'} \middle| R_{dd}^{\vec{\kappa}} \right\rangle = \delta^3 (\vec{\kappa}' - \vec{\kappa})$$

$$\left\langle \begin{matrix} \vec{\kappa}'_{d_i} \\ \varphi_{np_i} \end{matrix} \middle| \begin{matrix} \vec{\kappa}_{d_i} \\ \varphi_{np_i} \end{matrix} \right\rangle = \delta^3 (\vec{\kappa}'_{d_i} - \vec{\kappa}_{d_i})$$

We now construct the initial and final states of our reaction:

Initial State $\left| R^{\vec{\kappa}}_{dd} \varphi_{d_1} \varphi_{d_2} \right\rangle$ with energy $E-2B_d$

Final State $\left| R^{He}_{dd} \varphi_{d_1} \varphi_{d_2} \right\rangle$ with energy $- B^{dd}_{He} - 2B_d$.

$$E_\gamma = E + B^{dd}_{He}$$

Putting the unperturbed solutions and the perturbative Hamiltonian into the second order term of the perturbation theory expansion;

$$H' = H^P_C + H_{em}$$

$$H^P_C = - \frac{e^2}{2s^2} \hat{s} \cdot (\vec{r} - \vec{r}')$$

$$H_{em} = \underbrace{c\sqrt{\frac{2\pi\hbar}{\omega}}\left(\frac{-i\omega}{c}\right)}_{f} \frac{e}{2} \hat{\varepsilon} \cdot (\vec{r} + \vec{r}') \equiv f \frac{e}{2} \hat{\varepsilon} \cdot (\vec{r} + \vec{r}')$$

where we have defined the factor 'f'.

Now we can compute the second order contribution to the transition matrix element (eq.1):

$$\sum_n \frac{\left\langle {}^4He \left| H_C^P + H_{em} \right| n \right\rangle \left\langle n \left| H_C^P + H_{em} \right| d\ d \right\rangle}{(E - 2B_d - E_n + i\varepsilon)}$$

$$= \sum_n \frac{\left\langle {}^4He \left| H_C^P \right| n \right\rangle \left\langle n \left| H_C^P \right| d\ d \right\rangle}{(E - 2B_d - E_n + i\varepsilon)}$$

$$+ \sum_n \frac{\left\langle {}^4He \left| H_C^P \right| n \right\rangle \left\langle n \left| H_{em} \right| d\ d \right\rangle}{(E - 2B_d - E_n + i\varepsilon)}$$

$$+ \sum_n \frac{\left\langle {}^4He \left| H_{em} \right| n \right\rangle \left\langle n \left| H_C^P \right| d\ d \right\rangle}{(E - 2B_d - E_n + i\varepsilon)}$$

$$+ \sum_n \frac{\left\langle {}^4He \left| H_{em} \right| n \right\rangle \left\langle n \left| H_{em} \right| d\ d \right\rangle}{(E - 2B_d - E_n + i\varepsilon)}$$

Comments on these terms:

In the pure H^P_c term, i.e. the first term, while the amplitude doesn't vanish, no photons are emitted so it isn't relevant to this discussion. It violates conservation of energy since it takes us from the d-d continuum to the ground state of ^{4}He with no release of energy.

The pure H_{em} term, i.e. the fourth term, corresponds to a final state with two photons. It should be ignored since it will be extremely small (down by a factor of 1/137 from one photon emission).

Now consider

$$\sum_n \frac{\left\langle {}^4He \left| H_C^P \right| n \right\rangle \left\langle n \left| H_{em} \right| d\ d \right\rangle}{\left(E - 2B_d - E_n + i\varepsilon \right)}$$

Possible intermediate states:

$\left| {}^4He\ \varphi_{d_1}\ \varphi_{d_2} \right\rangle$ won't contribute because even in $\vec{r}$'s and $\hat{s}$;

$\left\langle \varphi_d \left| \vec{r} \right| \varphi_d \right\rangle = 0$, and $\left\langle {}^4He \left| \hat{s} \right| {}^4He \right\rangle = 0$.

$\left| R_{dd}^{\vec{\kappa}'}\ \varphi_{d_1}\ \varphi_{d_2} \right\rangle$ won't contribute, because even in $\vec{r}$'s.

$\left| R_{dd}^{\vec{\kappa}'}\ \varphi_{np_1}^{\vec{\kappa}_{d_1}}\ \varphi_{np_2}^{\vec{\kappa}_{d_2}} \right\rangle$ won't contribute, because $\left\langle \varphi_{np_i} \left| \varphi_{d_i} \right\rangle = 0 \right.$.

But, $\left| R_{dd}^{\vec{\kappa}'}\ \varphi_{np_1}\ \varphi_{d_2} \right\rangle$ and $\left| R_{dd}^{\vec{\kappa}'}\ \varphi_{d_1}\ \varphi_{np_2} \right\rangle$ <u>are not</u> immediately excluded by these symmetry arguments. Working these through the equations;

$$\sum_n \ldots =$$

$$\int d^3\kappa'\ d^3\kappa_{d_1} \frac{\left\langle R_{dd}^{He} \varphi_{d_1}\ \varphi_{d_2} \left| H_C^P \right| R_{dd}^{\vec{\kappa}'}\ \varphi_{np_1}^{\kappa_{d_1}}\ \varphi_{d_2} \right\rangle \left\langle R_{dd}^{\vec{\kappa}'} \varphi_{np_1}^{\kappa_{d_1}}\ \varphi_{d_2} \left| H_{em} \right| R_{dd}^{\vec{\kappa}} \varphi_{d_1}\ \varphi_{d_2} \right\rangle}{E - 2B_d - E - \frac{\kappa_{d_1}^2}{2\mu_{np}} + B_d}$$

$$+ \int d^3\kappa'\ d^3\kappa_{d_2} \frac{\left\langle R_{dd}^{He} \varphi_{d_1}\ \varphi_{d_2} \left| H_C^P \right| R_{dd}^{\vec{\kappa}'}\ \varphi_{d_1}\ \varphi_{np_2}^{\kappa_{d_2}} \right\rangle \left\langle R_{dd}^{\vec{\kappa}'}\ \varphi_{d_1}\ \varphi_{np_2}^{\kappa_{d_2}} \left| H_{em} \right| R_{dd}^{\vec{\kappa}} \varphi_{d_1}\ \varphi_{d_2} \right\rangle}{E - 2B_d - E - \frac{\kappa_{d_2}^2}{2\mu_{np}} + B_d}$$

$$= -\int d^3\kappa_{d_1} \frac{\left\langle R_{dd}^{He}\ \varphi_{d_1}\middle| H_C^P \middle| R_{dd}^{\bar{\kappa}'}\ \varphi_{np_1}^{\kappa_{d_1}}\right\rangle \left\langle R_{dd}^{\bar{\kappa}'}\ \varphi_{np_1}^{\kappa_{d_1}}\middle| H_{em}\middle| R_{dd}^{\bar{\kappa}}\ \varphi_{d_1}\right\rangle}{B_d + \frac{\kappa_{d_1}^2}{2\mu_{np}}}$$

Completeness implies;

$$-\int d^3\kappa_{d_2} \frac{\left\langle R_{dd}^{He}\ \varphi_{d_2}\middle| H_C^P \middle| R_{dd}^{\bar{\kappa}'}\ \varphi_{np_2}^{\kappa_{d_2}}\right\rangle \left\langle R_{dd}^{\bar{\kappa}'}\ \varphi_{np_2}^{\kappa_{d_2}}\middle| H_{em}\middle| R_{dd}^{\bar{\kappa}}\ \varphi_{d_2}\right\rangle}{B_d + \frac{\kappa_{d_2}^2}{2\mu_{np}}}$$

$$= -\int d^3\kappa_{d_1} \frac{\left\langle R_{dd}^{He}\ \varphi_{d_1}\middle| -\frac{e^2}{2s^2}\hat{s}\cdot\vec{r}\middle|\varphi_{np_1}^{\kappa_{d_1}}\right\rangle \left\langle \varphi_{np_1}^{\kappa_{d_1}}\middle| f\frac{e}{2}\hat{\varepsilon}\cdot\vec{r}\middle| R_{dd}^{\bar{\kappa}}\ \varphi_{d_1}\right\rangle}{B_d + \frac{\kappa_{d_1}^2}{2\mu_{np}}}$$

$$-\int d^3\kappa_{d_2} \frac{\left\langle R_{dd}^{He}\ \varphi_{d_2}\middle| +\frac{e^2}{2s^2}\hat{s}\cdot\vec{r}\middle|\varphi_{np_2}^{\kappa_{d_2}}\right\rangle \left\langle \varphi_{np_2}^{\kappa_{d_2}}\middle| f\frac{e}{2}\hat{\varepsilon}\cdot\vec{r}\middle| R_{dd}^{\bar{\kappa}}\ \varphi_{d_2}\right\rangle}{B_d + \frac{\kappa_{d_2}^2}{2\mu_{np}}}$$

$\equiv 0$ No contribution due to the nature of H_C^P.

In the above we have used the completeness of R-states to eliminate the $R_{dd}^{\bar{\kappa}'}$'s in the final step, and the $\left\langle \varphi_{d_i} \middle| \varphi_{d_i} \right\rangle = 1$ relations.

One could also use the relation $\left\langle R_{dd}^{He} \middle| \hat{s} \middle| R_{dd}^{\bar{\kappa}} \right\rangle \equiv 0$ to reach the same conclusion because the operands are even, and the operator is odd.

This result is therefore zero for two reasons: 1) each term above is identically zero, and 2) the two terms are equal but opposite in sign.

We still have the $H_{em}...H_C^P$ term to consider.

$\left| {}^4He \quad \varphi_{d_1} \quad \varphi_{d_2} \right\rangle$ won't contribute because of $\vec{r}$'s.

$\left| R^{\vec{\kappa}'}_{dd} \quad \varphi_{d_1} \quad \varphi_{d_2} \right\rangle$ likewise, and

$\left| R^{\vec{\kappa}'}_{dd} \quad \varphi^{\kappa_{d_1}}_{np_1} \quad \varphi^{\kappa_{d_2}}_{np_2} \right\rangle$ won't contribute because

$\left\langle \varphi_{d_i} \middle| \varphi^{\vec{\kappa}_{d_i}}_{np_i} \right\rangle = 0.$

The remainder of the proof follows in parallel to the $H_C^P...H_{em}$ case thus the result $\equiv 0$. So, to leading order in the definition of the polarization potential, no E1 radiation is produced!

<u>What about higher terms in the binomial expansion?</u>

$$\frac{1}{\sqrt{1+x}} \approx 1 - \frac{x}{2} + \frac{3}{8}x^2$$

$$\frac{e^2}{\rho} = \frac{e^2}{s}\frac{1}{\sqrt{1+\frac{\hat{s}\cdot(\vec{r}-\vec{r}')}{s}+\frac{|\vec{r}-\vec{r}'|^2}{4s^2}}}$$

$$\approx \frac{e^2}{s}\left\{1-\frac{\hat{s}\cdot(\vec{r}-\vec{r}')}{2s}-\frac{|\vec{r}-\vec{r}'|^2}{8s^2}+\frac{3}{8}\left[\frac{\hat{s}\cdot(\vec{r}-\vec{r}')}{s}+\frac{|\vec{r}-\vec{r}'|^2}{4s^2}+\right]\right\}$$

$$\approx \frac{e^2}{s}-\frac{e^2\hat{s}\cdot(\vec{r}-\vec{r}')}{2s^2}-\frac{e^2|\vec{r}-\vec{r}'|^2}{8s^3}+\frac{3}{8}\frac{e^2[\hat{s}\cdot(\vec{r}-\vec{r}')]^2}{s^3}$$

$$\approx \frac{e^2}{s}-\frac{e^2\hat{s}\cdot(\vec{r}-\vec{r}')}{2s^2}$$

$$-\frac{e^2}{8s^3}\left\{r^2+r'^2-2\vec{r}\cdot\vec{r}'+3(\hat{s}\cdot\vec{r})^2+3(\hat{s}\cdot\vec{r}')^2-6(\hat{s}\cdot\vec{r})(\hat{s}\cdot\vec{r}')\right\}$$

Clearly, the new terms are quadrupole in nature, so they do not produce E1 radiation due to deuteron polarizability.

Summary:

To leading order in the polarization potential, no E1 radiation is emitted in d + d -> ^{4}He + γ. This occurs because the polarization-potential matrix element vanishes. Specifically, in the spin independent case,

$$\left\langle \quad R_{He} \quad \left|\frac{\hat{s}}{s^2}\right| \quad R^{\bar{\kappa}}_{dd} \quad \right\rangle \equiv 0$$

because this is $\langle$ S-waves | odd operator | even waves only $\rangle$.

When spin is taken into account;

$$\left\langle \begin{array}{ll} s\text{-}wave(spin\ 0) & \left|\frac{\hat{s}}{s^2}\right| \quad Even\ waves(spin\ 0) \\ d\text{-}wave(spin\ 2) & \left|\frac{\hat{s}}{s^2}\right| \quad or \qquad (spin\ 2) \end{array} \right\rangle \equiv 0$$

This follows since the integrand is odd except for the case of odd waves (spin 1), which gives zero because the E1 operator used here is spin independent. The spin dependent part of the E1 operator could give a finite result (this is not the part we are discussing here).

Appendix B. Legendre Coefficients and Transition Amplitudes and Phases used in fitting these Data.

$$A0=(3.0000)(3P1)^2+(5.0000)(1D2)^2+(5.0000)(5D2)^2+(5.0000)(5S2)^2$$

$$A2=(1.5000)(3P1)^2+(3.5710)(1D2)^2+(-0.7650)(5D2)^2+(-5.9760)(5S2)(5D2)\cos(5S2-5D2)$$

$$A4=(-8.5710)(1D2)^2+(-2.4490)(5D2)^2$$

$$B1=(-4.5000)(1D2)(3P1)\sin(1D2-3P1)+(-5.9530)(5D2)(3P1)\sin(5D2-3P1)+(-3.5580)(5S2)(3P1)\sin(5S2-3P1)$$

$$B2=(-2.2410)(5S2)(5D2)\sin(5S2-5D2)$$

$$B3=(-3.0000)(1D2)(3P1)\sin(1D2-3P1)+(-1.1340)(5D2)(3P1)\sin(5D2-3P1)$$

$$C0=(-1.0610)(3P1)^2+(0.7580)(5D2)^2+(-5.3450)(5D2)(1D2)\cos(5D2-1D2)+(4.4720)(5S2)(1D2)\cos(5S2-1D2)+(5.9160)(5S2)(5D2)\cos(5S2-5D2)$$

C2=(-0.5300)(3P1)^2 +(-2.2550)(5D2)^2 +(-1.7680)(5S2)2+(-
3.8180)(5D2)(1D2)COS(5D2-
1D2)+(3.1940)(5S2)(1D2)COS(5S2-1D2)

+(-0.9060)(5S2)(5D2)COS(5S2-5D2)

C4=(0.8660)(5D2)^2+(9.1630)(5D2)(1D2)COS(5D2-1D2)
+(-7.6670)(5S2)(1D2)COS(5S2-1D2)
+(-2.8980)(5S2)(5D2)COS(5S2-5D2)

C1=(3.6080)(5D2)(3P1)COS(5D2-3P1)+(-
6.0370)(5S2)(3P1)COS(5S2-3P1)

Ayy(pure D-wave approximation)
=(7.5510)(5D2)(1D2)cos(5D2-1D2)

Appendix C. Electronics Diagrams.

Scintillator electronics used in the runs at LBL. The lower part of the circuit is used for diagnosing accidental vetoes.

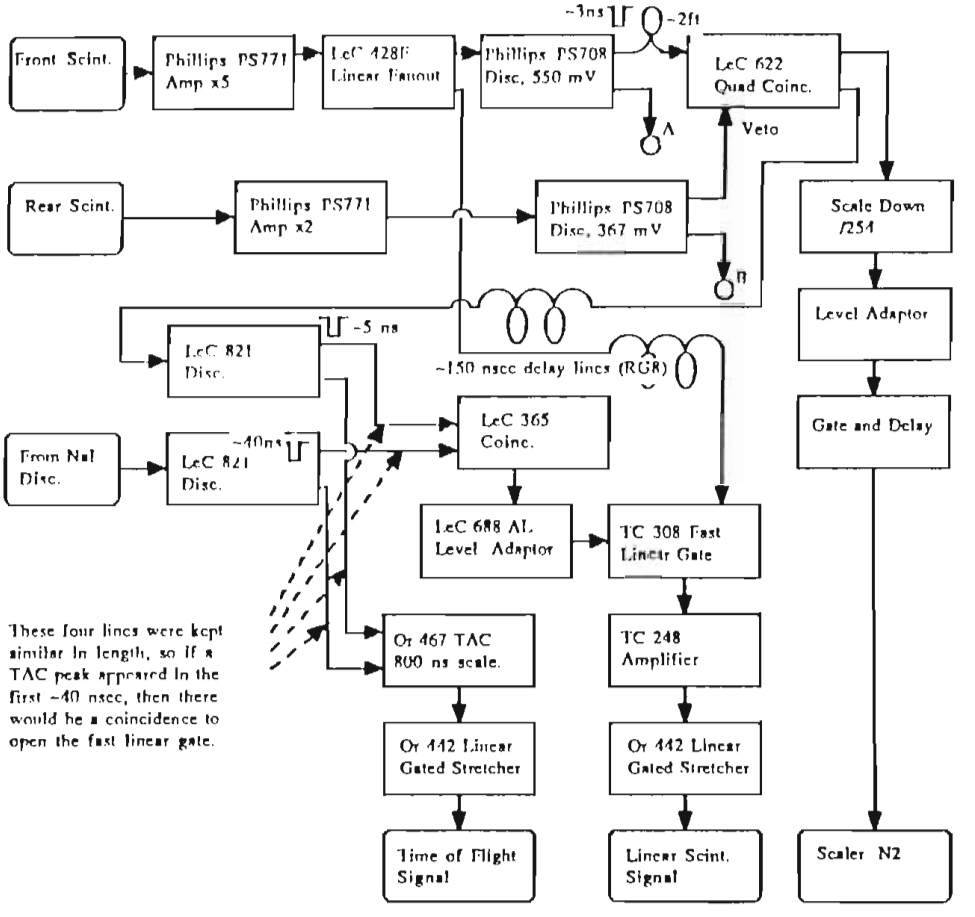

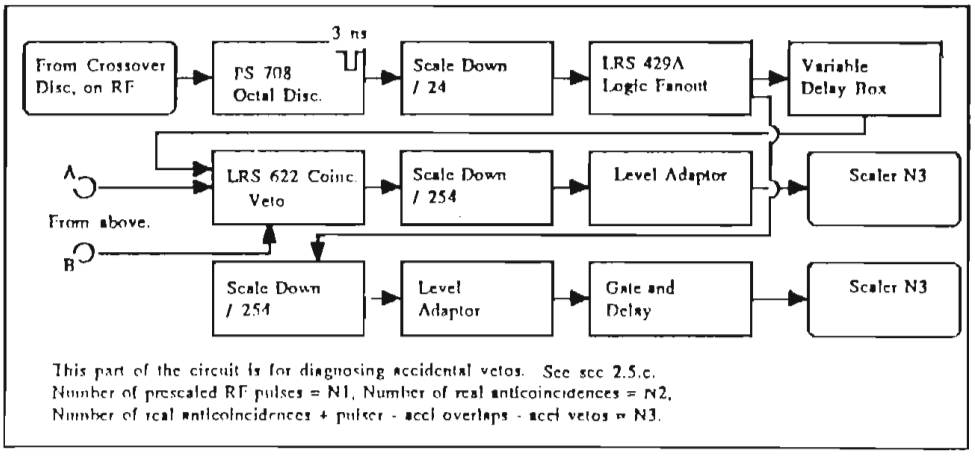

Sodium Iodide Electronics.used in the runs at LBL. Right side referred to as LNL because of the origin of the NaI.

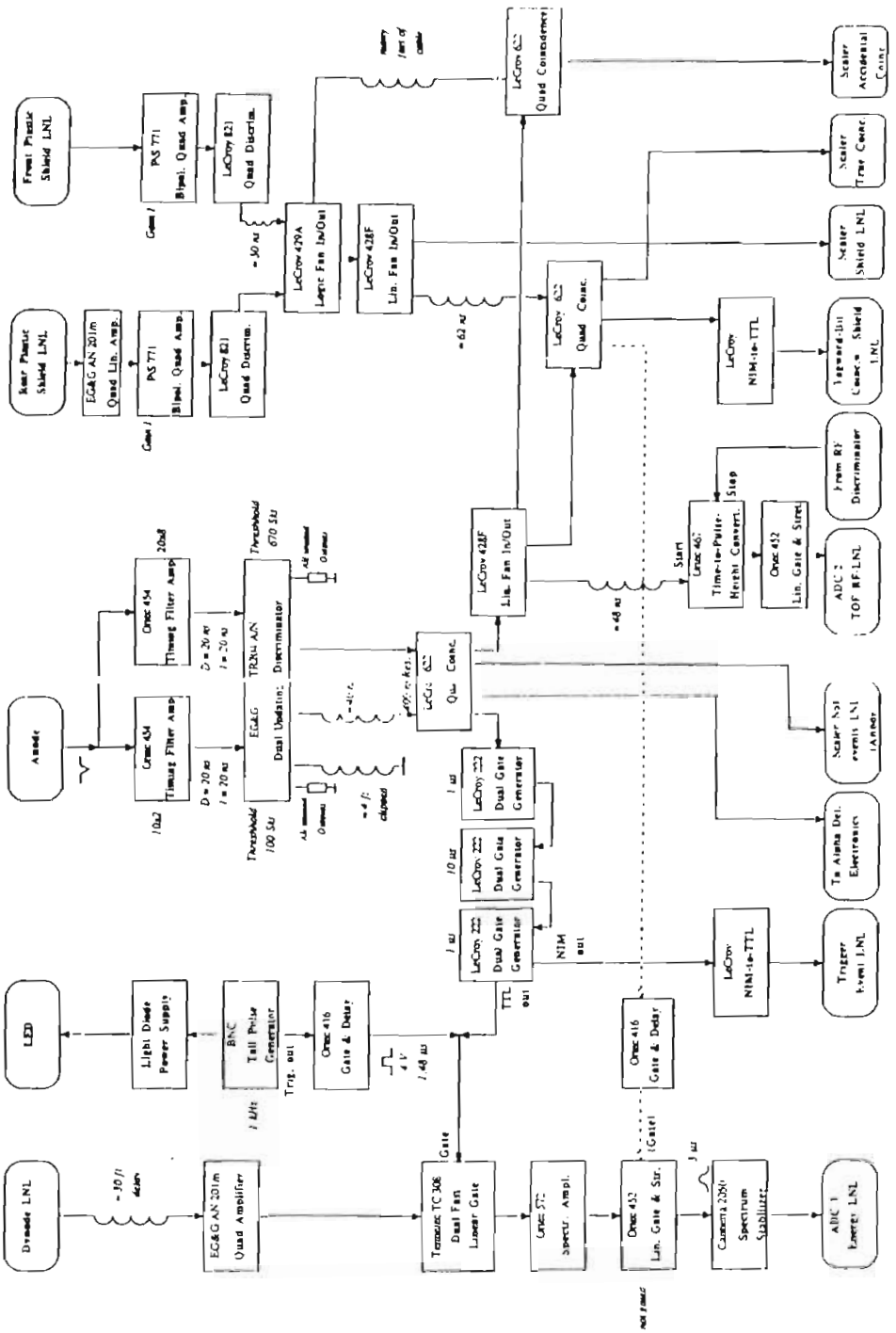

Sodium Iodide Electronics.used in the runs at LBL. Left side referred to as NBS because of the origin of the NaI.

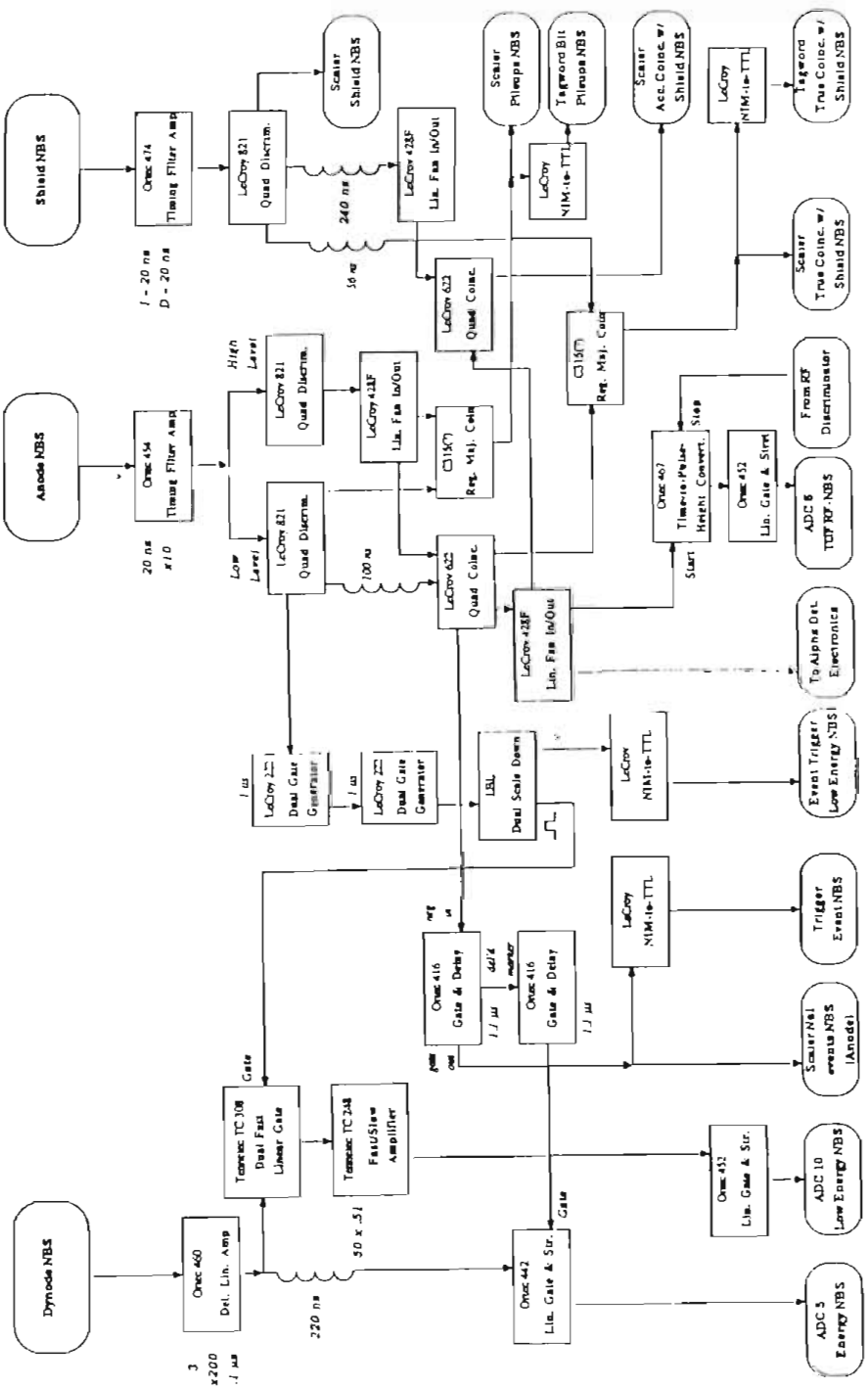

Interface electronics

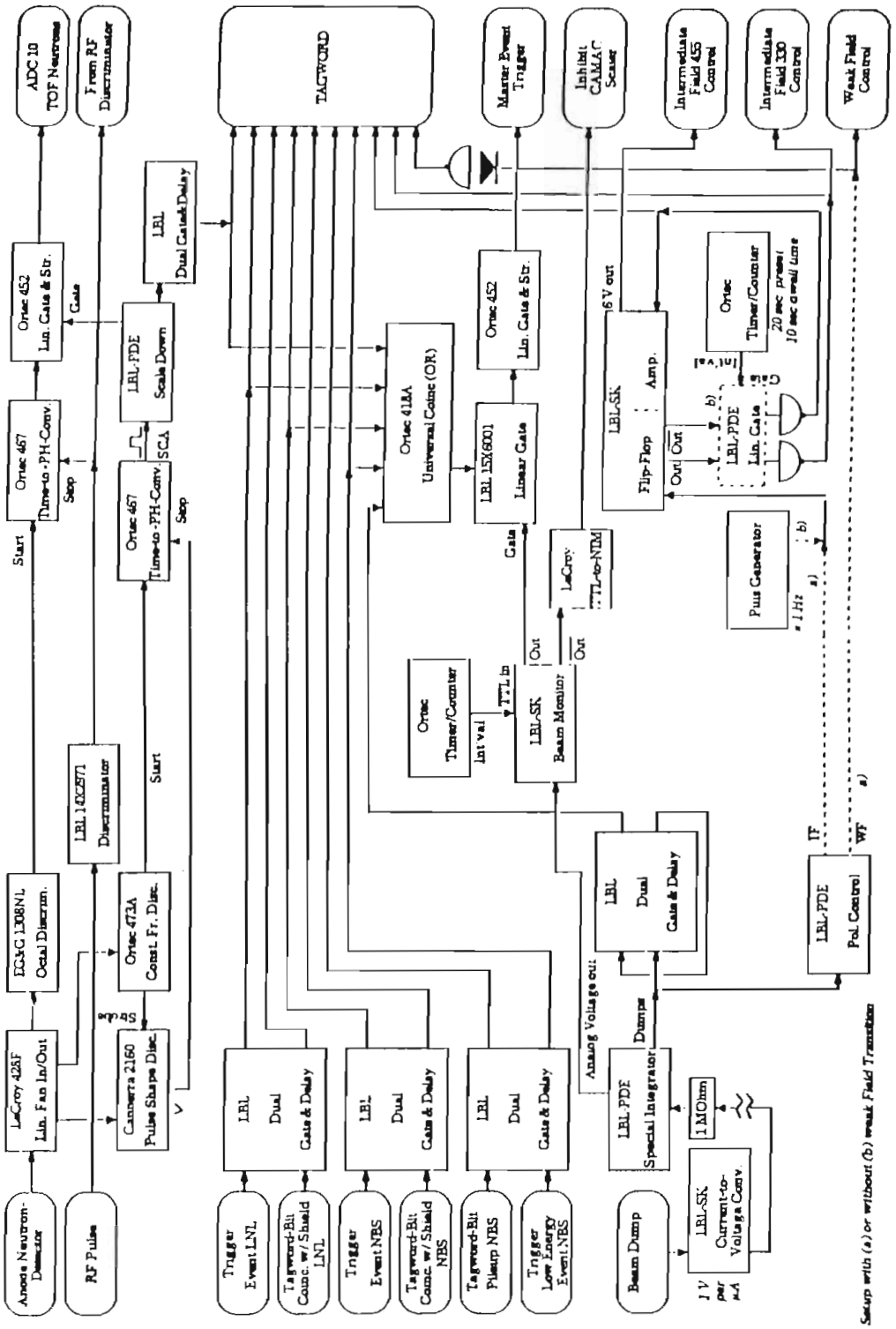

Appendix D. The Program CORRECT.

This program was used to estimate the locus of the ^4He recoils in order to optimize the target thickness, and the position of the scintillators, and make corrections to the data. It is included here as a reference to the logic only. It should not be taken as an example of programming style. The subroutine MULTSCAT which calculates the characteristic spreading angle according to (Marian, 1968; Morrill, 1987) was written by Sinan Utku while an undergraduate assistant to the lab. The relativistic kinematics subroutine SRKIN has been written an modified by many.

```
C       Correct is a Fortran program to correct for multiple
C       scattering and imperfect geometry in the detection of
C       4He nuclei in coincidence with the gamma spectrometers
C       at the 88. Through a monte carlo procedure, a place on
C       the front of a 10" gamma spectrometer is chosen, and
C       and a random place on the axis of the beam for a 5"
C       thick target is selected. All kinematics and angular
C       straggling are calculated and the point that the test
C       particle passes the scintillator plane two meters down-
C       stream is checked to see if it is a hit or miss. The
C       efficiency of the geometry is thus estimated.
C
      IMPLICIT REAL (A-H,O-Z)
      INTEGER I, ISEED
C     DATA EBEAM,THETA,DISTANCE,XSCINT1,XSCINT2,YSCINT,
C    1   KAPTON,PRESSURE,COLDFAC,BEAMSPRD/50.0,135.0,85.0,
C     2     10.025,17.02,5.715,1.0,4.0,3.0,0.25/
      READ (100,*)EBEAM,THETA,DISTANCE,XSCINT1,XSCINT2,YSCINT,KAPTON,
     1   PRESSURE,COLDFAC,BEAMSPRD,N
      PRINT *,'EBEAM=',EBEAM,'ANG=',THETA,'DIST=',DISTANCE
     1  ,'SCINT FROM',XSCINT1,'TO',XSCINT2,', AND',YSCINT,'VERTICALLY.'
      WRITE(009,*)XSCINT1,YSCINT
      WRITE(009,*)XSCINT2,YSCINT
      WRITE(009,*)XSCINT2,YSCINT*(-1.0)
      WRITE(009,*)XSCINT1,YSCINT*(-1.0)
      WRITE(009,*)XSCINT1,YSCINT
C
C       This loop increments the horizontal position of the the scints
C       by .1 cm 20 times to optimize positioning.
C5      DO 60J=1,20
      XMISS=0
      ISEED =549632111
      DO 50I=1,N
10     X=RAN(ISEED)*25-12.5
      Y=RAN(ISEED)*25-12.5
      IF (X**2+Y**2 .GT. 156.0) THEN
      GO TO 10
```

```
      ELSE
      END IF
      Z=RAN(ISEED)*12.5
      THETAR=THETA*3.14159/180
     THEATAC=ATAN2(X-((Z-6.25)*SIN(THETAR)),
     1  (DISTANCE+(Z-6.25)*COS(THETAR)))
     THEATA=THEATAC+THETAR
      PHI=ATAN2(Y,(COS(THEATA-3.14159265/2)*(DISTANCE+(Z-6.25)
     1  *COS(THEATA))))
     PHIS=ATAN2(Y,(DISTANCE+(Z-6.25)*COS(THETAR)))
     THEATAS=ACOS(COS(THEATA)*COS(PHIS))
     ZPC=Z*PRESSURE*COLDFAC
      DENOM=5.38*ZPC+17.35*KAPTON
      THICKNESS=0.002794*KAPTON+0.00018*ZPC
     ATARG=(10.76*ZPC+167.1*KAPTON)/DENOM
     ZTARG=(5.38*ZPC+86.23*KAPTON)/DENOM
     THEATASD=THEATAS*180/3.14159
C      WRITE (*,*)'ITERATION #',I,'-', X,Y,Z,THEATAD
       CALL SRKIN(EBEAM,2.014102,2.014102,0.0,4.002603,0.0,THEATASD,
     1  ANG3P,T3P,ANG4P,T4P,RATIOP,SHIFTP,QP,
     2  ANG3M,T3M,ANG4M,T4M,RATIOM,SHIFTM,QM,ECM,ANGL4P)
      IF (T4P.EQ.0.00) THEN
      T4P=T4M
      ELSE
      END IF
     CALL MULTSCAT(ZTARG,2,ATARG,THICKNESS,T4P,3760.0,CONTROL,XW
     1  ,THEMLT,THEOE,SIG)
      BEAMSPRDR=BEAMSPRD*3.14159265/180
      SIGMA= (SIG**2+BEAMSPRDR**2)**0.5
      ANGL4R= ANGL4P*(3.14159265/180)
     Y1=SIGMA*((-2*LOG(RAN(ISEED)))**0.5)
     1   *COS(2*3.14159365*RAN(ISEED))+ANGL4R
      RALPHA=(193.75+Z)*SIN(Y1)
      Y2=SIGMA*((-2*LOG(RAN(ISEED)))**0.5)
     1   *COS(2*3.14159265*RAN(ISEED))*(1/SIN(Y1))+PHI
     XALPHA=RALPHA*COS(Y2)
     YALPHA=RALPHA*SIN(Y2)
     WRITE(008,*)XALPHA,YALPHA
     IF (XALPHA .LT. XSCINT1) THEN
      GO TO 20
      ELSE
      END IF
     IF (XALPHA .GT. XSCINT2) THEN
      GO TO 20
      ELSE
      END IF
     IF (YALPHA**2 .GT. YSCINT**2) THEN
      GO TO 20
      ELSE
      END IF
      GOTO 40
20     XMISS=XMISS+1
C      WRITE(*,*)XALPHA,YALPHA,Y2
C      CALCULATE TIME OF FLIGHT.
40     THICKMG=THICKNESS*1000
C      WRITE(6,*)'T4P=',T4P,'AZ=',ATARG,ZTARG,'THI=',THICKNESS,THICKMG
      TIPOTL=0.
      CALL ENLOSS(T4P,4.0,2.0,ATARG,ZTARG,THICKMG,TIPOTL,0.0,0.0,
     1 ELOSS,IERROR)
C      WRITE(6,*)T4P,ELOSS,IERROR,TOF
      TOF=1.445*(Z+193.51)/SQRT(T4P-ELOSS)
```

```
      ITOF=INT(TOF)
       WRITE(010,*)ITOF
50     CONTINUE
      RATIO=(1-(XMISS/FLOAT(N)))*100
       PRINT *,'SCINT IS FROM',XSCINT1,'CM, TO',XSCINT2,'CM, AND',
    1  YSCINT,'CM VERTICALLY.'
      PRINT *,'THE EFFICIENCY FOR THIS GEOMETRY IS',RATIO,'PERCENT.'
           PRINT  *,'_._._._._._._._._._._._._._._._._._._._._._._._.'
C       XSCINT1=XSCINT1+0.1
C       XSCINT2=XSCINT2+0.1
C60     CONTINUE
C          PRINTS OUT TARGET THICKNESS AT END OF RUN.
       Z=12.5
      ZPC=Z*PRESSURE*COLDFAC
       THICKNESS=0.002794*KAPTON+0.00018*ZPC
      ATARG=(10.76*ZPC+167.1*KAPTON)/DENOM
      ZTARG=(5.38*ZPC+86.23*KAPTON)/DENOM
      PRINT *,'FOR THE THICKEST CASE,TH=',THICKNESS,'  A=',ATARG,
    1   '  Z=',ZTARG,2.794*KAPTON,' MILLIGR OF KAPTON, AND',
     2   0.18*ZPC,' MILLIGR OF GAS.',
    3   'ENERGY OF LAST 4HE SAMPLED IS',T4P
      END
C
C
C
      SUBROUTINE SRKIN (T1, TM1, TM2, TM3, TM4, EX, ANGLAB,
     .         ANG3P, T3P, ANG4P, T4P, RATIOP, SHIFTP, QP,
     .         ANG3M, T3M, ANG4M, T4M, RATIOM, SHIFTM, QM,
     .         ECM,ANGL4P)
C
C------------------------------------------------------------
C
C     Subroutine to perform relativistic kinematics.
C
C FUNCTION: To perform relativistic kinematics calculations for
C        general users.  Returns most useful kinematic quantities
C        through argument list.
C
C ARGUMENTS: (All arguments are DOUBLE PRECISION)
C
C     Arguments supplied by user:
C
C        T1 - lab frame kinetic energy of incoming particle, MeV
C       TM1 - projectile mass, AMU
C       TM2 - target mass, AMU
C       TM3 - scattered particle mass, AMU
C       TM4 - residual particle mass, AMU
C       EX  - excitation energy of residual nucleus,MeV
C       ANGLAB - lab angle of scattered particle, degrees
C
C     Arguments returned by SRKIN: (P implies usual allowed solution
C        and first solution if two allowed.  M is second)
C
C
C        ANG3P - Center of Mass angle of scattered particle
C        T3P    - kinetic energy of scattered particle
C        ANG4P - COM angle of residual particle
C        T4P    - kinetic energy of residual particle
C        RATIOP - ratio of CoM to Lab cross sections
C        SHIFTP - rate of change of energy with angle
C        QP      - momentum transfer in reaction
```

```
C           ANGL4P -LAB ANGLE OF RECOIL(WHITTON,NOV30'87)
C     Similar definitions hold for M arguments
C
C       In addition, ECM the center of mass incident energy is returned.
C
C     Assembled from RKIN by R L Varner 3-DEC-1982
C       Modified to return ECM          4-OCT-1983
C
C-----------------------------------------------------------------
C
      IMPLICIT REAL*8 (A-H, O-Z)
      COMMON /RELKIN/ AM1, AM2, AM3, AM40, AM1SQ, AM2SQ, AM3SQ, E1, EIN,
     1 P1, ELAB, P1CHK, P1CM, GAMMA, BETA, D, TCM
C
C       Call initial calculation routine
C
      CALL MASSET (T1,TM1,TM2,TM3,TM4)
        ECM = TCM
C
C       Call main calculation routine
C
      CALL RELKIN (EX, ANGLAB,
     .          ANG3P, T3P, ANG4P, T4P, RATIOP, SHIFTP, QP,
     .          ANG3M, T3M, ANG4M, T4M, RATIOM, SHIFTM, QM, ANGL4P)
C
      RETURN
      END
C
C-----------------------------------------------------------------
C
      SUBROUTINE MASSET(T1,TM1,TM2,TM3,TM4)
C
C   THIS SUBROUTINE SETS UP THE MASS AND ENERGY VALUES THAT ARE
C   INDEPENDENT OF THE SCATTERING ANGLE AND THE EXCITATION OF
C   THE RESIDUAL NUCLEUS.
C
C     B.C. KARP, 8/82
C
      IMPLICIT REAL*8 (A-H, O-Z)
      COMMON /RELKIN/ AM1, AM2, AM3, AM40, AM1SQ, AM2SQ, AM3SQ, E1, EIN,
     1 P1, ELAB, P1CHK, P1CM, GAMMA, BETA, D, TCM, ANGL4P
      PARAMETER (AMU=931.5016)
C
      AM1=TM1*AMU
      AM2=TM2*AMU
      AM3=TM3*AMU
      AM40=TM4*AMU
      AM1SQ = AM1*AM1
      AM2SQ = AM2*AM2
      AM3SQ = AM3*AM3
C
      E1=T1 + AM1
      EIN = DSQRT(AM1SQ + AM2SQ + 2.*AM2*E1)
      TCM = EIN - AM1 - AM2
      ELAB = E1 + AM2
      P1 = DSQRT(E1*E1 - AM1SQ)
      P1CHK = 1.E-4*P1
      P1CM = P1*AM2/EIN
     GAMMA=ELAB/EIN
      BETA=P1/ELAB
C
```

```
      D=(P1*AM3)
      D = D*D
      RETURN
      END
C
C-----------------------------------------------------------------
C
      SUBROUTINE RELKIN (EX, ANGLAB,
     .          ANG3P, T3P, ANG4P, T4P, RATIOP, SHIFTP, QP,
     .          ANG3M, T3M, ANG4M, T4M, RATIOM, SHIFTM, QM, ANGL4P)
C
C     THIS IS A DOUBLE PRECISION SUBROUTINE TO DO RELATIVISTIC KINEMATICS
C     INPUT AND OUTPUT ENERGIES IN MEV, MASSES IN AMU, ANGLES IN DEGREES
C     OUTPUTS BOTH SOLUTIONS.  IF ONLY ONE SOLUTION IS ALLOWED, THE OTHER
C      IS SET TO 0.0
C
C     IF THE REACTION IS NOT ALLOWED BECAUSE ENERGY IS BELOW THE
C     THRESHOLD, SUBROUTINE SETS ANG3P=-1.0
C     IF THE REACTION IS NOT ALLOWED FOR A GIVEN ANGLE, ANG3P=-2.0
C     AM1=PROJECTILE MASS, AM2=TARGET MASS, AM3=SCATTERED PARTICLE
C     MASS, AM4=RESIDUAL NUCLEUS MASS
C
C      MODIFIED BY B.C. KARP     5/82
C
      IMPLICIT REAL*8 (A-H,O-Z)
       PARAMETER (DTR=0.01745329, DTRKEV=-17.45329, PI=3.1415927)
      COMMON /RELKIN/ AM1, AM2, AM3, AM40, AM1SQ, AM2SQ, AM3SQ, E1, EIN,
     1 P1, ELAB, P1CHK, P1CM, GAMMA, BETA, D, TCM
C
      AM4 = AM40 + EX
      AM4SQ = AM4*AM4
C
C     ENERGY THRESHOLD CHECK
C
      EOUT=AM3 + AM4
      IF (EIN.LT.EOUT) GO TO 20
C
      ANGLB=ANGLAB*DTR
C  CHECK FOR LAB ANGLE OF 0 OR 180 DEGREES
      IZERO=0
      IF(DABS(ANGLAB).LT.0.01) THEN
       ANGLB=0.0001D0
      IZERO=1
      ENDIF
      IF(DABS(ANGLB-PI).LT.0.00001) THEN
       ANGLB = 3.14159
      IZERO = -1
      ENDIF
C
      COSLAB = DCOS(ANGLB)
      SINLAB = DSIN(ANGLB)
      SIN2LB = DSIN(2.*ANGLB)
C
      X=(AM2*E1 + (AM1SQ + AM2SQ - AM3SQ -
     1 AM4SQ)/2.0)**2 - AM3SQ*AM4SQ -
     2 D*(SINLAB)**2
      IF(X.LT.0.0) GO TO 80
      X=DSQRT(X)
      E3A=ELAB*(AM2*E1 + (AM1SQ + AM2SQ + AM3SQ
     1 - AM4SQ)/2.0)
      E3B=P1*COSLAB*X
```

```
      E3C = ELAB**2 - (P1*COSLAB)**2
      SUMAB = E3A + E3B
      DIFAB = E3A - E3B
      E3P = SUMAB/E3C
      E3M = DIFAB/E3C
      T3P=E3P - AM3
      T3M=E3M - AM3
      A=EIN*SINLAB
C
C     CALCULATE THE KINEMATIC SHIFT
C
      DXDT = -0.5*D*SIN2LB/X
      DE3BDT = P1*(COSLAB*DXDT - SINLAB*X)
      DE3CDT = P1*P1*SIN2LB
C
      FACTOR1 = DE3BDT/E3C
      FACTOR2 = DE3CDT/(E3C*E3C)
      SHIFTP = FACTOR1 - FACTOR2*SUMAB
      SHIFTM = -FACTOR1 - FACT0R2*DIFAB
C
C     CONVERT TO KEV/DEGREE
C
      SHIFTP = SHIFTP*DTRKEV
      SHIFTM = SHIFTM*DTRKEV
C
      IF(E3P.LT.AM3) THEN
      IF(E3M.LT.AM3) GO TO 80
      T3P = T3M
      E3P = E3M
      SHIFTP = SHIFTM
      T3M = 0.
      E3M = 0.
      SHIFTM = 0.
      ENDIF
      P3P=DSQRT(E3P*E3P - AM3SQ)
      E4P=E1 + AM2 - E3P
      T4P=E4P - AM4
C  MOMENTUM CONSERVATION CHECK
      P4P=DSQRT(E4P*E4P - AM4SQ)
      DIFFA=(P1 - P3P*COSLAB)/P4P
      CHECKA=DABS(DIFFA)
      IF (CHECKA.GT.1.01) GO TO (80,40,40),IZERO+2
      IF(DIFFA.GE.1.0) THEN
      THETA1 = 0.
      ELSE
      IF(DIFFA.LE.-1.0) THEN
      THETA1 = PI
      ELSE
      THETA1 = DACOS(DIFFA)
      ENDIF
      ENDIF
      DIFFB=P3P*SINLAB/P4P
      CHECKB=DABS(DIFFB)
      IF(CHECKB.GT.1.01) GO TO 40
      IF(DIFFB.GE.1.0) THEN
      THETA2 = 0.5*PI
      ELSE
      THETA2 = DASIN(DIFFB)
      ENDIF
      CHECKC=DABS(THETA1-THETA2)
      CHECKD=DABS(THETA1-PI+THETA2)
```

```
      IF(CHECKC.LT.0.0001 .OR. CHECKD.LT.0.0001 .OR.
     1 IZERO.EQ.1) GO TO 100
      GO TO 40
100   CONTINUE
C
      BP=(E1 + AM2)*(COSLAB - P1*E3P/(E1 + AM2)/P3P)
      ANG3P = DATAN2(A,BP)
C
C     CALCULATE THE MOMENTUM TRANSFER
C
      E3CM = (EIN*EIN + AM3SQ - AM4SQ)/(2.*EIN)
      P3CM = DSQRT(E3CM*E3CM - AM3SQ)
      P3CMX = P3CM*DSIN(ANG3P)
      P3CMZ = P3CM*DCOS(ANG3P)
      DELDZ = P3CMZ - P1CM
      QP = DSQRT(P3CMX*P3CMX + DELPZ*DELPZ)
C
C     LAB ANGLE FOR FOURTH PARTICLE
C
      ANGL4P = SINLAB*(P3P/P4P)
      IF(ANGL4P.GE.1.0) THEN
       ANGL4P = 0.5*PI
      ELSE
      ANGL4P = DASIN(ANGL4P)
      ENDIF
C
C     DETERMINE QUADRANT OF RECOIL
C
      I = 0
      DIFFA = P1 - P3P*COSLAB
      P4PZ = P4P*DCOS(ANGL4P)
110   CHECKA = DABS(DIFFA - P4PZ)
      IF(CHECKA.LT.P1CHK) GO TO 120
      IF(I.EQ.1) GO TO 40
      I = 1
      ANGL4P = PI - ANGL4P
      P4PZ = -P4PZ
      GO TO 110
120   CONTINUE
C
      Z=((DSIN(ANG3P))**3/SINLAB)*(GAMMA + 1.0/(DTAN(ANGLB)*
     1 DTAN(ANG3P)))
      R=BETA*GAMMA*(DSIN(ANG3P))**3/(SINLAB)**2
        Y=(1.0/P3P - E3P**2/P3P**3)*(-SINLAB/E3C)*(+P1*X*(1.0 +
     1 D*(COSLAB)**2/X**2) + 2.0*E3P*P1**2*COSLAB)
      RATIOP=1.0/(Z + R*Y)
      GO TO 50
40     ANG3P=0.0
       T3P=0.0
       SHIFTP = 0.
       T4P=0.0
       RATIOP=0.0
50     IF(E3M.LT.AM3) GO TO 60
       P3M=DSQRT(E3M*E3M - AM3SQ)
       E4M=E1 + AM2 - E3M
       T4M=E4M - AM4
C  MOMENTUM CONSERVATION CHECK
       P4M=DSQRT(E4M*E4M - AM4SQ)
       DIFFA=(P1 - P3M*COSLAB)/P4M
      CHECKA=DABS(DIFFA)
       IF(CHECKA.GT.1.01) GO TO 60
```

```
      IF(DIFFA.GE.1.0) THEN
      THETA1 = 0.
      ELSE
      IF(DIFFA.LE.-1.0) THEN
      THETA1 = PI
      ELSE
      THETA1 = DACOS(DIFFA)
      ENDIF
      ENDIF
      DIFFB=P3M*SINLAB/P4M
      CHECKB=DABS(DIFFB)
      IF(CHECKB.GT.1.01) GO TO 60
      IF(DIFFB.GE.1.0) THEN
      THETA2 = 0.5*PI
      ELSE
      THEAT2 = DASIN(DIFFB)
      ENDIF
      CHECKC=DABS(THETA1-THETA2)
      CHECKD=DABS(THETA1-PI+THETA2)
      IF(CHECKC.LT.0.0001 .OR. CHECKD.LT.0.0001)  GO TO 101
      GO TO 60
101   CONTINUE
C
      BP=(E1 + AM2)*(COSLAB - P1*E3M/(E1 + AM2)/P3M)
      ANG3M=DATAN2(A,BP)
C
C     CALCULATE THE MOMENTUM TRANSFER
C
      P3CMX = P3CM*DSIN(ANG3M)
      P3CMZ = P3CM*DCOS(ANG3M)
      DELPZ = P3CMZ - P1CM
      QM = DSQRT(P3CMX*P3CMX + DELPZ*DELPZ)
C
C     LAB ANGLE FOR FOURTH PARTICLE
C
      ANGL4M = SINLAB * (P3M/P4M)
      IF(ANGL4M.GE.1.0) THEN
      ANGL4M = 0.5*PI
      ELSE
      ANGL4M = DASIN(ANGL4M)
      ENDIF
C
C     DETERMINE QUADRANT OF RECOIL
C
      I = 0
      DIFFA = P1 - P3M*COSLAB
      P4MZ = P4M*DCOS(ANGL4M)
130   CHECKA = DABS(DIFFA - P4MZ)
      IF(CHECKA.LT.P1CHK) GO TO 140
      IF(I.EQ.1) GO TO 60
      I = 1
      ANGL4P = PI - ANGL4P
      P4MZ = -P4MZ
      GO TO 130
140   CONTINUE
C
      CHECKE=DABS(ANG3P-ANG3M)
      IF(CHECKE.LT.0.0001) GO TO 60
      Z=((DSIN(ANG3M))**3/SINLAB)*(GAMMA + 1.0/(DTAN(ANGLB)
     1 *DTAN(ANG3M)))
      R=BETA*GAMMA*(DSIN(ANG3M))**3/(SINLAB)**2
```

```
      Y=(1.0/P3M - E3M**2/P3M**3)*(-SINLAB/E3C)*(-P1*X*(1.0 +
     1 D*(COSLAB)**2/X**2) + 2.0*E3M*P1**2*COSLAB)
     RATIOM=1.0/(Z + R*Y)
     GO TO 70
60    ANG3M=0.0
     ANGL4M = 0.
      T3M=0.0
     SHIFTM = 0.
      T4M=0.0
     RATIOM=0.0
     GO TO 70
80    ANG3P=-2.0
     GO TO 200
20    ANG3P=-1.0
     GO TO 200
C
C    CONVERT RADIANS TO DEGREES
C
70   CONTINUE
     ANG3P=ANG3P/DTR
     ANG3M=ANG3M/DTR
     ANGL4P = ANGL4P/DTR
     ANGLM = ANGL4M/DTR
C
      IF(IZERO) 180,200,160
160   ANG3P=0.0D0
     IF(DABS(ANGL4P-180.).LT.0.5) THEN
       ANGL4P = 180.
     ELSE
       ANGL4P = 0.
     ENDIF
      ANG3M=0.0D0
     ANGL4M = 0.
     GO TO 200
180   ANG3P = 180.
     ANGL4P = 0.
     ANG3M = 0.
     ANGL4M = 0.
200  CONTINUE
     RETURN
     END

C
C
C

    SUBROUTINE MULTSCAT(BIGZ,SMALLZ,A,T,EKIN,EREST,CONTRL,XW
    1                  ,THEMLT,THEOE,THEOE1)

**********CODE BY SINAN UTKU, 7/9/87, TUNL**********

*****************************INPUT  CARDS*****************************
******  SMALLZ: ATOMIC NUMBER OF INCIDENT PARTICLE
******  BIGZ: ATOMIC NUMBER OF SCATTERER
******  A: ATOMIC WEIGHT OF SCATTERER
******  T: THICKNESS OF FOIL IN g/cm^2
******  EKIN: KINETIC ENERGY OF INCIDENT PARTICLE IN MeV
******  EREST: REST MASS OF INCIDENT PARTICLE IN MEV
*****************************OUTPUT  CARDS*****************************
******  CONTRL(LOGICAL): IF FALSE INDICATES THAT INPUT IS BAD
***********************************************************************
```

```
      REAL A,T,EKIN,EREST,BETASQ,BETA,PVSQ,XCSQ,FOFB,FPRB,B1,B2
     1    ,XC,XW,THEMLT,THEOE,THEOE1,BIGZ
      INTEGER SMALLZ
      LOGICAL CONTRL
        DATA B2,EPS/5.5,0.00001/

C               CALCULATION OF VARIOUS PARAMETERS
C     WRITE (*,*) BIGZ, A, T, EKIN

      BETASQ=1.-(1.+EKIN/EREST)**(-2)
      BETA=SQRT(BETASQ)
      SMALLB=ALOG(2730.*(BIGZ+1)*BIGZ**(1./3.)*SMALLZ**2*T/(A*BETASQ))
     1   -0.1544
      PVSQ=(EKIN**2+2.*EKIN*EREST)*BETASQ
      XCSQ=0.1569*BIGZ*(BIGZ+1)*SMALLZ**2*T/(A*PVSQ)
      XC=SQRT(XCSQ)
      IF (SMALLB .LT. 1.) THEN
        WRITE(*,50)
   50   FORMAT(//,' INVALID INPUT PARAMETERS. CHECK YOUR INPUT',//)
        CONTRL=.FALSE.
        RETURN
      ENDIF

C             NEWTON-RAPSON ITERATION TO FIND BIGB
 1010 CONTINUE
        B1=B2
       FOFB=B1-ALOG(B1)-SMALLB
        FPRB=1.-1./B1
        B2=B1-FOFB/FPRB
      IF (ABS(B2-B1) .GT. EPS) GOTO 1010
      BIGB=B2
      IF (BIGB .LE. 4. .OR. BIGB .GE. 15.) THEN
        WRITE(*,100)
  100   FORMAT(//,' WARNING: YOUR INPUT PARAMETERS ARE OUT'
     1        ' OF RANGE OF THE THEORY')
      ENDIF
        XW=-1.5475753E-05*BIGB**4+7.2736619E-04*BIGB**3
     1    -1.3252208E-02*BIGB**2+0.1158611*BIGB
     2    +0.5280014
      THEMLT=1./(XC*SQRT(BIGB))
      THEOE=XW*XC*SQRT(BIGB)
        FOFZ=1.024-.01*BIGZ+8.*10.**(-5)*BIGZ**2
        BB=-0.013+2.2*10.**(-3)*BIGZ-2.3*10.**(-5)*BIGZ**2
      THEOE1=THEOE*FOFZ*(1.+BB*(EKIN-3.))
      RETURN
      END
      SUBROUTINE ENLOSS (E,AI,ZI,AT,ZT,TT,TIPOTL,C,DELTA,ELOSS,IERROR)
C                                                              *
C     THIS ROUTINE CALCULATES THE MEAN ENERGY LOSS (IN MEV), USING THE
C     RELATIVISTICALLY CORRECT BETHE FORMULA, DIVIDING THE TARGET UP
C     INTO REGIONS OF SMALL ENERGY LOSS.    REFERENCES FOR EQUATION -
C       BETHE AND ASHKINS ARTICLE IN SEGRE S NUCL. PHYSICS BOOK.     *
C       S. M. SELTZER AND M. J. BERGER, ENERGY-LOSS STRAGGLING OF    *
C        PROTONS AND MESONS0 TABULATION OF THE VAVILOV DISTRIBUTION, *
C          NAS-NRC PUBL. 1133 (NUCLEAR SCIENCE SERIES  REPORT NO. 39,  *
C          STUDIES IN PENETRATION OF CHARGED PARTICLES IN MATTER),    *
C            P. 187 (1964).                                          *
C       J. F. JANNI, CALCULATIONS OF ENERGY LOSS, RANGE, PATHLENGTH,  *
C          STRAGGLING, MULTIPLE SCATTERING,  (ETC.),TECHNICAL REPORT  *
C            NO.1AFWL-TR-65-150 (1966).    AVAILABLE FROM U. S. FEDERAL  *
```

```
C         CLEARINGHOUSE.                                        *
C                                                               *
C      INPUT PARAMETERS ARE  INCIDENT ENERGY (MEV), ATOMIC MASS OF
C      INCIDENT PARTICLE (AMU), CHARGE OF INCIDENT PARTICLE, ATOMIC  *
C      MASS OF TARGET (AMU), CHARGE OF TARGET, TARGET THICKNESS      *
C      (MICROGRAMS PER SQUARE CM.), TARGET IONIZATION POTL. (EV),    *
C      SHELL CORRECTION FACTOR, AND DENSITY EFFECT CORRECTION TERM.  *
C
CT *    USES FUNCTION EMASS TO RETURN CURRENT VALUE OF ELECTRON REST
CT *     MASS AND AMU IN MeV.
CT
CT *    ERROR RETURN CODES.
CT *          IERROR=0 NORMAL CALCULATION
CT *           IERROR=1 BEAM STOPPED
CT *          IERROR=2 POSSIBLY NOT A VALID CALCULATION
CT *          IERROR=3 NEGATIVE STOPPING POWER
CT *
C                                                               *
C *    IONIZATION POTENTIAL DATA FOR Z<33
C
     DIMENSION POTLD(33)
       DATA POTLD/ 18.3, 41.7, 38.8, 61.0, 68.0, 75.1, 87.5,
        1         88.9,120.7,140.0,150.1,156.5,163.0,170.0,175.9,182.6,170.0,
        2         205.0,203.8,211.3,219.1,227.2,235.6,244.4,253.0,273.0,292.5,
       3       312.0,320.0,330. ,340. ,350. ,350. /
        DATA LOUT/6/
        IERROR=0
C
          AMU=931.5016
      WI=AI*AMU
      THICK=TT*1.E-03
      INDEX=0
         WE=EMASS(0,-1)
C
C *    TEST TO SEE IF IONIZATION POTENTIAL INPUT
C *    IF NOT THEN CALCULATE
C
      IF (TIPOTL.GT.0.) GO TO 03
C     TARGET Z 33 OR LESS, CALCULATE ION. POTL. USING LINEAR
C     INTERPOLATION OF VALUES IN TABLE ABOVE.
      IF (ZT.GT.33.) GO TO 02
      I=ZT
     ZDIFF=ZT-FLOAT(I)
C       WRITE(6,*)ZDIFF,POTLD(I),POTLD(I+1),I
      A1=1.-ZDIFF
     A2=A1*POTLD(I)
     A3=ZDIFF*POTLD(I+1)
      A4=A3+A2
C       WRITE(6,*)A1,A2,A3,A4
     TIPOTL=(1.-ZDIFF)*POTLD(I)+ZDIFF*POTLD(I+1)
      GO TO 3
02    CONTINUE
C     TARGET Z GREATER THAN 33, CALC. ION. POTL. FROM JANNI, EQ. (15).
       TIPOTL=9.78*ZT*(1.+0.196/(ZT**(2./3.)))
 3    CONTINUE
     POTL=TIPOTL*1.E-06
C
C     SET ELOSS TO 0.  AND SET ENERGY EPRIME TO INCIDENT ENERGY.
      ELOSS=0.
      EPRIM=E
C     CALCULATE PARTICLE VELOCITY  (C=1.)  AND PARAMETER EPSILON MAX.
```

```
10    BETASQ=(EPRIM**2+2.*WI*EPRIM)/((WI+EPRIM)**2)
     FACTOR=1.+2.*WE/(WI*SQRT(1.-BETASQ))+(WE/WI)**2
     EPSMAX=2.*WE*BETASQ/((1.-BETASQ)*FACTOR)
C                                                     *
C    CALCULATE  DE/DX  (BETHE FORMULA) FOR ENERGY EPRIME.
     FACTOR=2.*WE*BETASQ*EPSMAX/((POTL**2)*(1.-BETASQ))
     X=0.30058*(ZI**2)*(WE/BETASQ)*(ZT/AT)*(ALOG(FACTOR)-2.*BETASQ-2.*C
    1/ZT-DELTA)
C
C    BRANCH OUT IF CALCULATED STOPPING POWER IS NEGATIVE.
     IF (X.LE.0.0) GO TO 35
C                                                     *
C    BRANCH OUT IF PARTICLE IS STOPPED IN TARGET.
     IF (EPRIM.LT.X*THICK) GO TO 20
C    SET SMALL THICKNESS OF TARGET TO .5 PER CENT OF INCIDENT ENERGY
C    DIVIDED BY  DE/DX FROM BETHE FORMULA.
     TDELT=E/(200.*X)
C    BRANCH OUT IF THE TARGET THICKNESS REMAINING IS LESS THAN THE
C    SMALL THICKNESS JUST CALCULATED.
     IF (TDELT.GE.THICK) GO TO 30
C    LET PARTICLE PASS THROUGH SMALL THICKNESS, AND CALCULATE REMAINING
C    THICKNESS AND NEW PARTICLE ENERGY AFTER PASSING THROUGH.
     ELOSS=ELOSS+TDELT*X
     THICK=THICK-TDELT
     EPRIM=EPRIM-TDELT*X
C                                                     *
C    SET PRINT INDEX IF ENERGY IS SUCH THAT THE BETHE FORMULA IS NOT
C    VALID, THEN GO BACK TO CALCULATE NEW NOS. FOR NEW ENERGY IF
C    PARTICLE IS NOT STOPPED.
     EMIN=EPRIM/(WI*ZI**(4./3.))
     IF (EMIN.LT.0.0005) INDEX=1
     IF (EPRIM.GT.0.0) GO TO 10
C                                                     *
C    PARTICLE STOPPED IN TARGET. SET ENERGY LOSS TO INCIDENT ENERGY,
C    SET IERROR TO 1, AND RETURN.
  20 CONTINUE
     ELOSS=E
       IERROR=1
     RETURN
C                                                     *
C    ADD ON LAST CONTRIBUTION TO ENERGY LOSS AND PRINT MESSAGE IF
C    NECESSARY.
30   ELOSS=ELOSS+THICK*X
     IF (INDEX.NE.1) GO TO 34
       IERROR=2
  34 CONTINUE
     RETURN
  35 CONTINUE
     ELOSS=2.*E
       IERROR=3
     RETURN
C
CT      Former output messages printed for various errors.
C
C40   FORMAT (' THE INCIDENT ENERGY IS LESS THAN THE CALCULATED MEAN',
C    1 'ENERGY LOSS '/,
C    2' (I.E., THE PARTICLES ARE STOPPED IN THE TARGET, ON ',
C    3'THE AVERAGE)')
C50   FORMAT (' THE MEAN ENERGY LOSS RESULT IS QUESTIONABLE HERE,',
C    1' AS THE BETHE FORMULA'/,
C    2'IS NOT VALID (SHOULD USE EFFECTIVE CHARGE)')
```

```
C60   FORMAT (' THE MEAN ENERGY LOSS CALCULATION BREAKS DOWN WITH',
C     1' THESE PARAMETERS,'/,
C     2'AS IT GIVES A NEGATIVE STOPPING POWER')
      END
```

Biography

Born: Feb. 1, 1957 in Tallahassee FL

Education:

1984, M.A., Physics
Duke University, Durham, North Carolina

1982, B.S., Physics with minor in mathematics
Florida State University, Tallahassee, FL

1979, Associate of Arts degree
Tallahassee Community College, Tallahassee, FL

1975, National Merit Scholarship Finalist

Positions:

5/83-Present; Graduate Research Assistant
Triangle Universities Nuclear Laboratory (TUNL)
Physics Department, Duke University

9/82-4/83; Graduate Teaching Assistant
Physics Department, Duke University

80-5/82; Undergraduate Research Assistant
Electron Beam Precipitator Group
Physics Department, FSU

Publications and Abstracts:

Energy Dependence of Polarization Observables in the ^{2}H(d,g)^{4}He Reaction, H.R. Weller, R.M. Whitton, S. E. Kuhn, J.L. Langenbrunner, E. Hayward and W.R. Dodge, Phys. Lett. B213 (1988) 413.

Vector Analyzing powers for ^{1}H(d,g)^{3}He and ^{2}H(p,g)^{3}He, M.C. Vetterli, J.A. Kuehner, C. Bamber, N. Davis, A.J. Trudel, H.R. Weller and R.M. Whitton, Phys. Rev. C38 (1988) 2503-2508.

Gamma Decay of High Spin States in ^{25}Mg above 6.1 MeV, D.M. Headly, R.K. Sheline, S.L. Tabor, U.J. Huttmeier, C.J. Gross, E.F. Moore, B.H. Wildenthal, H.R. Weller, R.M. Whitton and I. Ragnarsson, Phys. Rev. C38 (1988) 1698-1721

High-Spin States and Rotational Coexistance in ^{25}Mg, D.M. Headly, R.K. Sheline, S.L. Tabor, U.J. Huttmeier, C.J. Gross, E.F. Moore, B.H. Wildenthal, H.R. Weller, R.M. Whitton and I. Ragnarsson, Phys. Lett. B198 (1987) 433-437.

The D-State of ^{4}He and the ^{2}H(d,g)^{4}He Reaction from E_d=600 keV-to-50MeV, H.R. Weller, R.M. Whitton, S. E. Kuhn, J.L. Langenbrunner, E. Hayward, W.R. Dodge, H.J. Hofmann, T.D. Poelhekken, S.K.B. Hesmondhalgh and S. Van der Werf, Submitted to the International Symposium on the Few-Body Problem in Nuclear Physics, Vancouver, July (1989)

The D-State in ^{4}He and the ^{2}H(d,g)^{4}He reaction at 30 and 50 MeV, R. M. Whitton, H. R. Weller, S.E. Kuhn, Evans Hayward and W. R. Dodge, Submitted to the meeting of the International Conference on Nuclear Physics, Sao Paulo, August (1989)

Tensor Polarized Deuteron Capture on Deuterium at 50 MeV Beam Energy: A Measurement of A_{zz}, R. M. Whitton, H. R. Weller, S.E. Kuhn, Evans Hayward and W. R. Dodge, Bull. Am. Phys. Soc. 33, No.4 (1988) 1099.

Tensor Polarized Deuteron Capture by Deuterium at Beam Energies of 20 to 50 MeV, R. M. Whitton, H. R. Weller, S.E. Kuhn, Evans Hayward and W. R. Dodge, Bull. Am. Phys. Soc. 32, No.8 (1987) 1547.

Radiative Capture of Tensor Polarized Deuterons by ^{3}He and ^{3}H, J.C. Riley, R.M. Whitton, H.R. Weller, and D.R. Tilley, Bull. Am. Phys. Soc. 30, No.4 (1985) 700.